Dynamics and Control of Cables in Cable-Actuated Systems

by

Donya Mohammadshahi

Department of Mechanical Engineering
McGill University, Montreal
Canada

August 2013

A thesis submitted to McGill University in partial fulfillment of the requirements for the degree of Master of Engineering

Abstract

This thesis deals with the dynamic modeling and control of a cable-actuated system consisting of a payload attached to several actuated cables. The objective of this thesis is to design a stabilizing controller that positions the payload and suppresses the cables vibrations. The dynamics of the system is modeled using the lumped-mass method. First, PID and LQG control algorithms are used to design a controller. Later, motivated by the robust nature of the passivity-based control, its application to cable-actuated systems is investigated. Cable-actuated systems are usually non-square with non-collocated actuators and sensors, which generally limits the use of passivity-based control. In order to overcome these limitations, first a dynamic embedding is considered where an observer is used to construct a new output that realizes a passive input-output map. Next, an alternative input-output map is considered where the output is a scaled version of the true payload velocity and the input is a modified winch torque.

Résumé

Cette thèse présente une étude de la modélisation dynamique et commande d’un système actionné par câbles, celui-ci composé d'un effecteur attaché à une série de câbles actionnés. L’objectif de cette thèse est de développer un contrôleur qui positionne l'effecteur et diminue les vibrations des câbles. La dynamique du système est modélisée en utilisant la méthode de masses localisées. D'abord, deux algorithmes de commande, PID et LQG sont utilisés pour développer la command. Puis, nous étudions l’application de la commande passive sur le système actionné pas câbles. Les systèmes actionnés par câbles sont généralement non carré avec des actionneurs et des senseurs non colocalisés, ce qui limite généralement l'utilisation de la commande passive. Pour trouver une solution pour ces contraintes, premièrement, nous considérons une intégration dynamique, où un observateur est utilisé pour construire une nouvelle sortie qui donne un système passif. Deuxièmement, nous considérons une entrée-sortie alternative, où la sortie est une version réduit de la vitesse réelle de l'effectuer et l'entrée est une modification du couple de treuil.

Contents

List of Figures

Acknowledgment

I would like to thank my husband, Hatef, for the love and support he has given me. His confidence in me and encouragement have greatly contributed to the completion of this work.

I would like to thank my parents for their everlasting love, sacrifice and support. I will always be grateful for their love.

I would like to thank my supervisors, Meyer Nahon and James Richard Forbes for their guidance.

Finally, I would like to thank my colleagues at McGill University for enriching discussion that I have had with them.

1 Introduction

Cables are flexible load carrying or force transmitting tension members used in many mechanical cable-actuated systems such as tethered aerostats, tethered satellites, elevators, towing vehicles, mooring ships, tethered under water vehicles, cranes, and cable-actuated robots. Figure 1.1 shows three such systems: a tethered aerostat, an elevator and a towed underwater vehicle. Cables are widely utilized in various engineering applications since they are more dynamically responsive than rigid systems. In addition, cables have better maximum payload to weight ratio and mobility compared to rigid elements [1].

(a) (b) (c)

Figure 1.1: Examples of cable-actuated systems: (a) multi-tethered aerostat [2], (b) elevator [3], (c) towed underwater vehicle [4]

Because of their wide usage in various structures and systems, cables have been the subject of extensive academic research. This thesis deals with dynamic modeling and control of cables which are actuated by several winches in order to position and orient a payload mass in a cable-actuated system as shown generically in Figure 1.2. There are two principal areas of research pertaining to cable-actuated systems: dynamic modeling and control of cables. Although the literature on dynamic modeling and control of cable-actuated systems has been ongoing for a number of decades, a number of issues remain, especially with respect to the control of these systems. Any cable that is used in a cable structure or cable-actuated system is prone to longitudinal and/or transverse vibration. In dealing with cable-actuated systems, a controller should be designed to reduce these vibrations. Moreover, in cable-actuated systems with an object to be moved, the controller should ensure tracking of a desired trajectory.

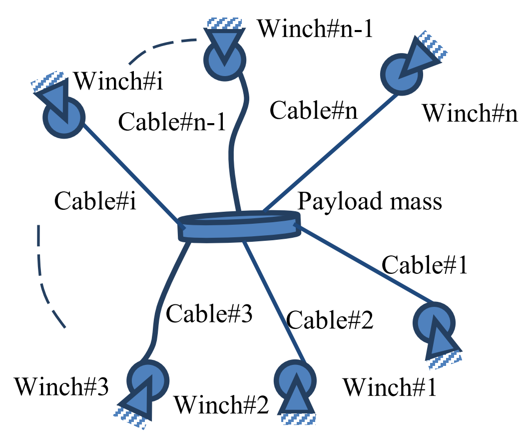

Figure 1.2: A generic cable-actuated system

1.1 Summary of previous work

This literature review surveys prior works relevant to dynamics modeling and control of cables in cable-actuated systems with a description and a summary of each work.

1.1.1 Dynamics

The dynamics of cable-actuated systems has been thoroughly studied. In this survey, the models reviewed are those that are more amenable to application in control, and some of their uses and limitations are discussed.

The motion of a cable-actuated system can be predicted if the forces and/or moments applied to the system through actuators are given. This is known as the forward cable dynamics problem. On the other hand, in robotics for example, given a prescribed end-effector path, inverse dynamics algorithms are used to calculate the required torques that the motors must produce to make the end-effector move properly. Similarly, in the cable inverse dynamics problem, we want to compute actuator forces and/or moments such that the desired motion of the payload is accomplished, given the known system properties, such as payload mass, cable density and maximum allowable cable tension. Two types of cable models are identified: continuous and discrete models.

1.1.1.1 Continuous models

In dynamic modeling of cable-actuated systems for the purpose of control, cables are usually modeled as continuous systems. In this approach cables are modeled using either beam or string equations. A string is a flexible element that shows no resistance to bending, so if the bending stiffness of a cable is relatively small, it can be modeled as a string. In contrast, if the cable has significant bending stiffness, it is modeled as a beam [5]. Zhu and Chen [6] investigated the forced response of a translating cable with variable length and tension, and found that a translating cable without any sag can be modeled as a string, a pinned-pinned beam or a fixed-fixed beam.

- **Beam model**

The dynamics of a cable have been investigated by modeling the cable as a vertically translating beam under tension [7]. The solution to a beam transverse vibration problem with time dependent boundary conditions was first addressed by reducing it into a free vibration beam problem [8]. Pota et al. [9] also used a beam equation of motion in order to model transverse vibration of a cable in a cable-actuated system. In this paper, a linear model was assumed to be valid around the final operating point.

Coupled vibration of a varying length flexible cable transporter system with arbitrary axial velocity was presented by Zhang and Agrawal [10] considering both transverse and longitudinal vibrations simultaneously. It was observed that an increase in internal damping can reduce longitudinal vibration, but has little effect on transverse vibration. Later, the problem of modeling longitudinal vibration of a flexible transporter system with varying cable length was presented by Zhang et al. [11]. In this research, the nonlinear Partial Differential Equations (PDE), governing the cable motion, were derived by applying Hamilton's principle. Subsequently, in order to solve the governing equations of motion, the assumed mode method was used. Zhang and Agrawal [12] performed an investigation of modeling transverse vibration of a cable. Similarly, the governing equation for transverse vibration of a cable was derived using Hamilton's principle. Since it is not possible to solve the coupled nonlinear PDE of motion analytically, Galerkin's method was used to transform the infinite dimensional PDE to finite dimensional ordinary differential equations (ODE).

- **String model**

Otsuki et al. [13] formulated the dynamics of a length-varying cable using the string equation. Later, they presented another paper on suppression of transverse vibration of an elevator cable that was also modeled with the string equation [14]. Zhu and Zheng [15] obtained the exact response of a string with arbitrary varying length under general excitation. In this research, the response of the string to a general excitation was also derived through a wave method. This wave method was proven to be more accurate and efficient than the spatial discretization method when the propagating wave was non-dispersive.

1.1.1.2 Discrete models

In the context of discrete modeling, the dynamics of cables can be formulated using different methods such as finite element and finite difference methods. In the finite difference method, the finite difference approximation is used to derive spatial and time derivatives to the system of equations. Howell [16] used the finite difference method to develop cable's differential equation of motion. Triantafyllou and Howell [17] studied the dynamic response of low tension cables using the finite difference method. Burgess [18] also developed the finite difference model with bending stiffness for simulation of undersea cables.

Buckham [19] performed a comprehensive literature review of discrete methods that are used for modeling the dynamics of cables, and then proceeded to use the lumped mass method (a specific instance of the finite element method) for dynamic modeling of an underwater vehicle system. In this thesis, cables are modeled using the discrete lumped mass model since it is more simple and versatile than other models. In addition, it has been confirmed that the lumped mass model can properly model longitudinal and transverse dynamics behavior of cables [20]. In the lumped mass method, a cable is modeled as a series of point masses connected by viscoelastic massless elements, and the equations of motion are derived for this approximate model. Lambert and Nahon [21] modeled a triple-tethered aerostat that supported the receiver in a very large radio telescope antenna, using a lumped mass model. The linear elements introduced in the lumped mass model do not tolerate torsion deformation. In order to consider the torsion deformation of the elements, Malahy [22] applied the finite element technique to third order 3D element and consider the element rotational equation of motion.

1.1.2 Control and its challenges

The control of cable-actuated systems has been addressed using different methods, including PID control, optimal and robust control. Cables are prone to longitudinal and/or transverse vibration. In dealing with cable-actuated systems with a payload to be moved, a controller is used to bring the object to its desired position. The controller should also reduce the cable vibration especially near the desired position of the object. In most research papers, author focus on damping the cable vibrations, and suggest using a separate simple feedback controller for positioning the object.

Early studies on vibration control focused on stabilizing the system using passive damping and stiffness. Considering more complicated and time-varying conditions, researchers later employed active vibration control. Few studies exist on active damping of multimodal oscillation of cables, and the problems of active damping of transverse and longitudinal vibrations are usually considered separately. As mentioned earlier, for the purpose of control, cables can be modeled as continuous or discrete systems. A control method based on a discrete cable model introduced for controlling a cable driven parallel mechanism is given in [23]. In this latter work, the system considered of eight cables whose varying length was controlled by ground-based winches, while an aerostat held the platform aloft. A cascade control architecture was designed with different control loops: the inner loop dealt with tension in the cables using the H_∞-optimal-control strategy, and the other loop controlled the position of the platform using inverse-dynamic control and PID control.

1.1.2.1 Damping transverse vibration

The locations of sensors and actuators in a cable-actuated system are limited to the two ends of the cable or near one of the two ends. This is one of the difficulties in dealing with active control of cables. In prior work, damping the transverse vibration of a cable is performed using a transverse actuator that is not attached to the cable [24]. Dealing with the gap between the actuator and the cable and positioning the actuator are two existing problems in active damping of the transverse vibration.

As mentioned in section 1.1.1.1, a translating cable without any sag can be modeled as a string, as a pinned-pinned beam, or as a fixed-fixed beam. For small vibrations, longitudinal and transverse vibrations are uncoupled [6]. In this research, longitudinal vibration was neglected, and it was shown that the three models mentioned for the cable have the same forced response owing to small assumed bending stiffness. Stability of a cable with varying length was investigated by Zhu and Ni [25] considering both beam and string equation for cable transverse vibration. Later, using an active control approach, they dissipated the transverse vibratory energy of a cable modeled again as both string and beam. In addition, optimal gains leading to fastest rates of decay of vibratory energy of a cable-actuated system were identified [26].

Zhang and Agrawal [12] designed a Lyapunov controller to damp transverse vibration of a cable transporter system. Two boundary controllers and one domain point-wise controller were proposed in order to dissipate transverse vibration. This controller simultaneously assured that the transporter object would reach its desired position and the closed-loop system would be stable. The length and the natural frequencies of cables in many cable-actuated systems change with time. In [12], the authors claimed that axially moving cables with arbitrary varying length and arbitrary axial velocity had not been properly studied before their research work.

Neglecting longitudinal vibration, a control method was presented by Zhu and Chen [7] for dissipating vibratory energy of an elevator cable. The optimal damping coefficient was calculated for applied nonlinear active damping in order to dissipate the increasing vibratory energy of the cable during upward movement. Otsuki, et al. [13] used non-stationary robust control that considers the effects of time varying characteristics as well as structured and unstructured uncertainties to damp the transverse vibrations of a cable. They also considered the application of non-stationary sliding mode control for suppression of transverse vibration of a cable-actuated system [14]. Here, there was a gap between the cable and the actuator which was located in the vicinity of one of the two ends of the cable. The actuator could apply a transverse force to the cable based on a non-stationary sliding mode control strategy. Both the non-stationary robust control strategy and the non-stationary sliding mode control strategy were shown to be able to robustly control the cable against tension fluctuations along the cable.

1.1.2.2 Damping longitudinal vibration

Pota et al. [9] focused on the damping of longitudinal vibration of cables, and they illustrated the modeling and robust control of a linear cable transporter system that tolerated the non-parametric uncertainties of the system. For bidirectional motion, two actuators were used at either end of the cable, one held the transporter object at its desired position and the other damped the residual longitudinal vibration. In further research by Zhang et al [11], the transporter object goal point was reached by applying a Lyapunov controller to the PDEs governing longitudinal vibration of a cable. The controller also dissipated vibratory energy due to longitudinal vibration and guaranteed the stability of the closed-loop system.

1.1.2.3 Multimodal control

One interesting control approach for active control of slightly sagged cables is using an actuator motion in the cable axial direction. Fujino and Susumpow [27] proposed two control schemes: active stiffness control and active sag-induced force control, for a slightly sagged cable using axial support movement. In this paper, multimodal response of a cable is controlled using a Lyapunov method that considers the stability of the system. They also showed that their control strategy leads to the reduction of cable vibratory energy [28]. A similar control approach was used by imposing a longitudinal action at one of the cable end supports, and a multimodal active control was designed to damp cable vibration by means of a longitudinal actuator at one movable support.

1.1.2.4 Passivity-based control

In the literature, there are many applications of passivity-based control for mechanical systems, such as flexible robotic manipulators, that are similar to cable-actuated systems in terms of structure and behavior. In the present work, we aim to design a stabilizing controller for cable-actuated systems using the Passivity Theorem that is well defined in [29] and [30]. Although passivity-based control has been widely used in many engineering applications, its use in cable-actuated systems has been limited to cranes as a particular application. Alli and Singh [31] designed an optimal passivity-based controller for an overhead crane.

In systems with flexible structures, the output (usually the payload motion) is not collocated with the actuators. This leads to nonminimum phase behavior and hence nonpassive input-output mapping. Wang and Vidyasagar [32] proposed an appropriate passive input-output transfer function for controlling a single flexible link by introducing a modified output. This idea is interesting, and will be investigated further and applied to a cable-actuated system in Chapters 5 and 6.

In the context of passive dynamic controller design, Juang et al. [33] proposed a controller consisting of passive second order systems with little knowledge of the system parameters. They claimed that in designing the controller, it is not necessary to use direct velocity feedback to have a stable controlled system, unlike the early framework for designing the passivity-based controllers. Moreover, this early framework required the system to be square and have collocated actuators and sensors. Lee, Flashner and Safonov [34] proposed a dynamic embedding that releases these two conditions in case the system itself is stable and does not have redundant actuators and sensors. Regarding the control of a linear time invariant (LTI) system, Collado, Lozano and Johansson [35] introduced an observer to render a LTI system strictly positive real (SPR). An interesting aspect of their passification technique is that the original system does not need to be square or even stable.

Using the idea by Wang and Vidyasagar [32], Damaren developed a new output involving the payload motion and the joint motions for multi-link manipulators that yields the passivity property in [36] and [37]. In his work, the payload is assumed to be much heavier than the links. He extended this passivity-based approach to the situation where two flexible multi-link arms manipulate a massive payload [38]. Later in [39], Damaren presented an adaptive controller which can track a prescribed payload trajectory with simultaneous vibration suppression for multi-link manipulators. In a recent work, Christoforou and Damaren [40] applied passivity–based techniques on control of structurally flexible gantry robots.

1.2 Thesis motivation, objective and outline

1.2.1 Example system

In this thesis, a particular horizontal cable-actuated system is used as a case study as shown in Figure 1.3. The system includes two cables extending from two winches and both attached to a payload mass which is supported from below. The two winches pull the cables to position the payload and reduce the vibrations in the cables. This will be accomplished by developing a controller that changes the cable lengths and regulates their tensions. The controller works in response to changes in the position of the payload. This example system exhibits all the key complexities of cable-actuated systems, while still being relatively simple. It is expected that controllers developed for this system could later be extended to more complex cable-actuated systems.

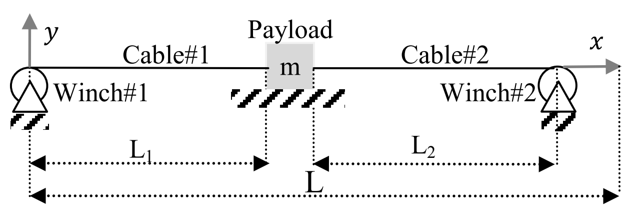

Figure 1.3: Schematic of example cable-actuated system

1.2.2 Motivation and objective

This thesis is in the field of dynamics and control of cable-actuated systems. In many cable-actuated systems, the purpose is to precisely position and orient a payload mass connected to several stretchable cables with varying lengths. The dynamics of a flexible cable is modeled continuously through nonlinear PDEs in terms of time and displacement. Different numerical approaches such as the finite element method and the finite difference method are used to model the nonlinear dynamics of a cable. The lumped mass method is a modular method that can model the behavior of a large variety of cables. Moreover, compared to other numerical techniques, this method requires fewer variables to define the state of each element [19]. Consequently, in the present work, the cables dynamics models are developed using the lumped mass method.

Any cable in a cable-actuated system is prone to longitudinal and transverse vibrations. Our objective is to design a stabilizing controller that brings the payload mass to a desired position, and at the same time suppresses the coupled vibrations of the cables. We have chosen to use the concept of the Passivity Theorem in the design of such controllers for cable-actuated systems because of the stability results that can be reached using this framework. Having seen applications of passivity-based control for flexible robotic manipulators that are similar to cable-actuated systems motivates us to use this control approach. The Passivity Theorem is conceptually connected with power dissipation, and is a popular input-output stability technique. It states that the negative feedback connection of a passive system and a strictly passive system is stable. Passive systems are common in engineering, such as mechanical systems composed of masses, springs, and dashpots. Regarding the control objective of this thesis, applying passivity-based control to cable-actuated systems can lead to new stability results if a passive input-output map can be found for the system. Passivity-based control design will guarantee the closed-loop stability of the cable-actuated system regardless of parameter violations and unmodeled dynamics.

In studies dealing with the vibration control of cable-actuated systems, the transverse vibration of a cable is usually reduced by means of a transverse actuator. However, in many applications, it is not convenient to implement such a control device. Therefore, another objective of this thesis is to achieve the control design goals (accurately positioning the payload mass, while suppressing the coupled vibrations in the cables) by regulating the tensions in the cables only through the action of the winches.

1.2.3 Outline

The research conducted is presented in seven chapters. In Chapter 2, the required mathematical background, the solution to the LQG optimal controller, the definition of various passive systems and the Passivity Theorem are reviewed.

The dynamics model is discussed in Chapter 3 in addition to static analysis of the lumped mass cable model. In this Chapter, the dynamic equations of motion of the example system introduced in section 1.2.1 are developed. The foundations of cable lumped mass model including element tension and internal damping are introduced and the dynamics model is validated. A linearized dynamics model obtained using numerical techniques is also presented.

The second topic of this thesis related to system control begins in Chapter 4 where we discuss two different methods of cable control. First, control objectives as well as application of control inputs are discussed. Then, a basic PID controller and optimal LQG controller are applied to the example system and their effectiveness in payload trajectory tracking and reducing cable vibrations are compared.

In Chapter 5, the idea of using passivity-based control and the required system modifications are studied using the premise that any LTI system can be modified and transferred into a SPR system. Applying this modification to an unstable system is then studied in Chapter 5. The open-loop system is made SPR by introducing an observer state-feedback. A state-feedback regulator including an integral action is required to track the desired payload trajectory. Later in Chapter 5, the positive realness of the modified system is verified and the performance of the designed passivity-based control in steady-state tracking and suppression of vibrations is evaluated.

In Chapter 6, another version of the linear system model is developed using relative coordinates and including the winch dynamics. A μ-tip output that depends on payload position and winch motions is developed that yields the passivity property with respect to a suitable combination of the winch torques. Theories related to μ-tip rate used to define a passive input-output map are reviewed. Furthermore, the effectiveness of the passivity-based controller designed using feedforward and feedback elements in tracking and vibration suppression is investigated.

Finally, a summary of the main contributions of this thesis and recommendations for future research are provided in Chapter 7.

2 Background Material

In this chapter, first, the basic notation of input-output L_2 stability is briefly described (section 2.1). Then, section 2.2 deals with linear quadratic Gaussian (LQG) control problem and its solution. Section 2.3 reviews the definitions and theorem related to passive systems. The basic version of the Passivity Theorem in the study of L_2-stability is also defined in this section.

2.1 Normed linear space

The norm of a vector on a linear space is the length of the vector. For example, the norm of $\boldsymbol{x}$ on the linear space is $\|\boldsymbol{x}\| = \sqrt{\sum_{i=1}^{n} x_i^2}$, and the norm of $\boldsymbol{x}$ associated with an inner product space is given by $\|\boldsymbol{x}\| = \sqrt{\langle \boldsymbol{x}, \boldsymbol{x} \rangle}$ [41].

2.1.1 L_2 space and extended L_2 space

Considering $S = \{\boldsymbol{u}: R^+ \rightarrow R^m\}$ as the set of measurable functions, the L_2 space is composed of functions whose second norm is finite, or otherwise stated, the L_2 space represents the class of finite energy functions [42].

$$L_2 := \left\{ \boldsymbol{u}: \mathbb{R}^+ \rightarrow \mathbb{R}^m : \int_0^\infty \boldsymbol{u}^T(t)\boldsymbol{u}(t)dt < \infty \right\} \tag{2.1}$$

The inner product in L_2 space is defined by [42]

$$\langle \boldsymbol{u}, \boldsymbol{v} \rangle := \int_0^{\infty} \boldsymbol{u}^T(t)\boldsymbol{v}(t)dt \ , \qquad \|\boldsymbol{u}\|_2 := \sqrt{\langle \boldsymbol{u}, \boldsymbol{u} \rangle} \tag{2.2}$$

The function truncation $\boldsymbol{u}_T: R^+ \to R^m$ is [29]

$$\boldsymbol{u}_T(t) := \begin{cases} \boldsymbol{u}(t), & 0 \le t \le T \\ \boldsymbol{0}, & t > T \end{cases} \quad T \in \mathbb{R}^+ \tag{2.3}$$

The extended L_2 space named L_{2e} is [29]

$$L_{2e} := \{\boldsymbol{u}: R^+ \to R^m: \boldsymbol{u}_T(t) \in L_2, \forall T \in \mathbb{R}^+\} \tag{2.4}$$

For a measurable function $\boldsymbol{u}(j\omega)$ with the conjugate transpose $\boldsymbol{u}^H(j\omega) = \boldsymbol{u}^T(-j\omega)$, the norm in frequency domain is defined using the Parseval's Theorem [41].

$$\|\boldsymbol{u}\|_2 = \left(\frac{1}{2\pi} \int_{-\infty}^{+\infty} \boldsymbol{u}^H(j\omega)\boldsymbol{u}(j\omega)d\omega \right)^{1/2} \tag{2.5}$$

2.1.2 L_∞ space

L_∞ is the space of measurable functions that are bounded [42]

$$L_\infty := \{\boldsymbol{u}: \mathbb{R}^+ \to \mathbb{R}^m: \|\boldsymbol{u}\|_\infty < \infty\} \ , \qquad \|\boldsymbol{u}\|_\infty = sup_{t\in\mathbb{R}^+}\left[max_{i=1\dots m}[u_i(t)]\right] \tag{2.6}$$

2.1.3 L_2 stability

The induced L_2 gain of a linear system is the maximum gain of the system. Considering $\boldsymbol{\mathcal{G}}$ as the LTI system mapping $\boldsymbol{u} \to \boldsymbol{y}$, the induced gain or the system gain is defined as [41]:

$$\|\mathcal{G}\|_\infty = sup_{0\neq \boldsymbol{u}\in L_2}\frac{\|\boldsymbol{y}\|_2}{\|\boldsymbol{u}\|_2} = sup_{0\neq \boldsymbol{u}\in L_2}\frac{\|\mathcal{G}\boldsymbol{u}\|_2}{\|\boldsymbol{u}\|_2} = sup_{\omega\in R}\sqrt{\lambda_{max}(\boldsymbol{G}^H(j\omega)\boldsymbol{G}(j\omega))}$$
$$= sup_{\omega\in R}\sigma_{max}(\boldsymbol{G}(j\omega)) \quad \textbf{(2.7)}$$

If $\boldsymbol{u}\in L_2$ then for a system with finite gain $\|\mathcal{G}\|_\infty < \infty$, $\|\mathcal{G}\boldsymbol{u}\|_2 \leq \|\mathcal{G}\|_\infty\|\boldsymbol{u}\|_2$ and the system is said to be L_2-stable. L_2-stability in terms of input and output energy implies that finite energy inputs lead to finite energy outputs [43].

2.2 Linear quadratic Gaussian (LQG) control

In this section we will discuss the LQG problem and its solution assuming that the system dynamics is linear and known, and the measurement noise $\boldsymbol{w_n}$ and the process noise $\boldsymbol{w_d}$ are white noise with constant power spectral density matrices $\boldsymbol{N}$ and $\boldsymbol{V}$.

$$\dot{\boldsymbol{x}} = \boldsymbol{A}\boldsymbol{x} + \boldsymbol{B}\boldsymbol{u} + \boldsymbol{w_d}$$
$$\boldsymbol{y} = \boldsymbol{C}\boldsymbol{x} + \boldsymbol{D}\boldsymbol{u} + \boldsymbol{w_n} \quad \textbf{(2.8)}$$

The LQG problem is to find the optimal control $\boldsymbol{u}(t)$ which minimizes [44]

$$J = E\left\{lim_{T\to\infty}\frac{1}{T}\int_0^T[\boldsymbol{x}^T\boldsymbol{Q}\boldsymbol{x} + \boldsymbol{u}^T\boldsymbol{R}\boldsymbol{u}]dt\right\} \quad \textbf{(2.9)}$$

where E is the expectation operator and $\boldsymbol{Q} = \boldsymbol{Q}^T \geq \boldsymbol{0}$ and $\boldsymbol{R} = \boldsymbol{R}^T > \boldsymbol{0}$ are design parameters. The solution to the LQG problem consists of first determining the optimal state-feedback gain $\boldsymbol{K_r}$ such that $\boldsymbol{u} = -\boldsymbol{K_r}\boldsymbol{x}$. This is the solution to the linear quadratic regulator (LQR) problem. The next step is to find an optimal estimate of the state named $\hat{\boldsymbol{x}}$ by a Kalman filter, so that $E\{[\boldsymbol{x}-\hat{\boldsymbol{x}}]^T[\boldsymbol{x}-\hat{\boldsymbol{x}}]\}$ is minimized. The solution of LQG problem is then defined by $\boldsymbol{u} = -\boldsymbol{K_r}\hat{\boldsymbol{x}}$.

Given the system $\dot{\boldsymbol{x}} = \boldsymbol{A}\boldsymbol{x} + \boldsymbol{B}\boldsymbol{u}$ with an initial state $\boldsymbol{x}(0)$, the LQR finds the input signal $\boldsymbol{u}(t)$ which takes the system to zero states in an optimal manner by minimizing $J_R = \int_0^\infty[\boldsymbol{x}^T\boldsymbol{Q}\boldsymbol{x} + \boldsymbol{u}^T\boldsymbol{R}\boldsymbol{u}]dt$. The optimal solution is $\boldsymbol{u}(t) = -\boldsymbol{K_r}\boldsymbol{x}$, where $\boldsymbol{K_r} = \boldsymbol{R}^{-1}\boldsymbol{B}^T\boldsymbol{X}$ and $\boldsymbol{X}$ is the unique positive semi-definite solution of the algebraic Riccati equation $\boldsymbol{A}^T\boldsymbol{X} + \boldsymbol{X}\boldsymbol{A} -$

$\boldsymbol{XBR^{-1}B^TX + Q = 0}$. The Kalman filter is a state estimator where $\dot{\hat{\boldsymbol{x}}} = \boldsymbol{A\hat{x} + Bu + K(y - C\hat{x})}$. The optimal $\boldsymbol{K} = [\boldsymbol{K}_x \quad \boldsymbol{K}_i]$ which minimizes $E\{[\boldsymbol{x} - \hat{\boldsymbol{x}}]^T[\boldsymbol{x} - \hat{\boldsymbol{x}}]\}$ is $\boldsymbol{K = YC^TV^{-1}}$, where $\boldsymbol{Y}$ is the positive semi-definite solution of the algebraic Riccati equation $\boldsymbol{YA^T + AY - YC^TV^{-1}CY + N = 0}$ [44].

A LQG controller is combined with integral action as shown in Figure 2.1 to ensure that the output $\boldsymbol{y}$ tracks the reference command $\boldsymbol{r}$ and reject measurement noise and process noise.

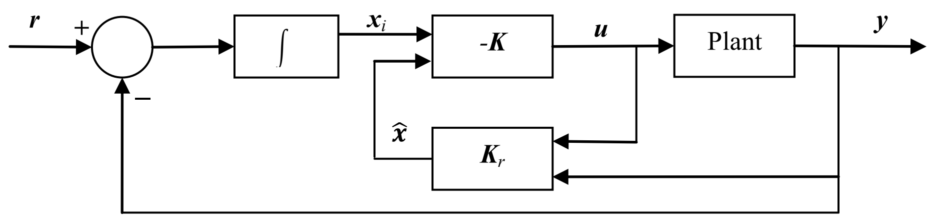

Figure 2.1: LQG controller with integral action and reference input

Combining optimal state estimation, optimal state-feedback and integral action, the LQG controller state-space equations are

$$\begin{bmatrix} \dot{\hat{\boldsymbol{x}}} \\ \dot{\boldsymbol{x}}_i \end{bmatrix} = \begin{bmatrix} \boldsymbol{A - BK_x - K_rC + K_rDK_x} & \boldsymbol{-BK_i + K_rDK_i} \\ \boldsymbol{0} & \boldsymbol{0} \end{bmatrix} \begin{bmatrix} \hat{\boldsymbol{x}} \\ \boldsymbol{x}_i \end{bmatrix} + \begin{bmatrix} \boldsymbol{0} & \boldsymbol{K}_r \\ \boldsymbol{I} & -\boldsymbol{I} \end{bmatrix} \begin{bmatrix} \boldsymbol{r} \\ \boldsymbol{y} \end{bmatrix}$$
$$\boldsymbol{u} = [-\boldsymbol{K}_x \quad -\boldsymbol{K}_i] \begin{bmatrix} \hat{\boldsymbol{x}} \\ \boldsymbol{x}_i \end{bmatrix} \tag{2.10}$$

2.3 Passive systems

Another stability theorem based on the input-output point of view is the Passivity Theorem which states that the negative feedback connection of one passive and one very strictly passive system is L_2-stable. The notation of passivity is associated with energy dissipation. A system represented by the operator $\boldsymbol{\mathcal{G}}$ such that $\boldsymbol{y} = \boldsymbol{\mathcal{G}y}$ where $\boldsymbol{u} \in L_{2e}$ and $\boldsymbol{y} \in L_{2e}$ is considered.

Definition 1. A square system $\boldsymbol{y} = \boldsymbol{\mathcal{G}y}$, $\boldsymbol{\mathcal{G}} : L_{2e} \to L_{2e}$, $\boldsymbol{u} \in L_{2e}$, $\boldsymbol{y} \in L_{2e}$ is very strictly passive (VSP) if there exist real constants $\delta > 0$, $\varepsilon > 0$ and β (that is zero assuming zero initial conditions) such that [42]

$$\int_0^T \boldsymbol{y}^T(t)\boldsymbol{u}(t)dt \geq \delta\|\boldsymbol{u}\|_{2T}^2 + \varepsilon\|\boldsymbol{y}\|_{2T}^2 + \beta, \qquad \forall \boldsymbol{u} \in L_{2e}, \forall T \in R^+ \tag{2.11}$$

A VSP is often referred to as input-output strictly passive system, or an input strictly passive system with finite gain. The system $\boldsymbol{y} = \boldsymbol{\mathcal{G}}\boldsymbol{y},\ \boldsymbol{\mathcal{G}}:\ L_{2e} \rightarrow L_{2e},\ \boldsymbol{u} \in L_{2e}\ ,\ \boldsymbol{y} \in L_{2e}$ is

- input strictly passive (ISP) when Eq. (2.11 holds with $\delta > 0\ , \varepsilon = 0$
- output strictly passive (OSP) when Eq. (2.11) holds with $\delta = 0\ , \varepsilon > 0$
- passive when Eq. (2.11) holds with $\delta = 0\ , \varepsilon = 0$

2.3.1 Passive linear time-invariant (LTI) systems

A LTI system $\boldsymbol{\mathcal{G}}$ with minimal state space representation *(**A**,**B**,**C**,**D**)* or with transfer matrix $\boldsymbol{G}(s)$ is considered. Using the Parseval's Theorem, [30] and [43]

$$\begin{aligned}
\int_0^T \boldsymbol{y}^T(t)\boldsymbol{u}(t)dt &= \int_0^\infty \boldsymbol{y}_T^T(t)\boldsymbol{u}_T(t)dt = \frac{1}{2\pi}Re\int_{-\infty}^{\infty} \boldsymbol{y}_T^H(j\omega)\boldsymbol{u}_T(j\omega)d\omega \\
&= \frac{1}{2\pi}Re\int_{-\infty}^{\infty}\left[\frac{1}{2}\boldsymbol{y}_T^H(j\omega)\boldsymbol{u}_T(j\omega) + \frac{1}{2}\boldsymbol{u}_T^H(j\omega)\boldsymbol{y}_T(j\omega)\right]d\omega \\
&= \frac{1}{4\pi}Re\int_{-\infty}^{\infty}[\boldsymbol{u}_T^H(j\omega)\boldsymbol{G}^H(j\omega)\boldsymbol{u}_T(j\omega) + \boldsymbol{u}_T^H(j\omega)\boldsymbol{G}(j\omega)\boldsymbol{u}_T(j\omega)]d\omega \\
&= \frac{1}{4\pi}Re\int_{-\infty}^{\infty}\boldsymbol{u}_T^H(j\omega)[\boldsymbol{G}^H(j\omega) + \boldsymbol{G}(j\omega)]\boldsymbol{u}_T(j\omega)d\omega
\end{aligned} \tag{2.12}$$

An LTI system $\boldsymbol{\mathcal{G}}$ is passive if $\boldsymbol{G}^H(j\omega) + \boldsymbol{G}(j\omega) \geq 0,\ \forall\omega \in R$; while it is ISP if $\boldsymbol{G}^H(j\omega) + \boldsymbol{G}(j\omega) \geq 2\delta\boldsymbol{I},\ \forall\omega \in R\ ,\ \delta > 0.$

2.3.2 Positive real and strictly positive real systems

Definition 2. A rational transfer matrix $\boldsymbol{G}(s)$ is positive real (PR) if all elements of $\boldsymbol{G}(s)$ are analytic in $R(s) \geq 0$, and $\boldsymbol{G}^H(s) + \boldsymbol{G}(s) \geq 0$ in $R(s) \geq 0$. Equivalent to the later condition is that the poles on the imaginary axis are simple and have nonnegative-definite residues, and $\boldsymbol{G}^H(j\omega) + \boldsymbol{G}(j\omega) \geq 0,\ \forall\omega \in R$ with $j\omega$ not a pole of any element of $\boldsymbol{G}(j\omega)$ [30].

An LTI system with a PR transfer matrix is passive. Moreover, a PR system is minimum phase (all zeros will be in the closed left half plane) and at least marginally stable. A transfer function g(s) is PR if its phase response satisfies $-\frac{\pi}{2} \leq \arg g(j\omega) \leq \frac{\pi}{2}$.

Definition 3. A stable rational transfer matrix $\boldsymbol{G}(s)$ is strictly positive real (SPR) if $\boldsymbol{G}(s-\delta)$ is PR for some $\delta > 0$; that is, 1st all elements of $\boldsymbol{G}(s)$ are analytic in $R(s) \geq 0$, 2nd $\boldsymbol{G}^H(j\omega) + \boldsymbol{G}(j\omega) \geq 0$, $\forall\omega \in \mathbb{R}$, and 3rd $\boldsymbol{Z} = \boldsymbol{G}^T(\infty) + \boldsymbol{G}(\infty) \geq 0$, or if $\boldsymbol{Z}$ is singular $lim_{\omega\to\infty}[\boldsymbol{G}^H(j\omega) + \boldsymbol{G}(j\omega)] > 0$ [30].

An LTI system's transfer functions $g(s)$ is SPR if it is Hurwitz, has a phase response that satisfies $-\frac{\pi}{2} < \arg g(j\omega) < \frac{\pi}{2}$, and either has a strictly positive feed through matrix (the transfer function is biproper), or $lim_{\omega\to\infty}\omega^2 Re\{g(j\omega)\} > 0$ if there is no feed through matrix (the transfer function is strictly proper).

Lemma 1. A LTI system described by

$$\begin{aligned} \dot{\boldsymbol{x}} &= \boldsymbol{A}\boldsymbol{x} + \boldsymbol{B}\boldsymbol{u}\,, \qquad \boldsymbol{x} \in \mathbb{R}^n\,, \boldsymbol{u} \in \mathbb{R}^m \\ \boldsymbol{y} &= \boldsymbol{C}\boldsymbol{x} + \boldsymbol{D}\boldsymbol{u}\,, \qquad \boldsymbol{y} \in \mathbb{R}^m \end{aligned} \tag{2.13}$$

that is controllable and observable is positive real (PR) if and only if there exist real matrices $\boldsymbol{P}=\boldsymbol{P}^T > \boldsymbol{0}$, $\boldsymbol{L}$, and $\boldsymbol{W}$ of appropriate dimension such that $\boldsymbol{PA} + \boldsymbol{A}^T\boldsymbol{P} = -\boldsymbol{L}^T\boldsymbol{L}$, $\boldsymbol{PB} = \boldsymbol{C}^T - \boldsymbol{L}^T\boldsymbol{W}$ and $\boldsymbol{D} + \boldsymbol{D}^T = \boldsymbol{W}^T\boldsymbol{W}$ [30].

Lemma 2. A LTI system described by Eq. (2.13) that is controllable and observable is strictly positive real (SPR) if and only if there exist real matrices $\boldsymbol{P}=\boldsymbol{P}^T > \boldsymbol{0}$, $\boldsymbol{L}$, and $\boldsymbol{W}$ of appropriate dimension, and $\upsilon > 0$ such that $\boldsymbol{PA} + \boldsymbol{A}^T\boldsymbol{P} = -\boldsymbol{L}^T\boldsymbol{L} - 2\upsilon\boldsymbol{P}$, $\boldsymbol{PB} = \boldsymbol{C}^T - \boldsymbol{L}^T\boldsymbol{W}$ and $\boldsymbol{D} + \boldsymbol{D}^T = \boldsymbol{W}^T\boldsymbol{W}$ [30].

If a system with a minimal state-space realization satisfies Lemma 1 then it is passive; while it is SPR if it satisfies lemma 2. If the system is strictly proper ($\boldsymbol{D} = \boldsymbol{0}$), the SPR Lemma reduces to that $\boldsymbol{PA} + \boldsymbol{A}^T\boldsymbol{P} = -\boldsymbol{L}^T\boldsymbol{L} - 2\upsilon\boldsymbol{P}$, $\boldsymbol{PB} = \boldsymbol{C}^T$ [43]. Lemma 2 is called the Kalman-Yakubovich-Popov Lemma (the KYP Lemma).

2.3.3 Passivity Theorem

Consider the negative feedback interconnection of the systems $\boldsymbol{\mathcal{G}} : L_{2e} \rightarrow L_{2e}$ and $\boldsymbol{\mathcal{H}} : L_{2e} \rightarrow L_{2e}$ in Figure 2.2. If $\boldsymbol{G}$ is passive and $\boldsymbol{H}$ is very strictly passive with finite gain then $\boldsymbol{u}_1, \boldsymbol{u}_2 \in L_2$ implies $\boldsymbol{y}_1, \boldsymbol{y}_2 \in L_2$ [45].

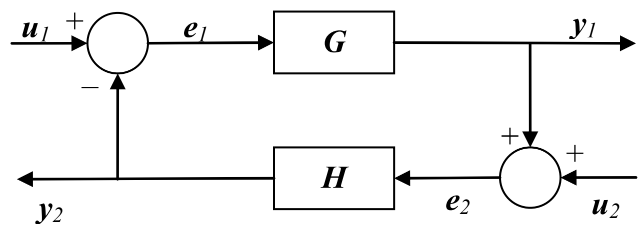

Figure 2.2: Negative feedback interconnection of two systems

2.4 Positive definite matrices

A symmetric matrix $\boldsymbol{P}$ is positive definite if $\forall\, \boldsymbol{V},\ \boldsymbol{V}^T\boldsymbol{P}\boldsymbol{V} > \boldsymbol{0}$.

A symmetric matrix is positive definite if all the diagonal entries are positive, and each diagonal entry is greater than the sum of the absolute values of all other entries in the corresponding row or column [46].

An arbitrary symmetric matrix is positive definite if and only if each of its principal sub-matrices has a positive determinant. This is known as Sylvester's criterion [46].

Theorem 1. Given two Hermitian matrices of the same dimensions $\boldsymbol{H}_1 > \boldsymbol{0}$ and $\boldsymbol{H}_2$, then there exist a non-singular matrix $\boldsymbol{M}$ such that $\boldsymbol{M}^H\boldsymbol{H}_1\boldsymbol{M} = \boldsymbol{I}$ and $\boldsymbol{M}^H\boldsymbol{H}_2\boldsymbol{M} = diag(\rho_1, \rho_2, \dots, \rho_n)$, where $\rho_i, i = 1 \dots n$ are eigenvalues of $\boldsymbol{H}_1^{-1}\boldsymbol{H}_2$.

2.4.1 Schur compliment condition

Let $\boldsymbol{P}$ be a symmetric matrix given by

$$\boldsymbol{P} = \begin{bmatrix} \boldsymbol{a} & \boldsymbol{b} \\ \boldsymbol{b}^T & \boldsymbol{c} \end{bmatrix}$$

$\boldsymbol{S} = \boldsymbol{c} - \boldsymbol{b}^T\boldsymbol{a}^{-1}\boldsymbol{b}$ is called the Schur compliment of $\boldsymbol{a}$ in $\boldsymbol{P}$. Then, $\boldsymbol{P}$ is positive definite if and only if $\boldsymbol{a}$ and $\boldsymbol{S}$ are both positive definite [47].

3 Dynamics Model

The dynamics of a continuous flexible cable is modeled through nonlinear PDEs in terms of time and displacement. In this approach, a cable can be modeled using either beam or string equations. However, our simulations show that using a beam equation will not lead to accurate results because the natural frequencies of longitudinal vibration of the cable do not change as long as the boundary conditions remain unchanged (e.g. changes in tension do not lead to changes of natural frequencies). Existing work on cables modeled using string equations, on the other hand, does not consider coupled vibrations of stretchable and varying length cables. The derivation of the continuous equation of motion of a planar cable *ab initio* and the model validation has been time consuming and the corresponding PDEs are not readily solvable. To simplify the modeling, a simpler discrete model of the cables has been selected for the purpose of control. As mentioned in section 1.1.1.2, in this thesis, cables are modeled using the lumped mass method that can properly model the longitudinal and transverse dynamics behavior of cables [20]. In addition, compared to other numerical techniques, the lumped mass method requires fewer variables to define the state of each element [48]. The lumped mass method leads to a series of ODEs that are solvable using standard numerical integration techniques.

3.1 Cable dynamics

The lumped mass method models the cable as a series of lumped masses called nodes that are connected by viscoelastic massless elements composed of springs and dampers, as shown in

Figure 3.1. For developing the mathematical model of the example system, a planar reference frame is considered with its origin at the left boundary as illustrated in Figure 3.1. In the model that will be developed in this chapter, the effect of the winches is defined by changing the unstretched length of the first elements of the cables, denoted as dl_1 and dl_4 [49]. As such the dynamics of the winches are not considered here.

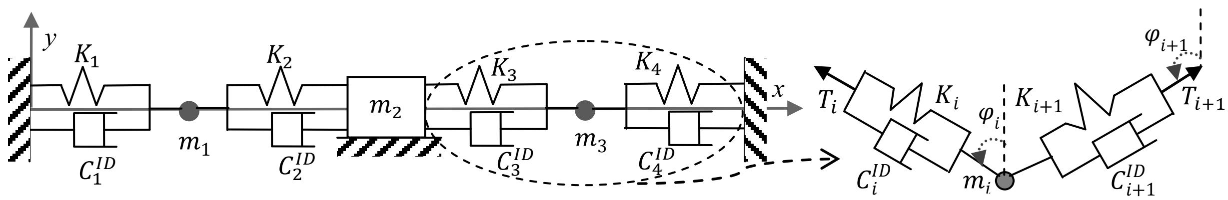

Figure 3.1: The lumped mass model of the cables

The accuracy of the lumped mass approach is controlled by the choice of element size. Increasing the number of elements used to model a cable leads to more precise calculation of the cable tension and smoother curvilinear profile, but increases the solver execution time. The number of elements on each cable is initially set to two allowing an approximate estimation of the first two cable natural frequencies in simulation. Later, the number of nodes on each cable and the number of cables will be set to arbitrary numbers N and N_C that can be changed to find a more accurate and general model of the system.

3.1.1 Element tension and damping

The tension and internal damping forces of the i^{th} cable element are calculated based on their linear relationship with the strain and strain rate of each element. The tension in the i^{th} cable element due to its stiffness, T_i^K, acting in the tangential direction is given by

$$T_i^K = EA\varepsilon_i \tag{3.1}$$

where, A is its cross sectional area and E is Young's modulus. It is ensured that the element strain, $\varepsilon_i = \frac{l_i - l_{u_i}}{l_{u_i}}$, remains positive by applying sufficient pretension to the cable. $l_i =$

$\sqrt{(x_i - x_{i-1})^2 + (y_i - y_{i-1})^2}$ is the stretched length of the i^{th} element and l_{u_i} is its unstretched length. The stiffness of each cable element is also defined as $k_i = \frac{EA}{l_{u_i}}$.

The damping behaviour of cables depends on their internal structure and is difficult to model [50]. In this thesis internal dissipation is simply modeled using a viscous damping term. The internal damping force, T_i^{ID}, generated in the i^{th} cable element is given by

$$T_i^{ID} = C_i^{ID}(V_i - V_{i-1}) \tag{3.2}$$

where, V_i and V_{i-1} are the tangential velocities of the two extreme nodes of the i^{th} cable element and C_i^{ID} is the internal damping coefficient of the element. The magnitude of the damping ratio in a cable, ξ, is typically considered to be between *1%* and *3%* [49], where $\xi = \frac{C^{ID}}{C_{cr}} = \frac{C^{ID}}{2\sqrt{Km}}$, and in this study the cable damping ratio,ξ, is set to *1%.* Although damping forces in cable systems are much smaller than elastic forces (cable tensions), they are included in dynamics model to prevent the instability that the system may experience due to numerical noise.

3.1.2 Model assembly

Given all the forces applied to the lumped masses, Newton's second law for the i^{th} node is expressed as

$$m_i \frac{d^2 x_i}{dt^2} = \left[T_{i+1}^K \sin(\varphi_{i+1}) - T_i^K \sin(\varphi_i)\right] + \left[T_{i+1}^{ID} \sin(\varphi_{i+1}) - T_i^{ID} \sin(\varphi_i)\right] \tag{3.3}$$

$$m_i \frac{d^2 y_i}{dt^2} = \left[-T_{i+1}^K \cos(\varphi_{i+1}) + T_i^K \cos(\varphi_i)\right] + \left[-T_{i+1}^{ID} \cos(\varphi_{i+1}) + T_i^{ID} \cos(\varphi_i)\right] - W_i \tag{3.4}$$

where, W_i is the weight of the i^{th} node, $W_i = 0.5\rho A\left(l_{u_i} + l_{u_{i+1}}\right)g$, and ρ is the density of the cable. For the node at the intersection of the two cables, W_i also includes the weight of the payload mass as shown in Figure 3.1. Here, φ_i is the angle that i^{th} cable element makes with vertical axis drew from i^{th} node, as shown in the free body diagram of Figure 3.1, and g is the acceleration of gravity.

Assembling the dynamics of all cable nodes expressed in Eqs. (3.3) and (3.4), the system dynamics is described by a set of second order ODEs. The original ODEs are then rewritten in state-space form consisting of first order ODEs for displacement and velocity of each node. The system dynamic is then simulated by solving the ODEs using a Runge-Kutta method intended for initial value problems. The initial condition for the dynamics simulation is provided by the static/equilibrium solution that will be derived in the next section.

3.2 Cable statics

Setting the position of all the lumped masses to their static equilibrium ones at the beginning of the simulation ensures that the observed results of the dynamic simulation is only due to external sources. Determining the equilibrium configuration of a stiff cable can be demanding because even a small perturbation in a node position can lead to considerable change in the cable's internal force. In order to find the cable equilibrium configuration, at first, the simulation was run using an arbitrary initial condition for the node positions until the transient oscillations decayed. This was found to be too time consuming.

Another approach named the shooting method [51] was later chosen to find the cable equilibrium configuration given the position of the first cable node ($\boldsymbol{r}_1$, at winch end) and the position of the last node ($\boldsymbol{r}_f$, at payload end). In this process, the initial estimate for L_u is found using [49]

$$\frac{\rho A L_u g}{2T_s} = \sinh\left[\frac{\rho A g}{2}\left(\frac{l_x}{T_s} - \frac{L_u}{EA}\right)\right] \tag{3.5}$$

where, l_x is the horizontal distance between the winch and the payload that is assumed as the initial guess for L_u, Figure 3.2, and T_s is the pretension applied to the cable.

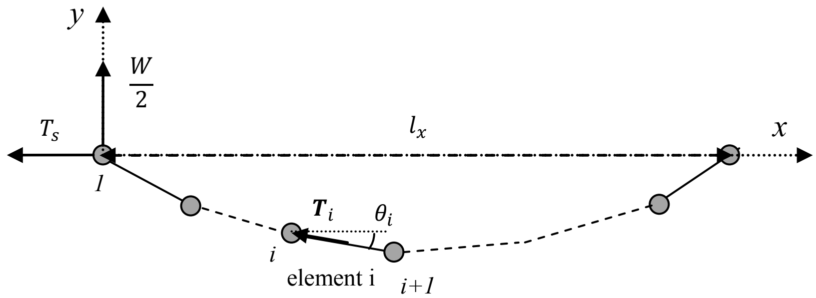

Figure 3.2: The lumped mass cable model equilibrium configuration

Given the applied force at the winch end of the cable (its horizontal component is equal to cable's initial pretension, T_s, and its vertical component is equal to half of the cable's weight, $\frac{W}{2} = \frac{\rho A L_u g}{2}$), Newton's second law is applied to the first cable node leading to the position of the next node, $\boldsymbol{r}_2$. The same procedure is performed for each node in succession. The horizontal force, T_s, remains constant along the cable, while the vertical component at i^{th} element is defined as

$$F_i = \frac{\rho A L_u g}{2} - \left(\frac{m}{2} + \sum_{1}^{i-1} m\right) g \tag{3.6}$$

where $m = \rho A g \frac{L_u}{N-1}$ is the weight of the i^{th} cable element. The element angle of inclination, θ_i, can now be calculated as $\theta_i = tan^{-1}\left(\frac{F_i}{T_s}\right)$, as well as the force in i^{th} cable element, $T_i = \frac{F_i}{sin(\theta_i)}$. The element stretched length is then defined as

$$l_i = \frac{L_u}{N-1}\left(1 + \frac{T_i}{EA}\right) \tag{3.7}$$

The position of $(i+1)^{th}$ element is $\boldsymbol{r}_{i+1} = \boldsymbol{r}_i + l_i(cos\,\theta_i \boldsymbol{i} + sin\,\theta_i \boldsymbol{j})$. This procedure is repeated until the position of the last node, $\boldsymbol{r}_N$ is found. In order find the best approximation for the unstretched cable length, L_u, the error $\boldsymbol{e} = \left\|\boldsymbol{r}_f - \boldsymbol{r}_N\right\|$ is minimized using the *fminsearch* command in MATLAB.

3.3 Cable internal damping coefficient

In order to specify the cable elements damping coefficient, the vertical spring-mass-damper system of Figure 3.3 is modeled in MATLAB. In this model, the nodes only move in vertical direction. The easiest way to show the effect of damping in the system is to introduce a velocity based term into the system equation of motion.

$$m_{eq}\ddot{y} + C_{eq}^{ID}\dot{y} + k_{eq}y = F(t) \tag{3.8}$$

Physically, the effect of the cable internal damping is modeled with a damper to dissipate energy. The equivalent cable damping coefficient is defined as

$$C_{eq}^{ID} = 2\xi m_{eq}\omega_n \tag{3.9}$$

where, $\omega_n = \sqrt{\frac{k_{eq}}{m_{eq}}}$ is the system natural frequency. Using the lumped mass method and considering the whole cable as one element with two end nodes, the cable mass is accumulated on the two extreme nodes, so $m_{eq} = m_{payload} + \frac{1}{2}\rho A L_u$ is the equivalent mass of the bottom node as shown in Figure 3.3, and $k_{eq} = \frac{EA}{L_u}$, where L_u the unstretched length of the cable.

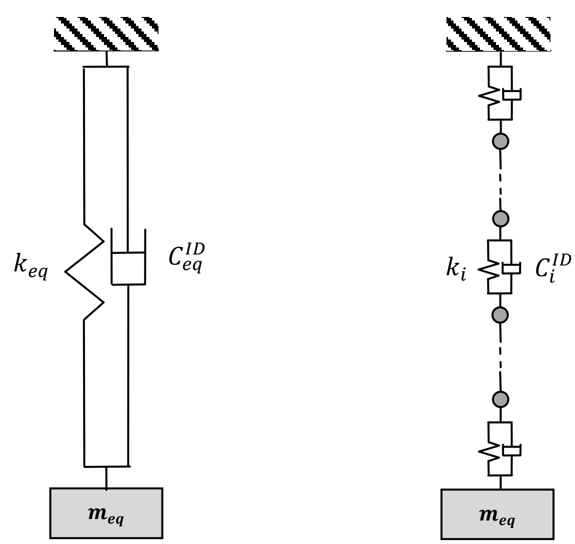

Figure 3.3: a vertical spring-mass-damper system

By discretizing the cable into *N-1* element with length $l_{ui} = \frac{L_u}{N-1}$ as shown in Figure 3.3, the stiffness of each cable element becomes $k_i = \frac{EA}{l_{u_i}} = k_{eq}(N-1)$. In the following analysis, it will be shown that the damping coefficient of each cable element can similarly be approximated as $C_i^{ID} = C_{eq}^{ID}(N-1)$.

The unique solution of Eq. (3.8) can be found for specified initial condition by assuming that the solution is of the form $y(t) = Ae^{\lambda t}$. In this section, the vibration of a spring–mass–damper system subjected to an external force is considered. Introducing the external force as a unit impulse function $F(t) = \delta(t)$ or an impulse applied at *t=0*, the impulse response is equivalent to giving the system at rest an initial velocity of $\frac{1}{m_{eq}}$. The transient response of the vertical spring–mass–damper system to the initial condition where all nodes are at rest and the payload node has the velocity of $\frac{1}{m_{eq}}$ is studied.

In order to determine the damping ratio of an under-damped system from its time domain response, $h_i(t)$, the concept of logarithmic decrement, denoted by γ and defined by $\gamma = ln\frac{h_i(t)}{h_i(t+T_d)}$ is used, where T_d is the period of oscillation in time domain response. The damping ratio in terms of the logarithmic decrement is derived as [52]

$$\xi = \frac{\gamma}{\sqrt{4\pi^2 + \gamma^2}} \tag{3.10}$$

Choosing the damping coefficient of each cable element as $C_i^{ID} = C_{eq}^{ID}(N-1)$, the transient response of both systems shown in Figure 3.3 is similar. For example, the payload position, Figure 3.4, and the cable tension, Figure 3.5, show the same logarithmic decreasing behavior for the system modeled with different number of elements. The cables parameters for this simulation are taken as follows: the Young's modulus $E = 437\,MPa$, the density $\rho = 2180\,kg/m^3$, the diameter of the cross sectional area $d = 6.16\,mm$, the damping ratio $\xi = 0.01$ and the starting lengths $L = 1\,m$. The payload mass is set to $10.19\,kg$ which yields to a pretension of $100\,N$ in the cable.

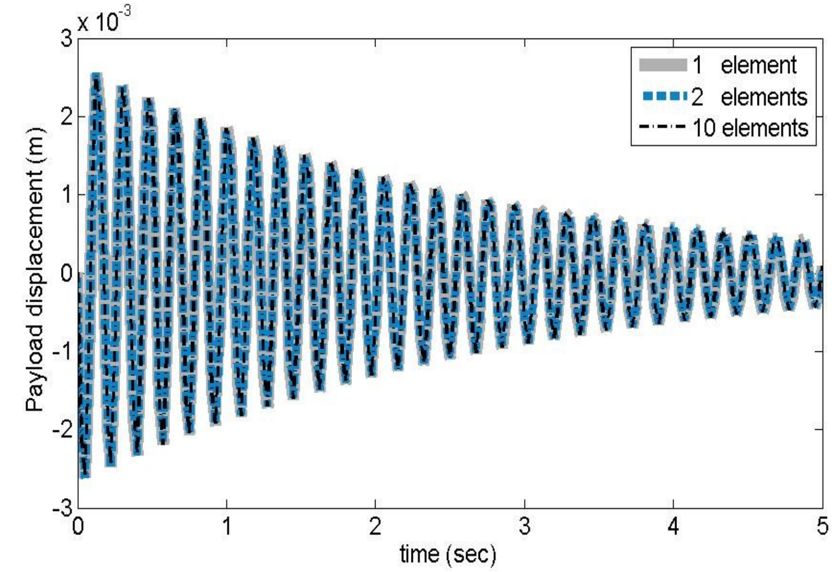

Figure 3.4: Payload position in response to unit impulse

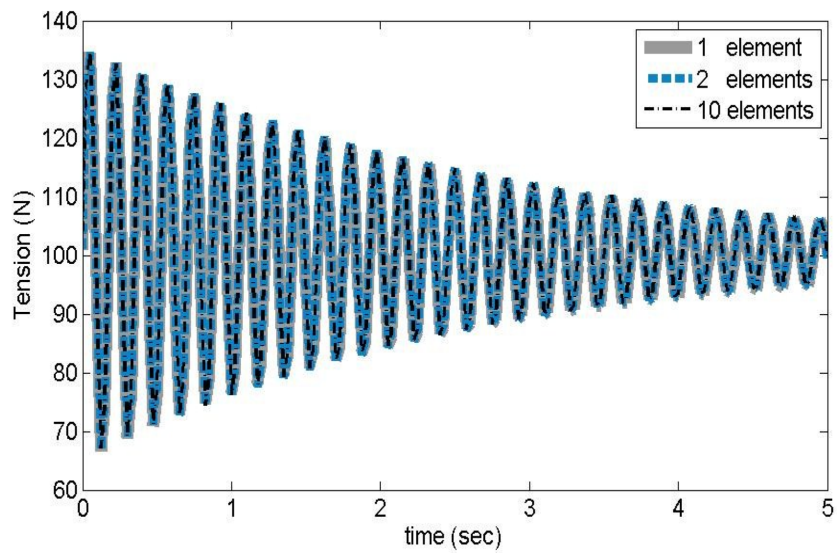

Figure 3.5: Cable tension in response to unit impulse

3.4 Modal analysis and model validation

Damping estimation is usually more accurate in modal coordinates, so the system's second order model is defined in modal coordinates. A cable-actuated system in nodal coordinates is represented by the second order matrix differential equation

$$\boldsymbol{M}\ddot{\boldsymbol{q}} + \boldsymbol{D}\dot{\boldsymbol{q}} + \boldsymbol{K}\boldsymbol{q} = \boldsymbol{B}\boldsymbol{u}$$
$$\boldsymbol{y} = \boldsymbol{C}_q\boldsymbol{q} + \boldsymbol{C}_{\dot{q}}\dot{\boldsymbol{q}} \tag{3.11}$$

where, $\boldsymbol{q}$ is the nodal vector of displacement . For the cable system of Figure 3.3 considering three moving nodes, $\boldsymbol{q} = [y_1 \quad y_2 \quad y_3]^T$. ***M, K*** and ***D*** are the mass, stiffness, and damping matrices.

$$\boldsymbol{M} = \begin{bmatrix} m_1 & 0 & 0 \\ 0 & m_2 & 0 \\ 0 & 0 & m_3 \end{bmatrix} \quad \boldsymbol{K} = \begin{bmatrix} k_1 + k_2 & -k_2 & 0 \\ -k_2 & k_2 + k_3 & -k_3 \\ 0 & -k_3 & k_3 \end{bmatrix} \quad \boldsymbol{D} = \begin{bmatrix} C_1^{ID} + C_2^{ID} & -C_2^{ID} & 0 \\ -C_2^{ID} & C_2^{ID} + C_3^{ID} & -C_3^{ID} \\ 0 & -C_3^{ID} & C_3^{ID} \end{bmatrix}$$

The cable damping ratio, ξ, is set to *1%* to define the damping matrix $\boldsymbol{D}$. In order to get a state-space representation from the nodal model, the state vector $\boldsymbol{X}$ is defined as the combination of the structural displacement, $\boldsymbol{q}$, and velocity, $\dot{\boldsymbol{q}}$, $\boldsymbol{X} = \begin{bmatrix} \boldsymbol{q} \\ \dot{\boldsymbol{q}} \end{bmatrix}$. Eqs. (3.11) can then be written as the following state-space representation. The dimension of the state-space model is twice the number of degrees of freedom of the system

$$\dot{\boldsymbol{X}} = \boldsymbol{A}\boldsymbol{X} + \boldsymbol{B}\boldsymbol{u} \tag{3.12}$$
$$\boldsymbol{y} = \boldsymbol{C}\boldsymbol{X}$$

where $\boldsymbol{A}$, $\boldsymbol{B}$ and $\boldsymbol{C}$ are defined as

$$\boldsymbol{A} = \begin{bmatrix} \boldsymbol{0} & \boldsymbol{I} \\ -\boldsymbol{M}^{-1}\boldsymbol{K} & -\boldsymbol{M}^{-1}\boldsymbol{D} \end{bmatrix} \qquad \boldsymbol{B} = \begin{bmatrix} \boldsymbol{0} \\ \boldsymbol{M}^{-1}\boldsymbol{B} \end{bmatrix} \qquad \boldsymbol{C} = [\boldsymbol{C}_q \quad \boldsymbol{C}_{\dot{q}}]$$

The matrix of natural frequencies, $\boldsymbol{\Omega}$, is defined as well as the matrix of mode shapes, $\boldsymbol{\phi}$ specifying the natural modes of the system. These are the eigen-pairs of the state matrix $\boldsymbol{A}$ such that $\boldsymbol{A}_n = \boldsymbol{\phi}^{-1}\boldsymbol{A}\boldsymbol{\phi}$ and $\boldsymbol{X} = \boldsymbol{\phi}\boldsymbol{Z}$. $\boldsymbol{A}_n$ is a diagonal complex matrix whose diagonal elements are eigen-values of the state matrix and $\boldsymbol{Z}$ is the state vector in modal representation. Assuming a matrix of proportional damping as $\boldsymbol{D} = \alpha\boldsymbol{M} + \beta\boldsymbol{K}$, the i^{th} and $(i+1)^{th}$ nonzero elements of $\boldsymbol{A}_n$ are given by

$$A_n(i,i) = -\xi_i\omega_i + j\omega_i\sqrt{1-\xi_i}$$
$$A_n(i+1,i+1) = -\xi_i\omega_i - j\omega_i\sqrt{1-\xi_i} \tag{3.13}$$

This way (e.g. assuming the damping ratio of the cable to be $\xi = 0.01$), the dimensionless modal damping ratio related to i^{th} mode found from the structural properties of the system.

$$\xi_i = \frac{-Re\big(A_n(i,i)\big)}{|A_n(i,i)|} \tag{3.14}$$

where, $Re\big(A_n(i,i)\big)$ is the real part of $A_n(i,i)$. The eigen-values of the state matrix are the roots of a polynomial equation of degree *2n*, where *n* is the number of degrees of freedom of the system, so it is not straight forward to present a closed-form expression to find the damping ratio of the cable, ξ, from the modal ones defined by $\xi_i\ ,\ i = 1, \dots, n$.

The vertical cable-actuated system of Figure 3.3 is simulated by solving the ODEs using a Runge-Kutta method. The model is validated by comparing the simulated frequencies with the theoretical longitudinal natural frequencies of a bar fixed at one end and attached to a mass, m, at the other end [50].

$$\omega_i^L = \frac{\lambda_i}{L}\sqrt{\frac{E}{\rho}}\ , \qquad cot(\lambda_i) = \lambda_i \frac{m}{\rho A L}\ , \qquad i = 1, \dots, n \tag{3.15}$$

Here, $E = 437\ MPa$, $A = 2.98e-5\ m^2, L = 1\ m$ and $\rho = 2180\ \frac{kg}{m^3}$ are the Young's modulus, cross sectional area, length and density of the cable, and $m = \frac{100}{9.81} kg$ is the payload mass. The first three simulated natural frequencies $\left(\omega_1^L = 35\ \frac{rad}{sec}, \omega_2^L = 1347\ \frac{rad}{sec}, \omega_3^L = 2337\ \frac{rad}{sec}\right)$ are within *2.8 %, 4.1 %* and *16 %* of the theoretical ones $\left(36\ \frac{rad}{sec}, 1405\ \frac{rad}{sec}, 2811\ \frac{rad}{sec}\right)$ respectively as shown in Figure 3.6. In this figure, the power spectrum of the transverse displacement of the vertical cable-actuated system in response to unit impulse is illustrated. The impulse response of the system in terms of the payload displacement was shown in Figure 3.4. It consists of response of three modes of natural frequencies ω_1^L, ω_2^L and ω_3^L. The impulse response spectrum of Figure 3.6 shows peaks at these frequencies.

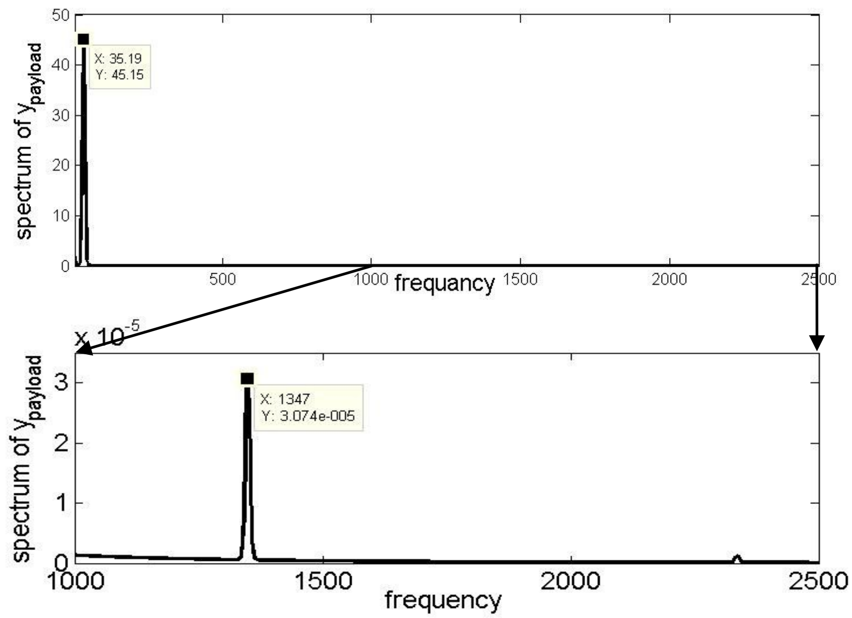

Figure 3.6: Spectrum of payload position of vertical cable-actuated system in response to unit impulse

The time domain impulse response of the closed-loop system can be written as $h(t) = \sum_{i=1}^{n} h_i(t)$, where $h_i(t)$ is the impulse response of the i^{th} mode (e.g. the system impulse response is the sum of modal responses). In Figure 3.7, the impulse response of modes 1, 2 and 3 are illustrated as sinusoids of frequency equal to ω_1, ω_1 and ω_3 respectively. The total response of Figure 3.4 is the sum of these impulse responses. Defining the logarithmic decrement, γ, in this simulation as shown in Figure 3.7, the first three modal damping ratios of the system are calculated using Eq. (3.10) as $\xi_1 = 0.0101, \xi_2 = 0.1203$ and $\xi_3 = 0.2010$, where the highest frequency modal response decays faster (e.g. the exponential decayed amplitude of i^{th} modal response is proportional to the modal damping ξ_i).

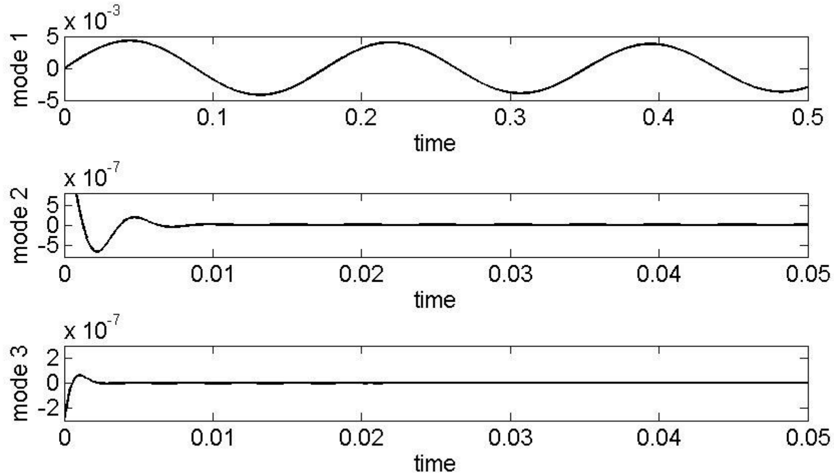

Figure 3.7: Impulse response of the first three modes

3.5 Dynamics model validation of the horizontal example system

The horizontal cable-actuated system of Figure 1.3 is simulated by solving the corresponding ODEs using *ode45* in MATLAB. The impulse response of the system in terms of the transverse vibration of the middle node on the first cable is shown in Figure 3.8.

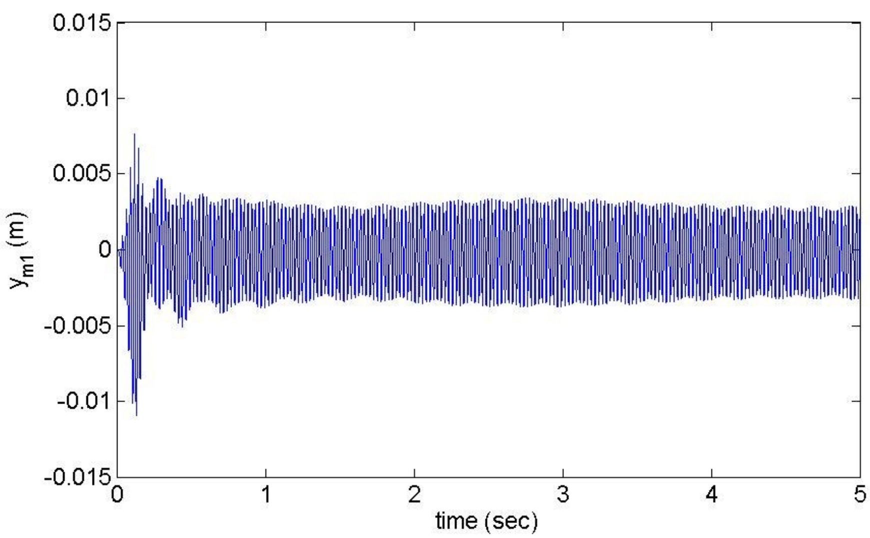

Figure 3.8: Transverse vibration of the middle node on the first cable in response to unite impulse

The model is validated by comparing the simulated frequencies of transverse vibrations of the first cable with the theoretical natural frequencies of a string with two fixed ends [53].

$$\omega_i^T = \frac{i\pi}{L}\sqrt{\frac{T}{\rho A}}, \quad i = 1, \dots, n \tag{3.16}$$

Here, $E = 437\ MPa$, $\rho A = 0.065\ \frac{kg}{m}$ and $L = 0.5\ m$ are the Young's modulus, mass per unit length and length of the cable, and $m = 1\ kg$ is the payload mass. A pretension of $T = 100\ N$ is applied to the cable. The first three simulated natural frequencies associated with the transverse vibration of the middle node on the first cable $\left(\omega_1^T = 226\ \frac{rad}{sec}, \omega_2^T = 452\ \frac{rad}{sec}, \omega_3^T = 684\ \frac{rad}{sec}\right)$ are within *8 %, 8.3 %* and *7.4 %* of the theoretical ones $\left(246\ \frac{rad}{sec}, 493\ \frac{rad}{sec}, 739\ \frac{rad}{sec}\right)$ respectively as shown in Figure 3.9. In this figure, the power spectrum of the transverse displacement of the first cable of the horizontal cable-actuated system in response to unit impulse is illustrated. The impulse response spectrum shows peaks at natural frequencies.

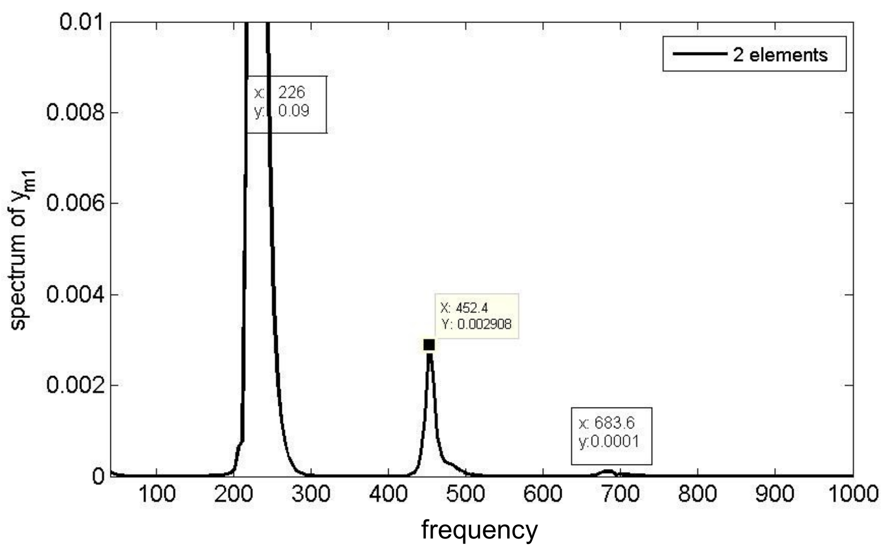

Figure 3.9: Spectrum of transverse oscillation of the cable with *2* elements in response to unit impulse

The accuracy of the lumped mass method improves by the increasing the number of elements. Increasing the number of elements used to model the cable from *2* elements to *10* elements leads to more precise calculation of the cable natural frequencies as shown in Figure 3.10 although increasing the solver execution time. Using *10* elements in modeling the cable, the simulated natural frequencies associated with the transverse vibration of the middle node on the first cable $\left(\omega_1^T = 246.3\ \frac{rad}{sec}, \omega_2^T = 472\ \frac{rad}{sec}, \omega_3^T = 719\ \frac{rad}{sec}\right)$ are within *0.04 %, 4.2 %* and *2.7%* of the theoretical ones $\left(246.4\ \frac{rad}{sec}, 493\ \frac{rad}{sec}, 739\ \frac{rad}{sec}\right)$ respectively.

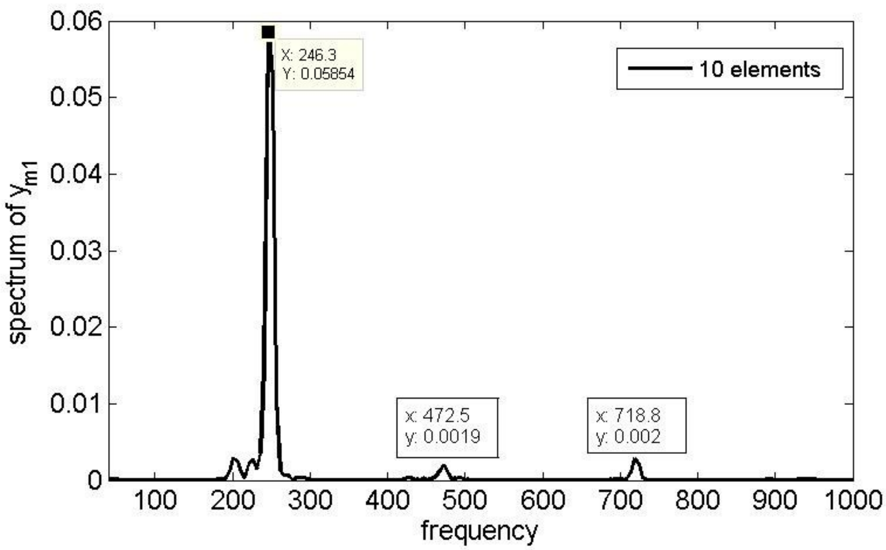

Figure 3.10: Spectrum of transverse oscillation of the cable with *10* elements in response to unit impulse

Ignoring the internal damping of the cables and the slider friction, an energy analysis is also performed to validate the system dynamics. The cables parameters for this simulation are taken as follows: the Young's modulus E=437 MPa, the density $\rho = 2180\ kg/m^3$, the diameter of the cross sectional area d=6.16 mm and the starting lengths $L_1 = L_2 = 0.5\ m$. The payload mass is set to 1 kg and a pretension of *100 N* in applied to the cables. The transient behavior of the example cable-actuated system of Figure 3.1 is studied in response to an impulse applied at the payload at *t=0*. The impulse response is equivalent to giving the system at rest an initial velocity of $\frac{1}{\hat{m}_{eq}}$, where $\hat{m}_{eq} = m_{payload} + \frac{1}{2}\rho A\left(l_{u_1} + l_{u_2}\right)$ with l_{u_i} be the unstretched length of the i^{th} cable. Each vibrating node has the greatest potential energy when it has the smallest kinetic energy. Since no work is done by the internal forces in the system, there should be no change in the total amount of mechanical energy of the system. The conservation of the mechanical energy of the system in absence of external forces is verified by the results shown in Figure 3.11.

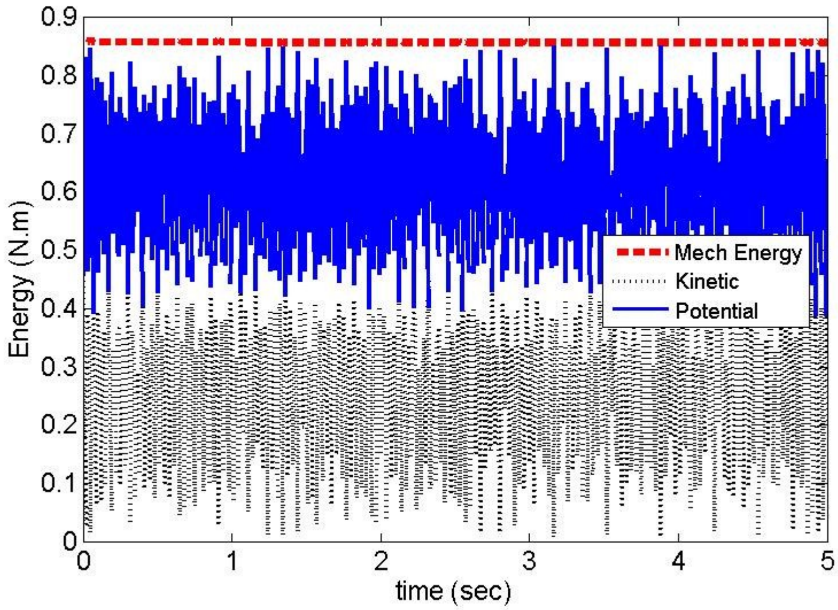

Figure 3.11: The conservation of the mechanical energy of the system

3.6 Linear model

The nonlinear cable model is linearized around its equilibrium configuration in order to design a cable controller which will be discussed in the following chapters. Initially, the equilibrium configuration of each cable was assumed to be horizontal, implying that the effect of gravity on each node was ignored. In this linearized model only the axial motion was considered. The initial unstretched length is the same for all elements, so all elements have the same mass. The assembled linearized equation of motion of the N moving nodes was defined. These N second order equations were then rewritten as a set of $2 \times N$ first order equations using intermediate states representing the time derivatives of the N node positions. The transverse vibrations of the lumped masses were not present in this linearized system. However, the control design goal of this thesis is to precisely position the payload and suppress the cables longitudinal and transverse vibrations. In order to accomplish this goal, we found the linearized system that considers cable deformations in both longitudinal and transverse directions by linearizing the nonlinear cable model around its true equilibrium configuration found in section 3.2 i.e. include the sag due to cables weight.

The system inputs are the changes in the unstretched lengths of the cable elements closest to the winches, $\boldsymbol{u} = [u_1 \;\; u_4]^T$. The output variable is the change in the position of the moving mass. The procedure of applying the control inputs will be discussed in detail in Chapter 4. The state-space realization of the linearized system is given by Eq. (3.17) where, $\boldsymbol{X} = \left[\Delta x_1 \;\; \Delta y_1 \;\; \Delta x_2 \;\; \Delta x_3 \;\; \Delta y_3 \;\; \Delta\dot{x}_1 \;\; \Delta\dot{y}_1 \;\; \Delta\dot{x}_2 \;\; \Delta\dot{x}_3 \;\; \Delta\dot{y}_3\right]^T$, and each state variable, e.g. Δx_i, is measured from its initial value, e.g. x_i.

$$\begin{aligned} \dot{\boldsymbol{X}} &= \mathbf{A}\boldsymbol{X} + \boldsymbol{B}\boldsymbol{u} \\ \boldsymbol{Y} &= \boldsymbol{C}\boldsymbol{X} \end{aligned} \tag{3.17}$$

4 Control System

In the context of control, the objective of this thesis is to design a controller that will apply force through the winches to position the payload of the cable-actuated systems precisely, and at the same time, suppress the cable vibrations. The winch control inputs are adjusted according to the payload tracking error. In dynamics model of the closed-loop system, the control input applied by each winch is approximated based on how the cable tension changes due to the change in the unstretched cable length, assuming that the cable remains straight during motion. If a cable has the unstretched length of L_{u_j} and the distance between the cable's two ends is d_j, then a change in the cable unstretched length of dl_j will cause a change in the cable tension of ΔT_j

$$\Delta T_j = EA\left(\frac{d_j - \left(L_{u_j} + dl_j\right)}{L_{u_j} + dl_j} - \frac{d_j - L_{u_j}}{L_{u_j}}\right) \tag{4.1}$$

The system control signal is then defined by changing of the unstretched length of the first element of each cable, $\boldsymbol{u} = \begin{bmatrix} u_1 \\ u_2 \end{bmatrix} = \begin{bmatrix} dl_1 \\ dl_4 \end{bmatrix}$. In the example system, each cable is initially $L_j = 0.5\ m$, and is discretized into $N_E = 2$ elements, so the method of changing the first cable element length is only valid up to $\frac{L_j}{N_E} = 0.25\ m$. In this chapter a PID controller and a LQG controller will be designed for the example system that responds to the payload positioning error. Later in this chapter, the application of passivity-based control to cable-actuated systems will be discussed.

4.1 PID and LQG for control system

In the process of designing a controller for the cable-actuated system to position the payload and damp the cables vibrations, a PID control algorithm is first selected because of its simplicity. Although it is simple to implement a PID controller to control the nonlinear system, the PID control performance is limited as a result of its suboptimal gains. Therefore, designing a more advanced controller such as LQG will be discussed later in order to improve the tracking performance of the system.

4.1.1 PID control

The PID control input of the j^{th} winch, that is located at x_{wi}, is adjusted according to the payload positioning error related to the j^{th} cable

$$e_j = |x_N - x_{wi}| - |x_{des} - x_{wi}| \tag{4.2}$$

where, x_N is the actual payload position and x_{des} is its desired position. Independent control inputs of the two winches are able to bring the payload to its desired position since the only possible x_{des} for $e_j = 0$, $j = 1,2$ is where $x_N = x_{des}$. The j^{th} PID controller is defined by

$$u_j = K_P e_j + K_I \int e_j dt + K_D \dot{e}_j \tag{4.3}$$

The three gains K_P, K_I and K_D are chosen to be the same for all the cables and are tuned manually. In MATLAB, *ode45* or *ode15s* is used to integrate the state-space equations. Each of the mentioned PID controllers adds one state variable of $\int e_j dt$ to the original system state vector. This way, the PID controller is combined with the nonlinear system in one *ode* routine. At each time-step, the unstretched lengths and the masses of the first cable elements are recalculated. The unstretched length the first cable element is adjusted using $l_{u_1} = l_{u_1}^0 + u_j$ where, $l_{u_1}^0$ is the original unstretched length.

4.1.2 LQG control

In section 2.2, the optimal LQG problem and its solution were defined for an LTI dynamics system. Given the linearized motion equations of the example system, Eq. (3.17), an LQG controller with integral action, as shown in Figure 2.1, is designed. The designed LQG controller ensures that the output, $\boldsymbol{Y} := x_N$ which is the payload position, tracks the reference input, $\boldsymbol{r} := x_{des}$ which is the desired payload trajectory. The LQG controller, Figure 2.1, state-space representation designed based on the strictly proper (***D=0***) and LTI system of Eq. (3.17) is given by

$$\begin{aligned} \begin{bmatrix} \dot{\hat{\boldsymbol{X}}} \\ \dot{\boldsymbol{X}}_i \end{bmatrix} &= \begin{bmatrix} \boldsymbol{A} - \boldsymbol{B}\boldsymbol{K}_x - \boldsymbol{K}_r\boldsymbol{C} & -\boldsymbol{B}\boldsymbol{K}_i \\ \boldsymbol{0} & \boldsymbol{0} \end{bmatrix} \begin{bmatrix} \hat{\boldsymbol{X}} \\ \boldsymbol{X}_i \end{bmatrix} + \begin{bmatrix} \boldsymbol{0} & \boldsymbol{K}_r \\ \boldsymbol{I} & -\boldsymbol{I} \end{bmatrix} \begin{bmatrix} \boldsymbol{r} \\ \boldsymbol{Y} \end{bmatrix} \\ \boldsymbol{u} &= \begin{bmatrix} -\boldsymbol{K}_x & -\boldsymbol{K}_i \end{bmatrix} \begin{bmatrix} \hat{\boldsymbol{X}} \\ \boldsymbol{X}_i \end{bmatrix} \end{aligned} \tag{4.4}$$

where, $\boldsymbol{K}_r$ is the optimal state-feedback gain, and $\boldsymbol{K} = [\boldsymbol{K}_x \quad \boldsymbol{K}_i]$ is the optimal Kalman filter gain. The design parameters of Eq. (2.9) are set to $\boldsymbol{Q} = \begin{bmatrix} \boldsymbol{0}_{nx\times nx} & \boldsymbol{0}_{nx\times p} \\ \boldsymbol{0}_{p\times nx} & \boldsymbol{I}_{p\times p} \end{bmatrix}$ and $\boldsymbol{R} = \boldsymbol{I}_{mx\times mx}$, where nx=10, mx=2 and p=1 are the number of states, inputs and outputs of the linearized system of Eq. (3.17). The parameter $\boldsymbol{Q}$ can be multiplied by an arbitrary integer *S* that is first set equal to one, in order to get a faster response of the closed-loop system. This controller is applied to the actual nonlinear example system of Figure 3.1, which is described by a set of second order ODEs obtained by assembling the dynamics of all cable nodes expressed in Eqs. (3.3) and (3.4). The closed-loop response of the same system is analysed and compared with the closed-loop response of the system with PID control in the next section.

4.2 Comparison of PID and LQG control

In order to study the closed-loop response of the system, the desired trajectory or the reference input is defined with a step change of *0.1 m* in the payload position at $t = 0$, starting from $x = 0.5\ m$. As shown with a brown line in Figure 4.1, the desired position of the payload is set to $x = 0.6\ m$ at $t = 0$. The cable parameters for this simulation are as follows: the Young's modulus $E = 675.62\ kPa$, the density $\rho = 1230\ kg/m^3$, the cable diameter $d = 3.8\ mm$, the damping ratio $\xi = 0.01$ and the starting lengths $L_1 = L_2 = 0.5\ m$. The payload mass is $0.11\ kg$ and the slider Coulomb friction is $C = 0.1\ N.sec/m$. The initial configurations of the cables are set to their equilibrium configurations, where the payload is located at x=0.5 m. In addition, no initial tension is considered in the cables.

The controllers designed using the methods in section 4.1 are evaluated using the nonlinear model shown in Figure 3.1, Eq. (3.3), and Eq. (3.4). Figure 4.1 shows the x-position of the payload, x_2, and the two lumped masses in the middle of the two cables, x_1 and x_3 of the cable-actuated system of Figure 3.1. Figure 4.2 shows the error in the payload position, x_2. Figure 4.3 shows the control signal, $\boldsymbol{u}$, or the system inputs which are the changes in the unstretched length of the first elements of the cables, u_1 and u_2.

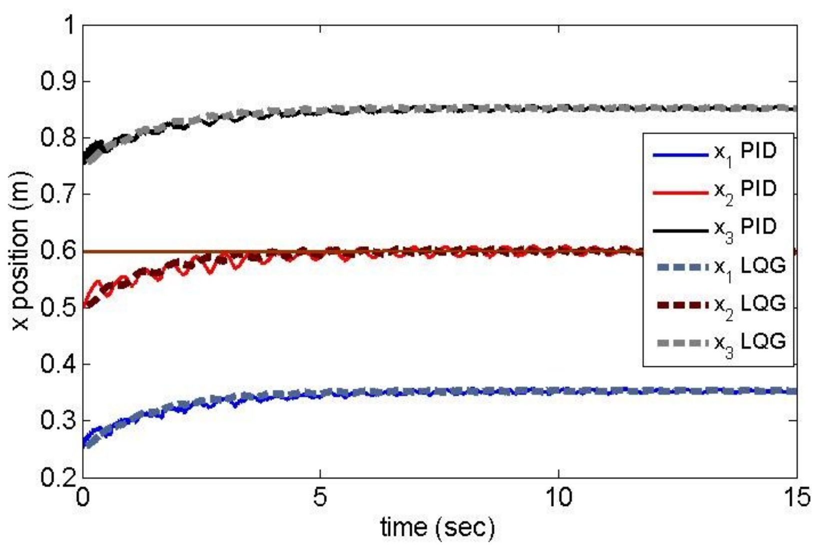

Figure 4.1: Longitudinal oscillations using the PID and LQG controllers

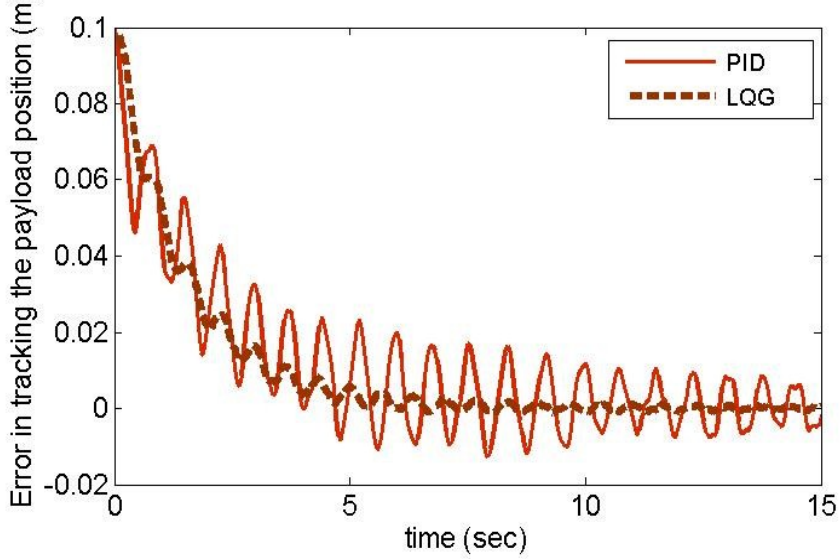

Figure 4.2: Error in tracking the payload using the PID and LQG controllers

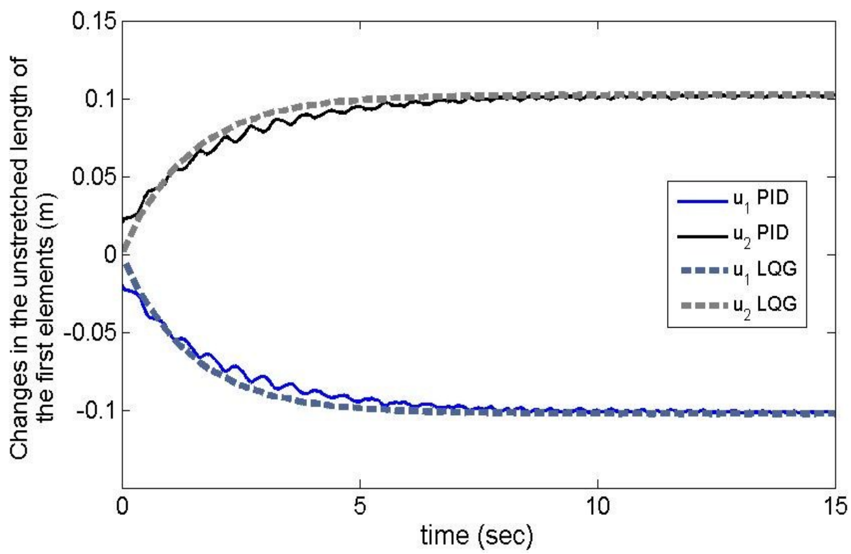

Figure 4.3: Control signals using the PID and LQG controls

In Figure 4.1, Figure 4.2 and Figure 4.3 the performance of the LQG controller and the PID controller ($K_P = 0.2,\ K_I = 0.6\ \frac{1}{sec},\ K_D = 0.001\ sec$) applied to the example system are compared. Clearly, using the LQG controller leads to smaller longitudinal oscillations of the lumped masses and smoother control signal. However, both controllers demonstrate a very slow convergence to the steady-state payload position, requiring more than 5 sec to converge.

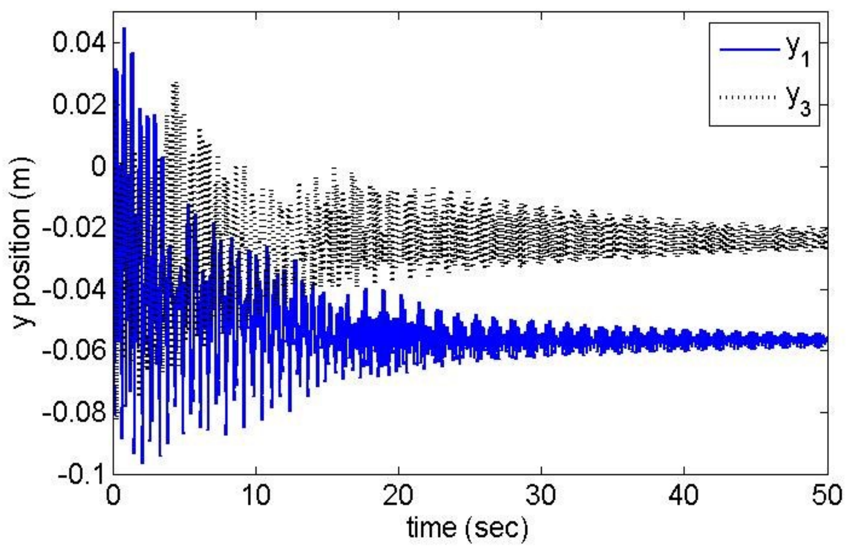

Figure 4.4: Transverse oscillations using the PID controller

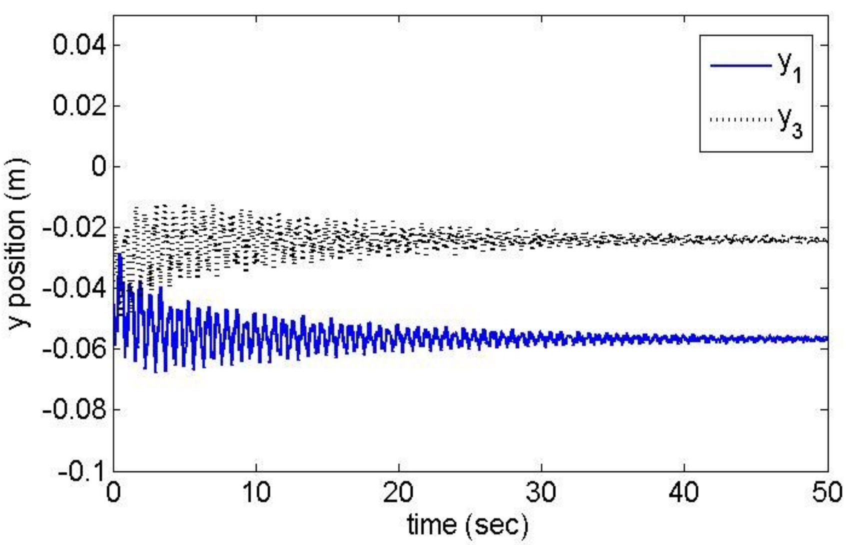

Figure 4.5: Transverse oscillations using the LQG controller with cables internal damping

Figure 4.4 shows the performance of the PID controller in damping the transverse vibrations of the cables. Figure 4.5 shows the corresponding oscillations with the LQG controller. Comparing Figure 4.4 with Figure 4.5 shows that the LQG controller has better performance in reducing the transverse vibrations of the cables.

We know that the friction between the braids of a cable dissipates the energy within the cable structure, and this is modeled in the nonlinear simulation by the internal damping forces. It is worth determining whether the reduction in the cables' transverse vibration is just as a result of the internal damping of the system (including the cables internal damping and the slider Coulomb damping) or whether the designed controller also affects these oscillations. It has been observed that ignoring all the internal damping sources, the closed-loop system becomes unstable during simulation. Therefore, the slider Coulomb damping is conserved in the dynamic model, and in order to see the performance of the PID controller and the LQG controller in reducing the transverse vibration of the cables, the dynamic system is simulated with zero cable internal damping, as shown in Figure 4.6 and Figure 4.7. In Figure 4.6 and Figure 4.7, the controller and the slider Coulomb friction are the only sources of damping in the system. These plots confirm that without the cables internal damping the PID controller is not effective at damping the transverse vibrations of the cables, while the LQG controller still damps the cables transverse vibrations effectively.

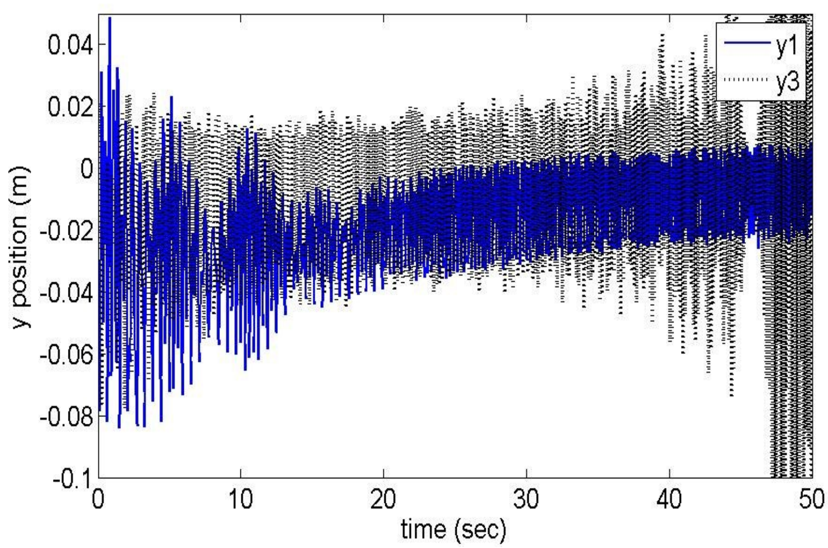

Figure 4.6: Transverse oscillations using the PID controller without cables internal damping

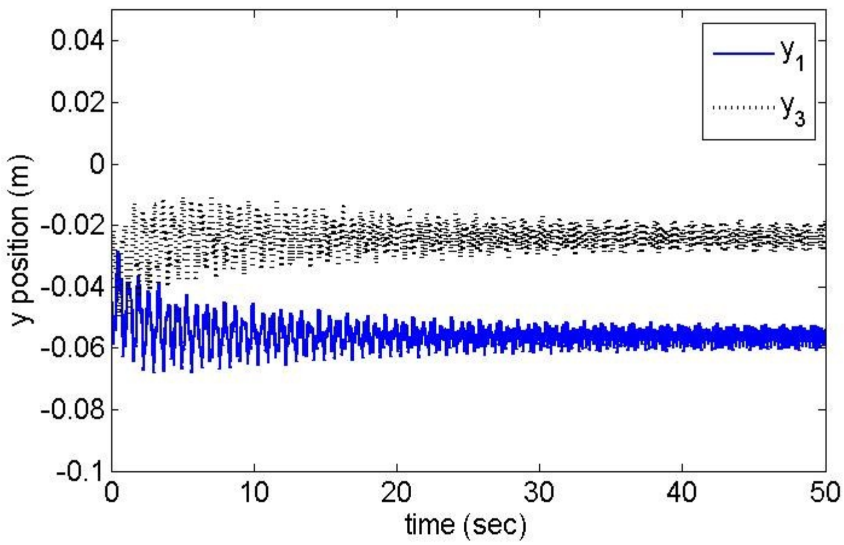

Figure 4.7: Transverse oscillations using the LQG controller without cables internal damping

Figure 4.8 and Figure 4.9 compare the PID controller and the LQG controller in terms of tension in the first cable element. Clearly, using the LQG controller, the cables experience much smaller tension oscillations.

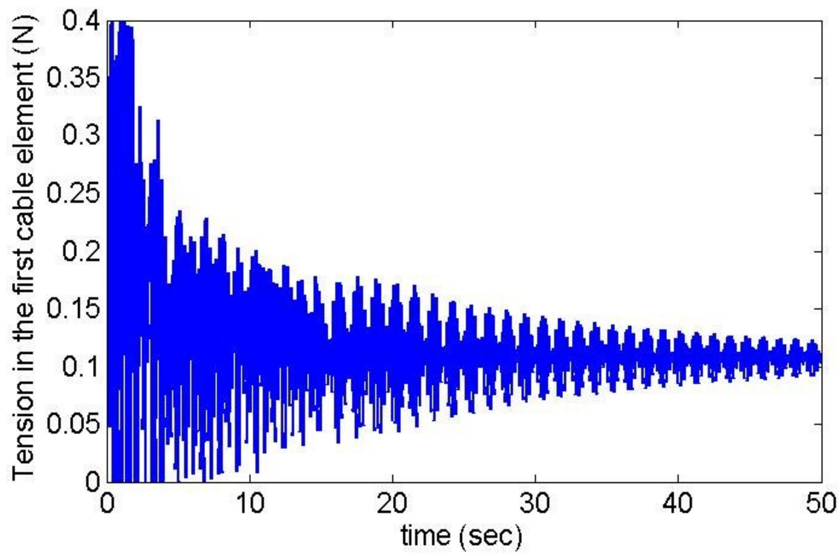

Figure 4.8: Variation of tension in the first cable element using the PID controller

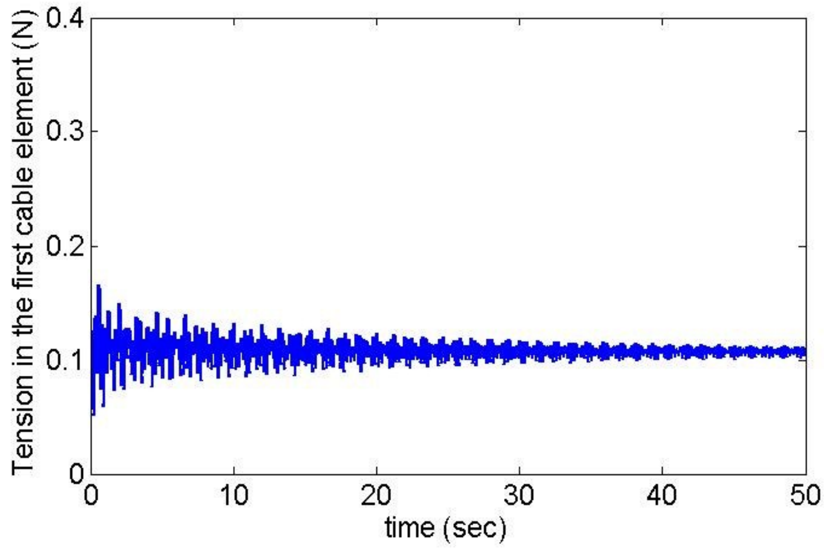

Figure 4.9: Variation of tension in the first cable element using The LQG controller

4.2.1 LQG control: a smoother trajectory

In the simulation of the previous section, the desired trajectory of the closed-loop system was defined with a step of *0.1 m* in the payload position. This reference input induces high amplitude vibrations in the cables. This may cause the actuators to fail or saturate in an attempt to move the payload and damp the cable vibrations. Therefore, a smooth desired trajectory is defined to move the payload smoothly from its initial position of *0.5 m* to its final desired position of *0.6 m*. The period of this trajectory is set to *T=0.2 s* and the payload is assumed to be at rest in its initial and final position. This smooth desired trajectory is defined by

$$r(t) = 0.5 + 0.05\left(1 - cos\left(\frac{\pi t}{T}\right)\right) \tag{4.5}$$

The cables parameters for the simulation are as follows: the Young's modulus $E = 437\ MPa$, the density $\rho = 2180\ kg/m^3$, the cable diameter $d = 6.16\ mm$ and the starting lengths $L_1 = L_2 = 0.5\ m$. The payload mass is set to $1\ kg$, the slider Coulomb friction is $0.1\ N.sec/m$ and a pretension of $100\ N$ is applied to the cables. Applying the LQG controller of Eq. (4.4) to the actual nonlinear example system of figure Figure 3.1, the closed-loop response to the desired trajectory of Eq. (4.5) is shown in Figure 4.10. The LQG controller is able to suppress the vibration of this cable that is more tight and stiffer than the previous test case. In the previous test case, a cable with small modulus of elasticity was chosen because the PID control was unable to produce stable results for a stiffer cable. It is shown in Figure 4.10 that the designed LQG controller can provide a faster response than that shown in the previous section by multiplying the design parameter $\boldsymbol{Q}$ of Eq. (2.9) by an integer S that is now set to 1×10^6. Figure 4.10 shows the x-position of the payload and the two nodes in the middle of the two cables in addition to the payload desired trajectory. Clearly defining a smoother trajectory leads to smaller oscillations.

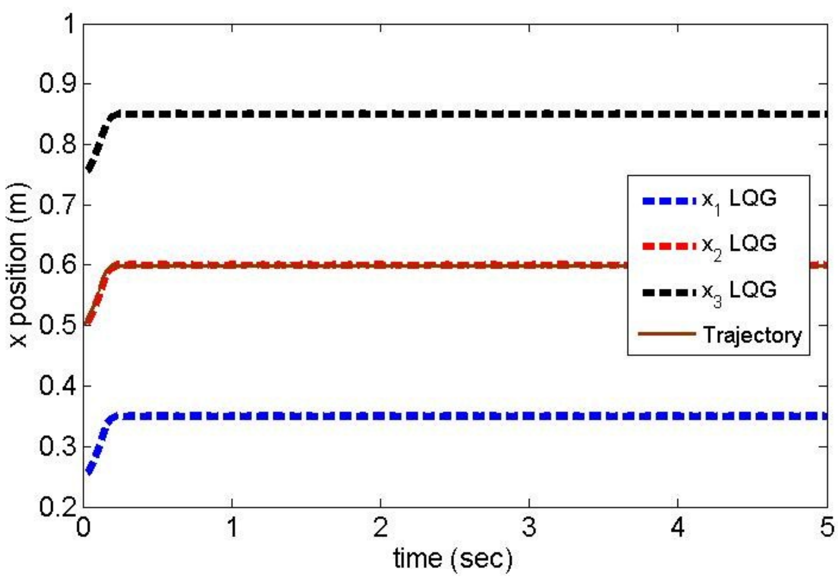

Figure 4.10: Closed-loop response to a smooth trajectory using the LQG controller

5 Passivity-Based Control: Observer-Based Strictly Positive Real Design

As mentioned in Chapter 2, the Passivity Theorem states that the feedback interconnection of a passive system and a very strictly passive (VSP) one is input-output stable. This section and the following chapters deal with illustrating the passivity property of the cable-actuated systems by defining suitable inputs and outputs, and applying passivity-based control scheme to cable-actuated systems. In the control design procedures, the controller is designed based on the linearized system of Eq. (3.17) and then the designed controller is applied to the original system.

5.1 Control design challenges

In dealing with LTI systems, passivity and positive real (PR) concepts are equivalent, and for a system to be PR, the relative degree of its transfer function must be -1, 0 or +1. The relative degree of the LTI transfer function of the example system, $\boldsymbol{G}(s) = \boldsymbol{C}(S\boldsymbol{I} - \boldsymbol{A})^{-1}\boldsymbol{B}$, exceeds +1, and consequently, it is not PR. The incentive to find a PR transfer function for the cable-actuated system is that, according to the Passivity Theorem, any finite gain very strictly passive controller will stabilize the closed-loop system. Unlike previously designed advanced controllers for cable-actuated systems, this would allow the design of very simple controllers for such systems, but there are some issues in the process of defining a passive input-output map for the system. First, in cable-actuated systems, the control actuators and the sensors measuring the position or the velocity of the payload are not usually collocated, while collocation usually leads to a passive input-output map. Second, the numbers of inputs and outputs of cable-actuated systems are not necessarily equal which also limits the use of the passivity-based control. In order to overcome these limitations, first a dynamic embedding is considered where an observer is used to construct a new output that realizes a passive input-output map. Next, an alternative input-output map is considered where the output is a scaled version of the true payload velocity and the input is a modified winch torque. These two techniques will be discussed in detail in this chapter.

5.2 Observer based strictly positive real design

The technique of designing an observer and a controller to transfer a non-square system with non-collocated actuators and sensors to a strictly positive real (SPR) system was introduced by Collado et al. [35]. They stated that any observable and stabilizable system (even an unstable system) can be transferred to a SPR system by introducing of an observer, constructing a new output based on the observer states and designing a state feed-back stabilizing controller.

As discussed in Chapter 3, the linearized time invariant system of the example cable–actuated system of Figure 3.1 in state-space realization is given by

$$\begin{aligned} \dot{\boldsymbol{X}} &= \mathbf{A}\boldsymbol{X} + \boldsymbol{B}\boldsymbol{u} \\ \boldsymbol{Y} &= \boldsymbol{C}\boldsymbol{X} \end{aligned} \tag{5.1}$$

where, $\boldsymbol{u} = \begin{bmatrix} u_1 \\ u_2 \end{bmatrix}$ is defined by changing of the unstretched length of the first element on each cable of Figure 3.1 and $\boldsymbol{Y} = x_3$ is the payload position. This linearized system is unstable because an eigenvalue pair of its state matrix lies in the open right half complex plane (RHP). The system has two complex conjugate poles in the RHP. The location of the poles of the linearized system are as follows: $-291.1 \pm 2546i$, $-288.8 \pm 2536i$, $-2.467 \pm 226.2i$, $0.145 \pm 223i$.

5.2.1 Design a stabilizing controller based on an observer

First, a full-order observer for the system of Eq. (5.1) is given by

$$\dot{\hat{\boldsymbol{X}}} = \boldsymbol{A}\hat{\boldsymbol{X}} + \boldsymbol{B}\boldsymbol{u} + \boldsymbol{L}(\boldsymbol{Y} - \boldsymbol{C}\hat{\boldsymbol{X}}) \tag{5.2}$$

where, $\boldsymbol{L}$ is the observer gain matrix and $\hat{\boldsymbol{X}}$ is the estimated state vector. Next, a stabilizing state feed-back controller based on the estimated state vector is introduced by

$$\boldsymbol{u} = -\boldsymbol{K}\hat{\boldsymbol{X}} + \boldsymbol{v} \tag{5.3}$$

where $\boldsymbol{v}$ is the input signal, thus the state-space realization of the system including the state feed-back is rewritten as

$$\dot{\boldsymbol{X}} = (\boldsymbol{A} - \boldsymbol{B}\boldsymbol{K})\boldsymbol{X} + \boldsymbol{B}\boldsymbol{v} - \boldsymbol{B}\boldsymbol{K}(\hat{\boldsymbol{X}} - \boldsymbol{X}) \tag{5.4}$$

Introducing the state estimation error $\tilde{\boldsymbol{X}} = \hat{\boldsymbol{X}} - \boldsymbol{X}$ the state-space representation of the system combined with the observer and the state feed-back controller is given by

$$\begin{bmatrix} \dot{\boldsymbol{X}} \\ \dot{\tilde{\boldsymbol{X}}} \end{bmatrix} = \boldsymbol{A}_0 \begin{bmatrix} \boldsymbol{X} \\ \tilde{\boldsymbol{X}} \end{bmatrix} + \boldsymbol{B}_0\boldsymbol{v}\,, \quad \boldsymbol{A}_0 = \begin{bmatrix} \boldsymbol{A} - \boldsymbol{B}\boldsymbol{K} & -\boldsymbol{B}\boldsymbol{K} \\ \boldsymbol{0} & \boldsymbol{A} - \boldsymbol{L}\boldsymbol{C} \end{bmatrix}, \quad \boldsymbol{B}_0 = \begin{bmatrix} \boldsymbol{B} \\ \boldsymbol{0} \end{bmatrix} \tag{5.5}$$

where, $\boldsymbol{K}$ and $\boldsymbol{L}$ are designed such that $\boldsymbol{A}_k = \boldsymbol{A} - \boldsymbol{B}\boldsymbol{K}$ and $\boldsymbol{A}_l = \boldsymbol{A} - \boldsymbol{L}\boldsymbol{C}$ are stable. Thus for all positive definite matrices $\boldsymbol{Q}_k$ and $\boldsymbol{Q}_l$, there exists positive definite matrices $\boldsymbol{P}_k$ and $\boldsymbol{P}_l$ as the solution for the Lyapunov equations

$$\boldsymbol{A}_k^T\boldsymbol{P}_k + \boldsymbol{P}_k\boldsymbol{A}_k = -\boldsymbol{Q}_k \tag{5.6}$$

$$\boldsymbol{A}_l^T\boldsymbol{P}_l + \boldsymbol{P}_l\boldsymbol{A}_l = -\boldsymbol{Q}_l \tag{5.7}$$

5.2.2 Positive realness requirements

In order to find conditions which guarantee positive realness of the modified system of Eq. (5.5), its corresponding Lyapunov equation is written as

$$\boldsymbol{A}_0^T\boldsymbol{P}_0 + \boldsymbol{P}_0\boldsymbol{A}_0 = -\boldsymbol{Q}_0 \tag{5.8}$$

Collado et al. [35] defined the matrix $\boldsymbol{P}_0 = \begin{bmatrix} \boldsymbol{P}_k & \boldsymbol{P}_k \\ \boldsymbol{P}_k & \zeta\boldsymbol{P}_l \end{bmatrix}$ containing the design parameter ζ to be determined such that the modified system becomes SPR. Therefore,

$$\boldsymbol{Q}_0 = \begin{bmatrix} \boldsymbol{Q}_k & \boldsymbol{Q}_k + \boldsymbol{P}_k\boldsymbol{LC} \\ \boldsymbol{Q}_k + \boldsymbol{C}^T\boldsymbol{L}^T\boldsymbol{P}_k & \zeta\boldsymbol{Q}_l \end{bmatrix} \tag{5.9}$$

For the modified system to be stable $\boldsymbol{P}_0$ and $\boldsymbol{Q}_0$ should be positive definite: $\boldsymbol{P}_0 > 0$ and $\boldsymbol{Q}_0 > 0$. Using the Schur complement positive definite condition stated in section 2.4.1, $\boldsymbol{P}_0 > 0$ if and only if

- $\boldsymbol{P}_k > 0$ (which is satisfied because of the positive definiteness of $\boldsymbol{A}_k$) and
- $\zeta\boldsymbol{P}_l - \boldsymbol{P}_k > 0$ which is satisfied if $\zeta > \zeta_1 := max_{i=1\ldots n}(\xi_i)$

where, $\xi_i\,, i = 1 \ldots n$ are the eigenvalues of $\boldsymbol{P}_l^{-1}\boldsymbol{P}_k$ based on the theorem stated in section 2.4 [35]. Similarly, $\boldsymbol{Q}_0 > 0$ if and only if

- $\boldsymbol{Q}_k > 0$ (which is satisfied because of the positive definiteness of $\boldsymbol{A}_k$) and
- $\zeta\boldsymbol{Q}_l - (\boldsymbol{Q}_k + \boldsymbol{C}^T\boldsymbol{L}^T\boldsymbol{P}_k)\boldsymbol{Q}_k^{-1}(\boldsymbol{Q}_k + \boldsymbol{P}_k\boldsymbol{LC}) > \boldsymbol{0}$
  which is satisfied if $\zeta > \zeta_2 := max_{i=1\ldots n}(\varsigma_i)$

where, $\varsigma_i\,, i = 1 \ldots n$ are the eigenvalues of $\boldsymbol{Q}_l^{-1}(\boldsymbol{Q}_k + \boldsymbol{C}^T\boldsymbol{L}^T\boldsymbol{P}_k)\boldsymbol{Q}_k^{-1}(\boldsymbol{Q}_k + \boldsymbol{P}_k\boldsymbol{LC})$ [35]. Therefore, the modified system is stable if and only if

$$\zeta > max(\zeta_1, \zeta_2) \tag{5.10}$$

5.2.2.1 Definition of the new output

Given the stable matrix $\boldsymbol{A}_0$ and defining the new output that depends on the observer states as

$$\boldsymbol{z} = \boldsymbol{M}_0 \begin{bmatrix} \boldsymbol{X} \\ \widetilde{\boldsymbol{X}} \end{bmatrix} \tag{5.11}$$

the modified system of Figure 5.1 defined by the following state-space representation is SPR from $\boldsymbol{v}$ to the new output $\boldsymbol{z}$.

$$\begin{aligned} \begin{bmatrix} \dot{\boldsymbol{X}} \\ \dot{\widetilde{\boldsymbol{X}}} \end{bmatrix} &= \boldsymbol{A}_0 \begin{bmatrix} \boldsymbol{X} \\ \widetilde{\boldsymbol{X}} \end{bmatrix} + \boldsymbol{B}_0 \boldsymbol{v} \\ \boldsymbol{z} &= \boldsymbol{M}_0 \begin{bmatrix} \boldsymbol{X} \\ \widetilde{\boldsymbol{X}} \end{bmatrix} = \boldsymbol{B}_0^T \boldsymbol{P}_0 \begin{bmatrix} \boldsymbol{X} \\ \widetilde{\boldsymbol{X}} \end{bmatrix} = \boldsymbol{B}^T \boldsymbol{P}_k \widehat{\boldsymbol{X}} = \boldsymbol{M} \widehat{\boldsymbol{X}} \end{aligned} \tag{5.12}$$

where, $\boldsymbol{M}$ is a dynamic embedded to the system which is combined with the observer and the state-feed-back.

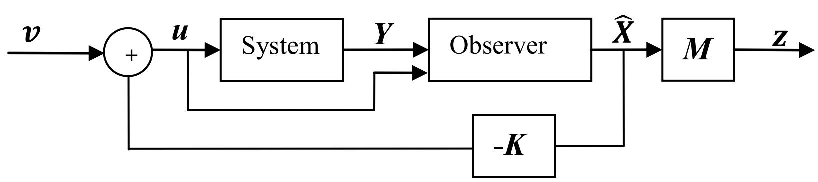

Figure 5.1: The modified SPR system: the observer state feedback controller and the dynamic embedding

As mentioned in Chapter 2, based on the KYP lemma, the transfer matrix of the modified LTI system, $\boldsymbol{G_0}(s) = \boldsymbol{M}_0(S\boldsymbol{I} - \boldsymbol{A}_0)^{-1}\boldsymbol{B}_0$, where $\boldsymbol{A}_0$ is stable, $(\boldsymbol{A}_0, \boldsymbol{B}_0)$ is stabilizable and $(\boldsymbol{A}_0, \boldsymbol{M}_0)$ is observable is SPR if and only if there exist positive definite symmetric matrices $\boldsymbol{P}$ and $\boldsymbol{Q}$ such that first, $\boldsymbol{P}_0\boldsymbol{A}_0 + \boldsymbol{A}_0^T\boldsymbol{P}_0 = -\boldsymbol{Q}_0$ and second, $\boldsymbol{B}_0^T\boldsymbol{P}_0 = \boldsymbol{M}_0$. The first condition is satisfied for $\zeta > max(\zeta_1, \zeta_2)$ and the second condition is satisfied by using the dynamic embedding $\boldsymbol{M}$ which defined the new output $\boldsymbol{z}$ as defined in Eq (5.12).

5.2.3 Checking if the modified system is SPR

Given the modified LTI system $\boldsymbol{G_0}(s) = \boldsymbol{M}_0(S\boldsymbol{I} - \boldsymbol{A}_0)^{-1}\boldsymbol{B}_0$, the positive realness of the system can be checked in the frequency domain. A square system from $\boldsymbol{v}(t)$ to $\boldsymbol{z}(t)$ is SPR if $\int_0^T \boldsymbol{z}^T(t)\boldsymbol{v}(t)dt > \boldsymbol{0}$ which is equivalent to $\boldsymbol{G}_0^H(j\omega) + \boldsymbol{G}_0(j\omega) > \boldsymbol{0}\,, \forall\omega \in R$ in the frequency domain as shown in section 2.3.1 using Parseval's theorem. The minimum Hermitian part of $\boldsymbol{G}_0(s)$ is defined as

$$\frac{1}{2}\lambda_{min}[\boldsymbol{G}_0^H(j\omega) + \boldsymbol{G}_0(j\omega)] \tag{5.13}$$

and its maximum singular value is defined as

$$\bar{\sigma}[\boldsymbol{G}_0(j\omega)] = \sqrt{\lambda_{max}[\boldsymbol{G}_0^H(j\omega)\boldsymbol{G}_0(j\omega)]} \tag{5.14}$$

where, λ_{min} and λ_{max} represent the minimum and maximum eigenvalues respectively. The minimum Hermitian part and the maximum singular value of the original system are shown in Figure 5.2 and those of the modified system are shown in Figure 5.3.

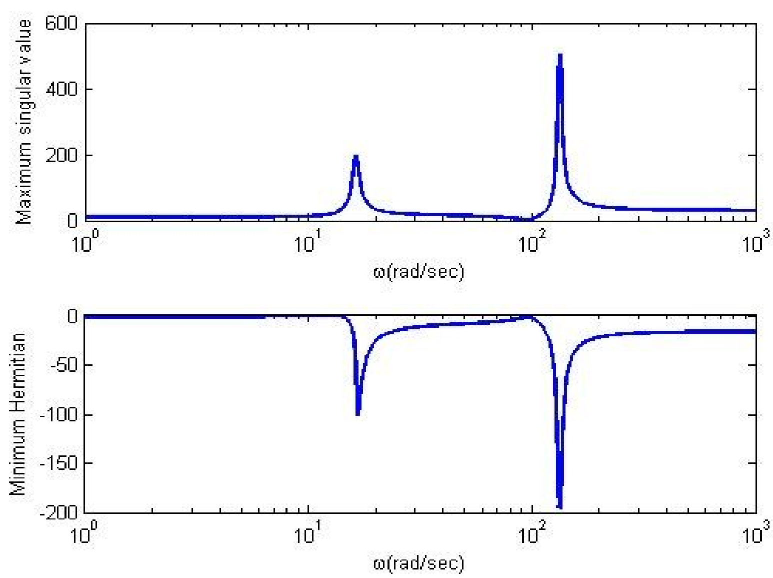

Figure 5.2: The maximum singular value and the minimum Hermitian part of the original systems

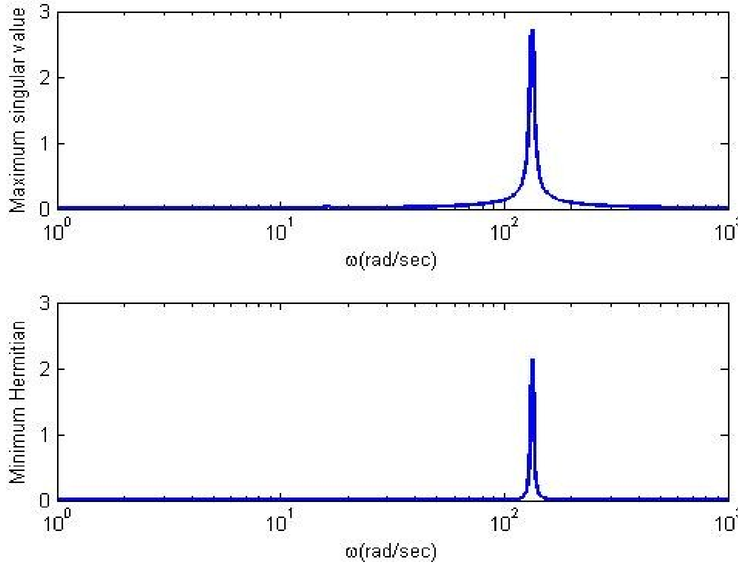

Figure 5.3: The maximum singular value and the minimum Hermitian part of the modified systems

Figure 5.2 shows the minimum Hermitian part and the maximum singular value of the original system. The minimum Hermitian part of the original system is negative, and consequently it is not even PR. The modified system consisting of the linearized system with the observer, state-feedback controller and the dynamic embedding is SPR over all frequencies since its minimum Hermitian part is positive, as shown in Figure 5.3.

5.3 Steady-state tracking

Up to now, it has been shown that the Kalman-Yakubovich-Popov (KYP) lemma holds for the system connected with an observer state-feedback and introducing a new output. Although by using this observer state-feedback technique the original system was transferred to a SPR system, it does not satisfy the steady-state tracking requirements for a desired reference trajectory. The observer state-feedback design procedure will be extended to address the steady-state tracking problem by including integral action on the tracking error. A schematic of the observer state-feedback controller augmented with integral action is shown in Figure 5.4. Adding an integral term to the control law guarantees obtaining a system that yields zero steady-state tracking error for a desired trajectory input $\boldsymbol{r}$ as long as the closed-loop stability is maintained.

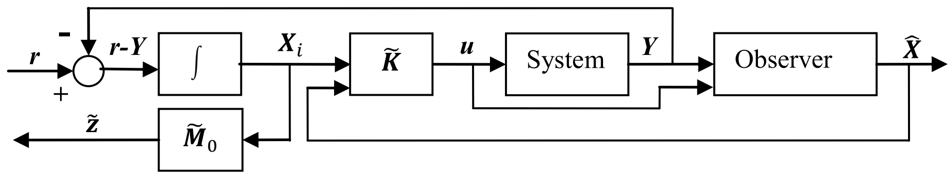

Figure 5.4: Schematic of the observer state-feedback controller augmented with an integral action

5.3.1 Positive realness of the modified system

Introducing the new state $\boldsymbol{X}_i = \int(\boldsymbol{r}-\boldsymbol{Y})dt$, the state-space representation of the modified system of Figure 5.4 including an integral term is given by

$$\begin{bmatrix}\dot{\boldsymbol{X}}\\ \dot{\widetilde{\boldsymbol{X}}}\\ \dot{\boldsymbol{X}}_i\end{bmatrix} = \widetilde{\boldsymbol{A}}_0\begin{bmatrix}\boldsymbol{X}\\ \widetilde{\boldsymbol{X}}\\ \boldsymbol{X}_i\end{bmatrix} + \widetilde{\boldsymbol{B}}_0\begin{bmatrix}\boldsymbol{r}\\ \boldsymbol{Y}\end{bmatrix}, \qquad \widetilde{\boldsymbol{A}}_0 = \begin{bmatrix}\boldsymbol{A}-\boldsymbol{BK}_x & -\boldsymbol{BK}_x & -\boldsymbol{BK}_i\\ \boldsymbol{0} & \boldsymbol{A}-\boldsymbol{LC} & \boldsymbol{0}\\ \boldsymbol{0} & \boldsymbol{0} & \boldsymbol{0}\end{bmatrix}, \qquad \widetilde{\boldsymbol{B}}_0 = \begin{bmatrix}\boldsymbol{0} & \boldsymbol{0}\\ \boldsymbol{0} & \boldsymbol{0}\\ \boldsymbol{I} & -\boldsymbol{I}\end{bmatrix} \tag{5.15}$$

where $\widetilde{\boldsymbol{v}} = \begin{bmatrix}\boldsymbol{r}\\ \boldsymbol{Y}\end{bmatrix}$ is the input vector and $\widetilde{\boldsymbol{K}} = [\boldsymbol{K}_x \quad \boldsymbol{K}_i]$ includes the state-feedback gain $\boldsymbol{K}_x$ and the gain $\boldsymbol{K}_i$ corresponding to the integral action. In order to find conditions which guarantee positive realness of the system with the state-space representation of Eq. (5.15), its corresponding Lyapunov equation is written as

$$\widetilde{\boldsymbol{A}}_0^T\widetilde{\boldsymbol{P}}_0 + \widetilde{\boldsymbol{P}}_0\widetilde{\boldsymbol{A}}_0 = -\widetilde{\boldsymbol{Q}}_0 \tag{5.16}$$

where, $\widetilde{\boldsymbol{P}}_0$ is chosen as

$$\widetilde{\boldsymbol{P}}_0 = \begin{bmatrix}\boldsymbol{P}_k & \boldsymbol{P}_k & \boldsymbol{0}\\ \boldsymbol{P}_k & \tilde{\zeta}\boldsymbol{P}_l & \boldsymbol{0}\\ \boldsymbol{0} & \boldsymbol{0} & \boldsymbol{I}\end{bmatrix} \tag{5.17}$$

which contains the design parameter $\tilde{\zeta}$ to be determined such that the modified system with integral action becomes SPR from $\widetilde{\boldsymbol{v}}$ to $\widetilde{\boldsymbol{z}}$. Therefore,

$$\widetilde{\boldsymbol{Q}}_0 = \begin{bmatrix} \boldsymbol{Q}_k & -\boldsymbol{P}_k\boldsymbol{A}_l + \boldsymbol{P}_k\boldsymbol{B}\boldsymbol{K}_x - \boldsymbol{A}_k^T\boldsymbol{P}_k & \boldsymbol{P}_k(\boldsymbol{B}\boldsymbol{K}_i) \\ -\boldsymbol{A}_l^T\boldsymbol{P}_k + (\boldsymbol{B}\boldsymbol{K}_x)^T\boldsymbol{P}_k - \boldsymbol{P}_k\boldsymbol{A}_k & -\tilde{\zeta}\boldsymbol{Q}_l + (\boldsymbol{B}\boldsymbol{K}_x)^T\boldsymbol{P}_k + \boldsymbol{B}\boldsymbol{K}_x\boldsymbol{P}_k & \boldsymbol{P}_k(\boldsymbol{B}\boldsymbol{K}_i) \\ (\boldsymbol{B}\boldsymbol{K}_i)^T\boldsymbol{P}_k & (\boldsymbol{B}\boldsymbol{K}_i)^T\boldsymbol{P}_k & \boldsymbol{0} \end{bmatrix} \quad \textbf{(5.18)}$$

For the modified system to be stable $\widetilde{\boldsymbol{P}}_0$ and $\widetilde{\boldsymbol{Q}}_0$ should be positive definite: $\widetilde{\boldsymbol{P}}_0 > 0$ and $\widetilde{\boldsymbol{Q}}_0 > 0$. Using Sylvester's criterion positive definite condition stated in section 2.4.1, $\boldsymbol{P}_0 > 0$ if and only if

- $\boldsymbol{P}_k > 0$ which is satisfied because of the positive definiteness of $\boldsymbol{A}_k$ and
- $\zeta\boldsymbol{P}_l - \boldsymbol{P}_k > 0$ which is satisfied if $\tilde{\zeta} > \tilde{\zeta}_1 := \zeta_1 := max_{i=1\ldots n}(\xi_i)$

where, $\xi_i\,, i = 1 \ldots n$ are the eigenvalues of $\boldsymbol{P}_l^{-1}\boldsymbol{P}_k$ based on the theorem stated in section 2.4. Similarly, $\boldsymbol{Q}_0 > 0$ if and only if

- $\boldsymbol{Q}_k > 0$ which is satisfied because of the positive definiteness of $\boldsymbol{A}_k$ and
- $[(\boldsymbol{B}\boldsymbol{K}_i)^T\boldsymbol{P}_k]^2[(-\boldsymbol{P}_k\boldsymbol{A}_l + \boldsymbol{P}_k\boldsymbol{B}\boldsymbol{K}_x - \boldsymbol{A}_k^T\boldsymbol{P}_k) - \left(-\tilde{\zeta}\boldsymbol{Q}_l + (\boldsymbol{B}\boldsymbol{K}_x)^T\boldsymbol{P}_k + \boldsymbol{B}\boldsymbol{K}_x\boldsymbol{P}_k\right) + \boldsymbol{Q}_k + \boldsymbol{A}_l^T\boldsymbol{P}_k - (\boldsymbol{B}\boldsymbol{K}_x)^T\boldsymbol{P}_k + \boldsymbol{P}_k\boldsymbol{A}_k] > \boldsymbol{0}$

  which is satisfied if $\tilde{\zeta} > \tilde{\zeta}_2 := max_{i=1\ldots n}(\tilde{\varrho}_i)$ and
- $\boldsymbol{Q}_k\left[-\tilde{\zeta}\boldsymbol{Q}_l + (\boldsymbol{B}\boldsymbol{K}_x)^T\boldsymbol{P}_k + \boldsymbol{B}\boldsymbol{K}_x\boldsymbol{P}_k\right] - [-\boldsymbol{A}_l^T\boldsymbol{P}_k + (\boldsymbol{B}\boldsymbol{K}_x)^T\boldsymbol{P}_k - \boldsymbol{P}_k\boldsymbol{A}_k]^2 > \boldsymbol{0}$

  Which is satisfied if $\tilde{\zeta} < \tilde{\zeta}_3 := min_{i=1\ldots n}(\tilde{\varsigma}_i)$

$\tilde{\varsigma}_i\,, i = 1 \ldots n$ are the eigenvalues of $\boldsymbol{Q}_l^{-1}\boldsymbol{Q}_k^{-1}\{\boldsymbol{Q}_k\boldsymbol{P}_k[(\boldsymbol{B}\boldsymbol{K}_x)^T + \boldsymbol{B}\boldsymbol{K}_x] - \boldsymbol{P}_k^2(\boldsymbol{B}\boldsymbol{K}_x - \boldsymbol{A}_l - \boldsymbol{A}_k)\}$ and $\tilde{\varrho}_i\,, i = 1 \ldots n$ are the eigenvalues of $\boldsymbol{Q}_l^{-1}\{-\boldsymbol{Q}_k + \boldsymbol{P}_k[2(\boldsymbol{B}\boldsymbol{K}_x)^T + \boldsymbol{A}_k^T - \boldsymbol{A}_k + \boldsymbol{A}_l - \boldsymbol{A}_l^T]\}$. Therefore, the modified system with integral action is stable if and only if

$$max\left(\tilde{\zeta}_1, \tilde{\zeta}_2\right) < \tilde{\zeta} < min\left(\tilde{\zeta}_3\right) \quad \textbf{(5.19)}$$

As a result, the first condition of the KYP lemma is satisfied. The second condition is satisfied by using the dynamic embedding $\widetilde{\boldsymbol{M}}$ which defined the new output $\tilde{\boldsymbol{z}}$

$$\tilde{\boldsymbol{z}} = \widetilde{\boldsymbol{M}}_0 \begin{bmatrix} \boldsymbol{X} \\ \widetilde{\boldsymbol{X}} \\ \boldsymbol{X}_i \end{bmatrix} = \widetilde{\boldsymbol{B}}_0^T \widetilde{\boldsymbol{P}}_0 \begin{bmatrix} \boldsymbol{X} \\ \widetilde{\boldsymbol{X}} \\ \boldsymbol{X}_i \end{bmatrix} = \begin{bmatrix} \boldsymbol{0} & \boldsymbol{0} \\ \boldsymbol{0} & \boldsymbol{0} \\ \boldsymbol{I} & -\boldsymbol{I} \end{bmatrix}^T \begin{bmatrix} \boldsymbol{P}_k & \boldsymbol{P}_k & \boldsymbol{0} \\ \boldsymbol{P}_k & \tilde{\zeta}\boldsymbol{P}_l & \boldsymbol{0} \\ \boldsymbol{0} & \boldsymbol{0} & \boldsymbol{I} \end{bmatrix} = \begin{bmatrix} 1 \\ -1 \end{bmatrix} \boldsymbol{X}_i \tag{5.20}$$

Given the new square LTI system $\widetilde{\boldsymbol{G}}_{\boldsymbol{0}}(s) = \widetilde{\boldsymbol{M}}_0\left(s\boldsymbol{I} - \widetilde{\boldsymbol{A}}_0\right)^{-1}\widetilde{\boldsymbol{B}}_0$ from $\widetilde{\boldsymbol{v}}$ to $\tilde{\boldsymbol{z}}$**,** the positive realness of the system is being checked. The system is SPR if $\widetilde{\boldsymbol{G}}_0^H(j\omega) + \widetilde{\boldsymbol{G}}_0(j\omega) > 0\,, \forall\omega \in R$ in the frequency domain and the minimum Hermitian part of $\widetilde{\boldsymbol{G}}_0(s)$ is defined as $\frac{1}{2}\lambda_{min}\left[\widetilde{\boldsymbol{G}}_0^H(j\omega) + \widetilde{\boldsymbol{G}}_0(j\omega)\right]$. The minimum Hermitian part and the maximum singular value of the new system of Figure 5.4 is shown in Figure 5.5. The new system consisting of the linearized system with the observer, state-feedback controller, the dynamic embedding and the integral action is SPR over all frequencies since its minimum Hermitian part is positive. The minimum Hermitian part and the maximum singular value shown in Figure 5.5 illustrate that the integrator is dominating in this design.

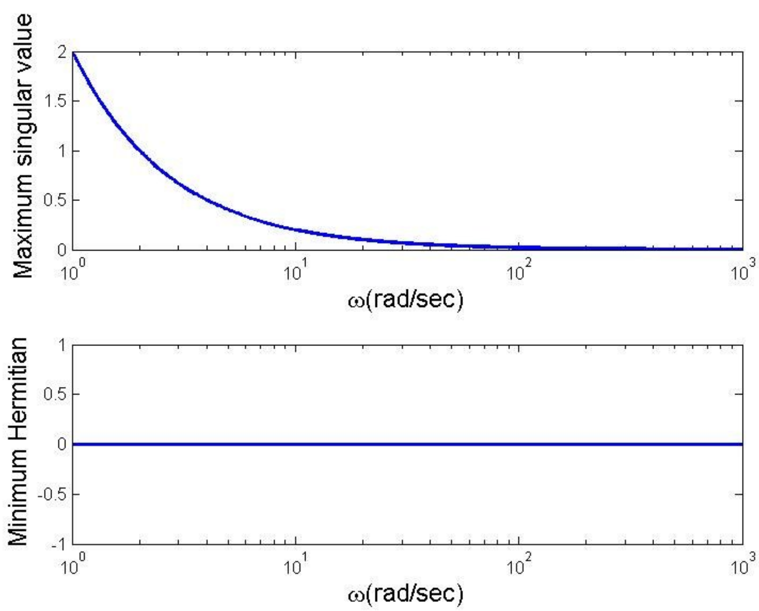

Figure 5.5: The maximum singular value and the minimum Hermitian part of the new systems

5.4 Passivity-based controlled response of the system

Applying the observer state-feedback controller of Figure 5.4 augmented with an integral action to the original nonlinear example system of Figure 3.1, Eq. (3.3), and Eq. (3.4), the closed-loop response to the desired trajectory of (5.21) is shown in Figure 5.6. The period of this trajectory is set to *T=0.2 s* and the payload is assumed to be at rest in its initial and final position.

$$r(t) = 0.5 + 0.05\left(1 - cos\left(\frac{\pi t}{T}\right)\right) \quad \textbf{(5.21)}$$

The cables parameters for this simulation are as follows: the Young's modulus $E = 437\ MPa$, the density $\rho = 2180\ kg/m^3$, the cable diameter $d = 6.16\ mm$ and the starting lengths $L_1 = L_2 = 0.5\ m$. The payload mass is set to $1\ kg$, the slider Coulomb friction is $0.1\ N.sec/m$ and a pretension of $100\ N$ is applied to the cables.

Figure 5.6 shows the x-position of the payload, $x_{payload}$, and the two lumped masses in the middle of the two cables, x_1 and x_3 of the cable-actuated system of Figure 1.3 in addition to the desired trajectory. Figure 5.6 shows reasonably good tracking and suppression of the longitudinal vibrations using the observer state-feedback controller. Figure 5.7 demonstrates the control signal, $\boldsymbol{u}$, or the system inputs which are the changes in the unstretched length of the first elements of the cables. Using the observer state-feedback controller leads to a smooth control signal as shown in Figure 5.7.

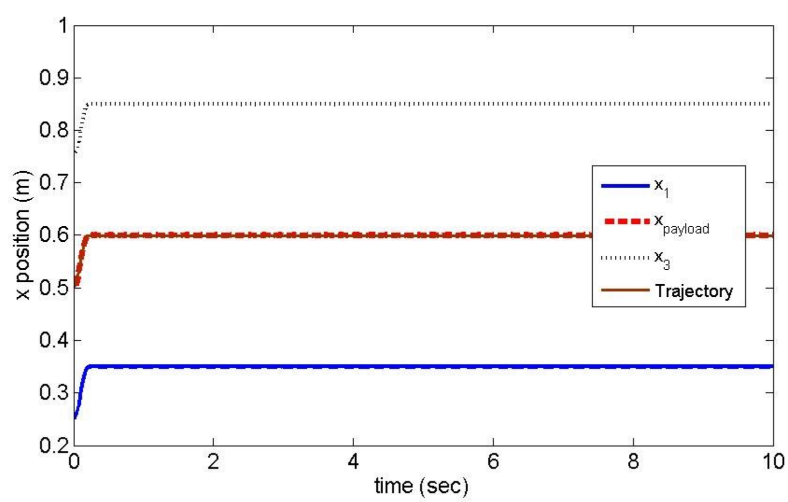

Figure 5.6: Longitudinal oscillations using the observer state-feedback controller

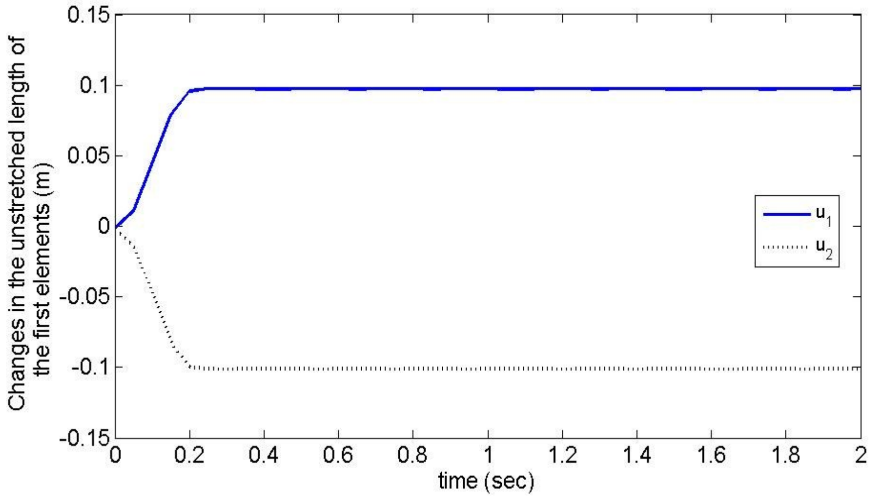

Figure 5.7: Control signal using the observer state-feedback controller

Figure 5.8 shows the performance of the observer state-feedback controller in damping the transverse vibrations of the node in the middle of the first cable. This figure shows that the observer state-feedback controller is effective in damping the transverse oscillations of the cables. Figure 5.9 shows the variation in the tension of the first cable element using the observer state-feedback controller.

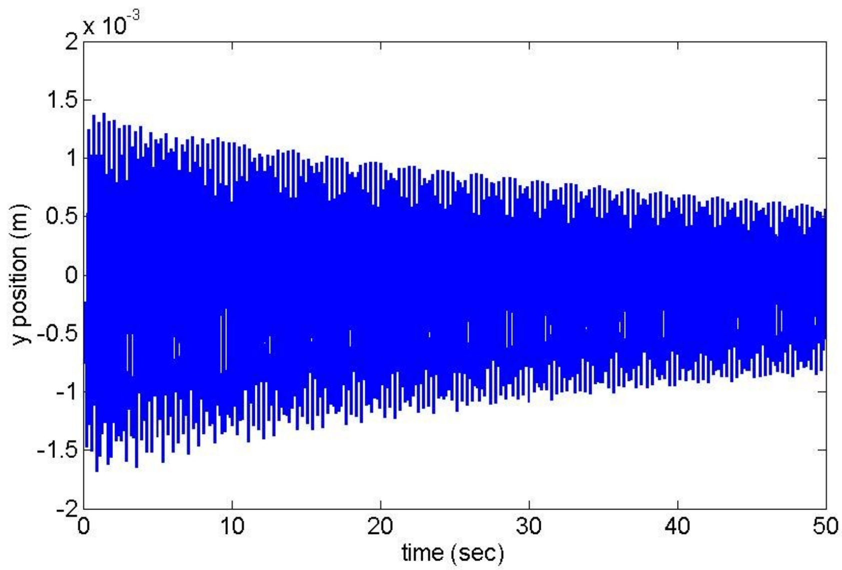

Figure 5.8: Transverse oscillations using the observer state-feedback controller

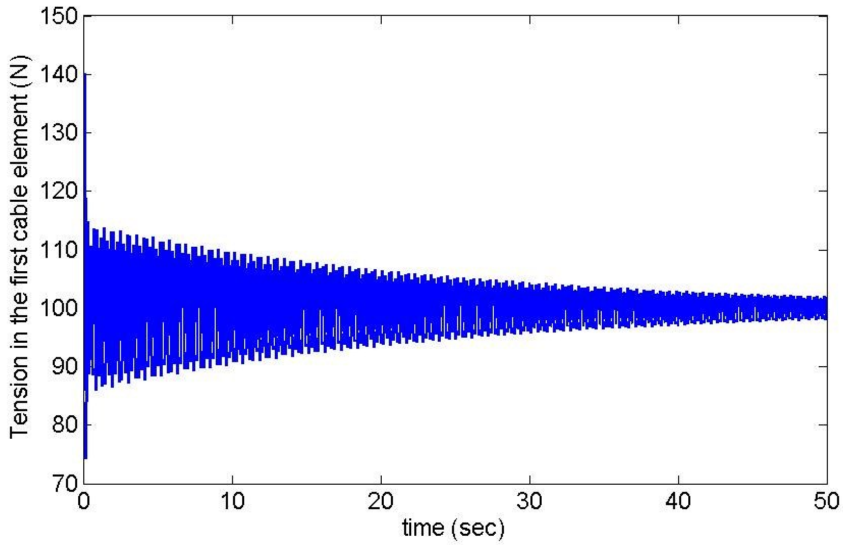

Figure 5.9: Variation in the tension of the first cable element using the observer state-feedback controller

6 Passive System Design: Introducing μ-tip Rate

Motivated by the robust nature of passivity-based control, its application to cable-actuated systems is investigated in this thesis. In addition, the Passivity Theorem has the potential to lead to a very simple controller design which can make the implementation of the controller simple and practical. As discussed in section 5.1, cable-actuated systems are usually non-square with non-collocated actuators and sensors, which generally limits the use of passivity-based control. In order to overcome these limitations, a dynamic embedding was considered in Chapter 5 where an observer state-feedback was used to construct a new output that realizes a passive input-output map. Later in Chapter 5, an integral term was added to the control law to guarantee a zero steady-state tracking error. Although a passive input-output map was found for the cable-actuated system by using this observer-based technique, the controller design procedure and thus its implementation became complicated for a steady-state tracking problem. We now consider an alternative passification technique which leads to the design of a more practical and simpler controller. In this alternative technique, an input-output map is considered where the output is a scaled version of the true payload velocity and the input is a modified winch torque. An overview of this technique, along with simulation results, will be presented in this chapter.

6.1 Dynamics model in relative coordinates

In order to derive the dynamic equations of motion of the example system, the generalized coordinate vector $\boldsymbol{q} = \begin{bmatrix} \boldsymbol{\theta} \\ \boldsymbol{q}_e \end{bmatrix}$ is considered that consists of rigid body motion coordinate vector $\boldsymbol{\theta} = \begin{bmatrix} r\theta_1 \\ r\theta_2 \end{bmatrix}$ and elastic coordinate vector $\boldsymbol{q}_e = \begin{bmatrix} \boldsymbol{q}_{1e} \\ \boldsymbol{q}_{2e} \end{bmatrix}$, where $\boldsymbol{q}_{1e}$ and $\boldsymbol{q}_{2e}$ are the vectors of relative coordinates on each cable. Considering three lumped masses on the first cable connected by springs $k_{i,1} = \frac{EA}{lu_{i,1}}$ and dashpots $d_{i,1} = C^{ID}$, *i=1,2* as shown in Figure 6.1, relative coordinates $\xi_{2,1}$ and $\xi_{3,1}$ will form $\boldsymbol{q}_{1e}$. The displacements of the lumped masses on the first cable with respect to their equilibrium position in absolute coordinates (with respect to inertial frame) are labeled as x_1, x_2, x_3. The first relative coordinate $\xi_{1,1} = x_1 = r\theta_1$ gives the position of the first mass relative to inertial frame. The two others $\xi_{i,1}$, $i = 2{,}3$, represent the relative displacement of the i^{th} mass on the first cable with respect to the previous one. That is, $\xi_{1,1} = x_1$, $\xi_{2,1} = x_2 - x_1$, $\xi_{3,1} = x_3 - x_2$.

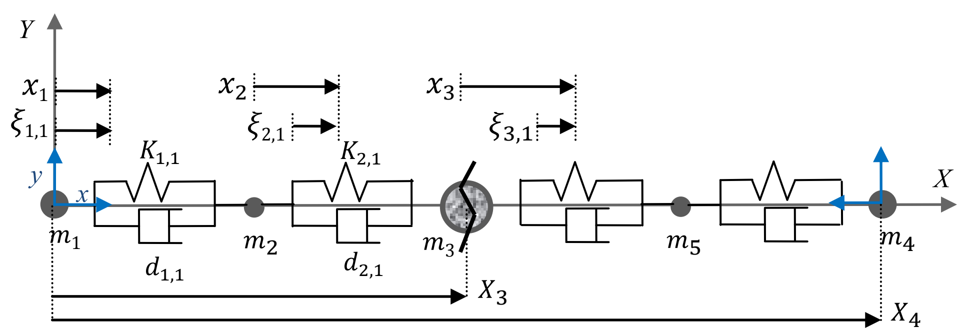

Figure 6.1: Lumped-mass model of the cables, payload and winches

Using relative coordinates the potential energy, *PE*, and the kinetic energy, *KE*, of the cable are given as

$$KE = \frac{1}{2}(m_1 + m_2 + m_3)\dot{\xi}_{1,1}^2 + \frac{1}{2}(m_2 + m_3)\dot{\xi}_{2,1}^2 + \frac{1}{2}(m_3)\dot{\xi}_{3,1}^2 + (m_2 + m_3)\dot{\xi}_{1,1}\dot{\xi}_{2,1} + m_3\dot{\xi}_{1,1}\dot{\xi}_{3,1} + m_3\dot{\xi}_{1,1}\dot{\xi}_{2,1} \quad \textbf{(6.1)}$$

$$PE = \frac{1}{2}k_{1,1}\xi_{2,1}^2 + \frac{1}{2}k_{2,1}\xi_{3,1}^2 = \frac{1}{2}\sum_{i=1}^{2} k_{i,1}\xi_{i+1,1}^2 \tag{6.2}$$

The virtual work of nonconservative forces is also given as

$$\delta W = \frac{\tau_1}{r}\delta\xi_{1,1} - C^{ID}\dot{\xi}_{2,1}\delta\xi_{2,1} - C^{ID}\dot{\xi}_{3,1}\delta\xi_{3,1} = \sum_{i=1}^{3} w_i\delta\xi_{i,1} \tag{6.3}$$

The nonconservative forces are due to internal damping of cable elements, $C^{ID}\dot{\xi}_{i,1}$, $i = 1,2$, and the torque applied to the first winch, τ_1. r represents the winch radius. Substituting into Lagrange's equations

$$\frac{d}{dt}\left(\frac{\partial L}{\dot{\xi}_{i,1}}\right) - \frac{\partial L}{\xi_{i,1}} = w_i \tag{6.4}$$

where, the Lagrangian function is defined as $L = KE - PE$. The equation of motion of the first cable is formulated as

$$\begin{bmatrix} m_1 + m_2 + m_3 & m_2 + m_3 & m_3 \\ m_2 + m_3 & m_2 + m_3 & m_3 \\ m_3 & m_3 & m_3 \end{bmatrix}\begin{bmatrix} \ddot{\xi}_{1,1} \\ \ddot{\xi}_{2,1} \\ \ddot{\xi}_{3,1} \end{bmatrix} + \begin{bmatrix} 0 & 0 & 0 \\ 0 & d_{1,1} & 0 \\ 0 & 0 & d_{2,1} \end{bmatrix}\begin{bmatrix} \dot{\xi}_{1,1} \\ \dot{\xi}_{2,1} \\ \dot{\xi}_{3,1} \end{bmatrix} + \begin{bmatrix} 0 & 0 & 0 \\ 0 & k_{1,1} & 0 \\ 0 & 0 & k_{2,1} \end{bmatrix}\begin{bmatrix} \xi_{1,1} \\ \xi_{2,1} \\ \xi_{3,1} \end{bmatrix} = \begin{bmatrix} \tau_1/r \\ 0 \\ 0 \end{bmatrix} \tag{6.5}$$

which can be rewritten in the form

$$\boldsymbol{M}_1\ddot{\boldsymbol{q}}_{1e} + \boldsymbol{D}_1\dot{\boldsymbol{q}}_{1e} + \boldsymbol{K}_1\boldsymbol{q}_{1e} = \boldsymbol{F}_1 \tag{6.6}$$

6.1.1 Incorporating winch dynamics

The equation of motion governing the dynamics of the first winch is

$$I_1\ddot{\theta}_1 = \tau_1 + \left(k_1\xi_{2,1} + d_1\dot{\xi}_{2,1}\right)r\,, \qquad I_1 = I + \frac{1}{2}\rho A l u_{1,1} r^2 \tag{6.7}$$

where I and r are the moment of inertia and the radius of the winch. Incorporating the winch dynamics to the dynamics of the cable, m_1, m_2 and m_3 in Eq. (6.5) are replaced by $\frac{I}{r^2} + \frac{1}{2}\rho A l u_{1,1}$, $\frac{1}{2}\rho A\left(lu_{1,1} + lu_{1,2}\right)$ and $\frac{1}{2}\rho A l u_{1,2} + \frac{1}{2}M_{PL}$ respectively. $\frac{I}{r^2}$ is the equivalent mass of the winch added to the mass of the first node of the cable and M_{PL} is the payload mass which is distributed on the last lumped masses of the two cables. Similarly, the equation of motion regarding the dynamics of the second cable is derived. Before the cable equations can be assembled, it is necessary to transform the cable matrices and vectors derived in local coordinate systems (*xy*) so that all the cable equations are referred to the inertial coordinate systems (*XY)* that is shown in Figure 6.1.

The next step is to construct the overall system equations of motion by assembling the cables matrices and vectors found in inertial coordinate system *XY*. In the assembly procedure, the value of the unknown variables is the same for all cables joining at nodes where cables are connected. The nodal stiffness, mass, damping and load of each of the cables sharing the node are added to get the net amount at that node. The boundary conditions must also be applied before solving for $\boldsymbol{q}$. It is known that the distance between the two winches, X_{N+1}, is constant, where *N* is the number of nodes on each cable chosen to be three in Figure 6.1. The payload position, X_N, is written down using the relative coordinates of each cable and then is set equal in order to find the appropriate kinematic constraint. Given *N=3*, the positions of the lumped masses of the second cable in absolute coordinates are labeled as x_4, x_5, x_3 and in relative coordinates are labeled as $\xi_{1,2} = x_4 = r\theta_2$, $\xi_{2,2} = x_4 - x_5$, $\xi_{3,2} = x_5 - x_3$, all written in inertial coordinate system. Using the relative coordinates of the first cable

$$X_3 = \sum_{i=1}^{2} lu_{i,1} + \sum_{i=1}^{3} \xi_{i,1} \tag{6.8}$$

Using the relative coordinates of the second cable

$$X_3 = X_4 - \sum_{i=1}^{2} lu_{i,2} + \xi_{1,2} - \sum_{i=2}^{3} \xi_{i,2} \tag{6.9}$$

Subtracting this equation from Eq. (6.8) gives $X_4 = \sum_{i=1}^{2} lu_{i,1} + \sum_{i=1}^{2} lu_{i,2} + \xi_{1,1} - \xi_{1,2} + \sum_{i=2}^{3} \xi_{i,1} + \sum_{i=2}^{3} \xi_{i,2}$, where X_4 represents the distance between the two winches that is constant. Taking the derivative of this equation, the kinematic constraint is derived as

$$\dot{X}_4 = \boldsymbol{J}_c\dot{\boldsymbol{q}} = \boldsymbol{0}\,, \qquad \boldsymbol{J}_c = [J_{1\theta} \quad J_{2\theta} \quad \boldsymbol{J}_{1e} \quad \boldsymbol{J}_{2e}] = [1 \quad -1 \quad 1 \quad 1 \quad 1 \quad 1] \tag{6.10}$$

where, $\boldsymbol{q} = [\xi_{1,1} \quad \xi_{1,2} \quad \xi_{2,1} \quad \xi_{3,1} \quad \xi_{2,2} \quad \xi_{3,2}]^T$, $\boldsymbol{J}_c$ is the Jacobian matrix, $J_{1\theta} = \frac{\partial X_4}{\partial \boldsymbol{q}_1}$, $J_{2\theta} = \frac{\partial X_4}{\partial \boldsymbol{q}_2}$, $\boldsymbol{J}_{1e} = \begin{bmatrix} \frac{\partial X_4}{\partial \boldsymbol{q}_3} & \frac{\partial X_4}{\partial \boldsymbol{q}_4} \end{bmatrix}$ and $\boldsymbol{J}_{2e} = \begin{bmatrix} \frac{\partial X_4}{\partial \boldsymbol{q}_5} & \frac{\partial X_4}{\partial \boldsymbol{q}_6} \end{bmatrix}$.

Using relative coordinates, the motion equation for example system of Figure 6.1 finally looks like

$$\boldsymbol{M}\ddot{\boldsymbol{q}} + \boldsymbol{D}\dot{\boldsymbol{q}} + \boldsymbol{K}\boldsymbol{q} = [\boldsymbol{I}\ \boldsymbol{0}]^T\boldsymbol{\tau} + \boldsymbol{J}_c^T\boldsymbol{\lambda} \tag{6.11}$$

subject to constraint of Eq. (6.10), where, $\boldsymbol{M}$, $\boldsymbol{D}$ and $\boldsymbol{K}$ are the mass, damping and stiffness matrices respectively. These positive definite matrices are partitioned as

$$\boldsymbol{M} = \begin{bmatrix} \boldsymbol{M}_{\theta\theta} & \boldsymbol{M}_{\theta e} \\ \boldsymbol{M}_{e\theta} & \boldsymbol{M}_{ee} \end{bmatrix}, \qquad \boldsymbol{D} = \begin{bmatrix} \boldsymbol{0} & \boldsymbol{0} \\ \boldsymbol{0} & \boldsymbol{D}_{ee} \end{bmatrix}, \quad \boldsymbol{K} = \begin{bmatrix} \boldsymbol{0} & \boldsymbol{0} \\ \boldsymbol{0} & \boldsymbol{K}_{ee} \end{bmatrix}$$

$\boldsymbol{\lambda}$ is the Lagrange multiplier, $\boldsymbol{\tau}$ is the winch torque vector and $\boldsymbol{J}_c$ is the Jacobian matrix from system kinematic constraint of (6.10).

6.1.2 Forward dynamics

In order to solve the motion Eq. (6.11) for $\ddot{\boldsymbol{q}}$, a new variable $\boldsymbol{z}$ and a matrix $\boldsymbol{R}$ are introduced such that $\boldsymbol{J}_c\boldsymbol{R} = \boldsymbol{0}$ which satisfies the constraint of Eq. (6.10).

$$\dot{\boldsymbol{q}} = \boldsymbol{R}\dot{\boldsymbol{z}} \tag{6.12}$$

Given $\boldsymbol{z} = \begin{bmatrix} \theta_1 \\ \boldsymbol{q}_e \end{bmatrix}$,

$$\boldsymbol{R} = \begin{bmatrix} \begin{bmatrix} 1 \\ \tilde{R}_{\theta r} \end{bmatrix} & \begin{bmatrix} \boldsymbol{0}_{1\times 4} \\ \tilde{\boldsymbol{R}}_{\theta e} \end{bmatrix} \\ \boldsymbol{0}_{4\times 1} & \boldsymbol{I}_{4\times 4} \end{bmatrix} \tag{6.13}$$

where $\tilde{R}_{\theta r} = 1$ and $\tilde{\boldsymbol{R}}_{\theta e} = [1 \quad 1 \quad 1 \quad 1]$ are found from the equation

$$\dot{\xi}_{1,2} = \tilde{R}_{\theta r}\dot{\xi}_{1,1} + \tilde{\boldsymbol{R}}_{\theta e}\left[\dot{\xi}_{2,1} \;\; \dot{\xi}_{3,1} \;\; \dot{\xi}_{2,2} \;\; \dot{\xi}_{3,2}\right]^T \tag{6.14}$$

Rewriting Eq. (6.11) in terms of the new variable $\boldsymbol{z}$ yields

$$\boldsymbol{M}_{zz}\ddot{\boldsymbol{z}} + \boldsymbol{D}_{zz}\dot{\boldsymbol{z}} + \boldsymbol{K}_{zz}\boldsymbol{z} = \boldsymbol{R}^T[\boldsymbol{I}\ \boldsymbol{0}]^T\boldsymbol{\tau} \tag{6.15}$$

where, $\boldsymbol{M}_{zz} = \boldsymbol{R}^T\boldsymbol{M}\boldsymbol{R} = \begin{bmatrix} M_{zz,rr} & \boldsymbol{M}_{zz,re} \\ \boldsymbol{M}_{zz,re} & \boldsymbol{M}_{zz,ee} \end{bmatrix}$, $\boldsymbol{D}_{zz} = \boldsymbol{R}^T\boldsymbol{D}\boldsymbol{R}$ and $\boldsymbol{K}_{zz} = \boldsymbol{R}^T\boldsymbol{K}\boldsymbol{R}$.

6.1.3 Modal analysis and dynamic verification

Introducing the state vector $\begin{bmatrix} \boldsymbol{z} \\ \dot{\boldsymbol{z}} \end{bmatrix}$, the state-space representation of the example system is formulated as

$$\begin{bmatrix} \dot{\boldsymbol{z}} \\ \ddot{\boldsymbol{z}} \end{bmatrix} = \begin{bmatrix} \boldsymbol{0} & \boldsymbol{I} \\ -\boldsymbol{M}_{zz}{}^{-1}\boldsymbol{K}_{zz} & -\boldsymbol{M}_{zz}{}^{-1}\boldsymbol{D}_{zz} \end{bmatrix}\begin{bmatrix} \boldsymbol{z} \\ \dot{\boldsymbol{z}} \end{bmatrix} + \begin{bmatrix} \boldsymbol{0} \\ \boldsymbol{M}_{zz}{}^{-1}\boldsymbol{R}^T[\boldsymbol{I}\ \boldsymbol{0}]^T \end{bmatrix}\boldsymbol{\tau} \tag{6.16}$$

The system is simulated by solving the above ODE using a Runge-Kutta method intended for initial value problems. The dynamics of the system is then validated by modal analysis and checking the energy conservation of the system. The corresponding eigen-value problem of Eq. (6.15) is written as

$$-\omega_i{}^2 \boldsymbol{M}_{zz}\boldsymbol{z}_i + \boldsymbol{K}_{zz}\boldsymbol{z}_i = \boldsymbol{0}\, , i = 1,2, \dots, NT \tag{6.17}$$

where, NT is total number of lumped masses that is the degrees of freedom of the system (chosen to be five in Figure 6.1) and ω_i is the i^{th} natural frequency of the system. $\boldsymbol{q}_i = \boldsymbol{R}\boldsymbol{z}_i$ is the i^{th} mode shape corresponding to ω_i. For simplicity, let us consider the simplest case where $NT = 3$. In this case, the cables parameters for the simulation are as follows: the Young's modulus $E = 437\ MPa$, the density $\rho = 2180\ kg/m^3$, the cable diameter $d = 6.16\ mm$ and the starting lengths $L_1 = L_2 = 0.5\ m$. The payload mass and the winches inertia are temporarily set to zero. The mode shapes are $\boldsymbol{q}_1 = [1 \quad 1 \quad 0 \quad 0]^T$, $\boldsymbol{q}_2 = [0.57 \quad -0.57 \quad -0.57 \quad -0.57]^T$ and $\boldsymbol{q}_3 = [-0.33 \quad -0.33 \quad 0.66 \quad -0.66]^T$ as shown in Figure 6.2. For each mode the mass displacements are oscillatory and have the same frequency.

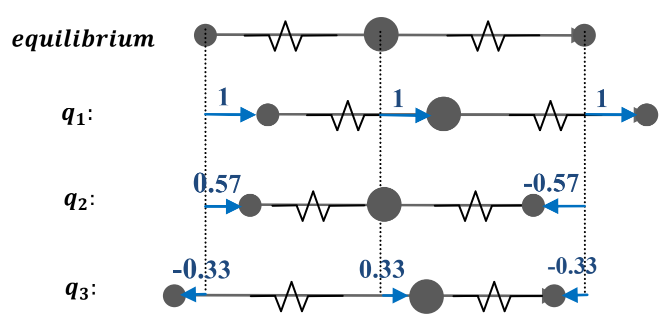

Figure 6.2: Modes of the example system

The mode shapes of this simple system composed of three masses $\frac{1}{2}\rho A L_1$, $\rho A(L_1 + L_2)$ and $\frac{1}{2}\rho A L_2$ are reasonable, verifying the accuracy of the dynamic model.

The dynamics model is also validated by performing an energy analysis while ignoring the internal damping of the cables and the slider friction for the system with the same cables parameters. The payload mass in this simulation is set to $1\ kg$ and a pretension of $100\ N$ is applied to the cables. The winches moment of inertia and radius are set to $0.001\ kg.m^2$ and $0.05\ m$. The transient behavior of the example cable-actuated system of Figure 6.1 is studied in response to an initial offset of $0.1\ m$ in the payload position. Since no work is done by the external forces on the system, there should be no change in the total amount of mechanical energy of the system. The conservation of the mechanical energy of the system in absence of external forces is verified by the results shown in Figure 6.3.

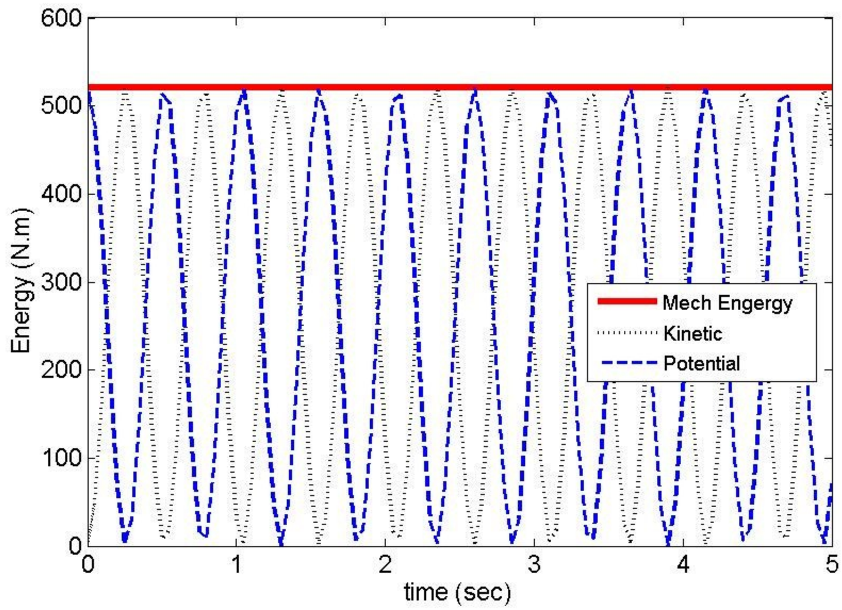

Figure 6.3: The kinetic, potential and mechanical energy of the system in absence of damping forces

6.2 Alternative input-output map

The motion control problem of a closed-loop and flexible multibody system manipulating a large payload was considered by Damaren [38]. He constructed a new system output, called $\mu -$ tip rate, that depends on the true payload position and the joint motions of the system. He also introduced an alternative input as a combination of the joint torques and illustrated the passivity property of the system from this alternative input to the $\mu -$ tip rate. The structural properties and the motion equations of the flexible multibody system modeled and controlled by Damaren are similar to those of a typical cable-actuated system. It therefore seems appropriate to use his idea to find an alternative input-output map for the cable-actuated system that is passive and apply the passivity-based control to the system for the purpose of the steady-state tracking of the payload and the vibration suppression of the cables.

- **$\boldsymbol{\mu}$ − tip rate**

The payload position of the cable-actuated system, shown in Figure 6.1 can be formulated by forward kinematic maps of the two cables as

$$\mathrm{P} = F_i(\theta_i, \boldsymbol{q}_{ie}), \qquad i = 1 \; or \; 2 \tag{6.18}$$

This equation is similar to Eq. (6.8) and Eq. (6.9), where, for simplicity the payload position X_3 is called P. In Figure 6.1, the number of nodes on each cable, N, is set to three. The payload velocity is then defined as

$$\dot{\mathrm{P}} = J_{i\theta}(\theta_i, \boldsymbol{q}_{ie})\dot{\theta}_i + \boldsymbol{J}_{ie}(\theta_i, \boldsymbol{q}_{ie})\dot{\boldsymbol{q}}_{ie}\,, \qquad i = 1 \; or \; 2 \tag{6.19}$$

where, $J_{i\theta}$ and $\boldsymbol{J}_{ie}$ are the Jacobian matrices. A more general output known as $\mu -$ tip rate is defined as a scaled version of the true payload velocity.

$$\begin{aligned}\dot{\mathrm{P}}_\mu = \sum_{i=1}^{2} C_i\left[J_{i\theta}\dot{\theta}_i + \mu\boldsymbol{J}_{ie}\dot{\boldsymbol{q}}_{ie}\right] &= \dot{\mathrm{P}} - (1-\mu)[C_1\boldsymbol{J}_{1e}\dot{\boldsymbol{q}}_{1e} + C_2\boldsymbol{J}_{2e}\dot{\boldsymbol{q}}_{2e}] \\ &= \mu\dot{\mathrm{P}} - (1-\mu)\left[C_1J_{1\theta}\dot{\theta}_1 + C_2J_{2\theta}\dot{\theta}_2\right]\end{aligned} \tag{6.20}$$

where, $0<C_1<1$ and $C_2=1-C_1$ are called the load sharing parameters. It is obvious that $\dot{\mathrm{P}}_\mu$ with $\mu = 1$ captures the velocity of the payload and with $\mu = 0$ it captures an output that only involves the winches motion.

- **Alternative control input, $\hat{\boldsymbol{\tau}}$**

The input vector $\boldsymbol{\tau}$ consisting of the two input torques applied to the cables through the two winched (located at nodes one and four in Figure 6.1) is determined as

$$\boldsymbol{\tau} = [C_1 J_{1\theta} \quad C_2 J_{2\theta}]^T \hat{\tau} \tag{6.21}$$

where, $\hat{\tau}$ is the alternative control input. The same load sharing parameters that are used in forming the $\mu -$ tip rate are used here for distributing the required torque between the two winches.

6.2.1 Positive realness analysis

The state-space representation of the example system follows

$$\dot{\mathbf{X}} = \boldsymbol{A}_{sys}\mathbf{X} + \boldsymbol{B}_{sys}\hat{\tau} \tag{6.22}$$

$$\dot{\mathrm{P}}_{\mu} = \boldsymbol{C}_{sys}\mathbf{X} \tag{6.23}$$

where, $\mathbf{X} = \begin{bmatrix} \boldsymbol{Z} \\ \dot{\boldsymbol{Z}} \end{bmatrix}$, $\boldsymbol{A}_{sys} = \begin{bmatrix} \mathbf{0} & \boldsymbol{I} \\ -\boldsymbol{M}_{zz}{}^{-1}\boldsymbol{K}_{zz} & -\boldsymbol{M}_{zz}{}^{-1}\boldsymbol{D}_{zz} \end{bmatrix}$, $\boldsymbol{B}_{sys} = \begin{bmatrix} \mathbf{0} \\ \boldsymbol{M}_{zz}{}^{-1}\boldsymbol{R}^T[\boldsymbol{I}\ \mathbf{0}]^T \end{bmatrix} \begin{bmatrix} C_1 J_{1\theta} \\ C_2 J_{2\theta} \end{bmatrix}$, and $\boldsymbol{C}_{sys} = \begin{bmatrix} \mathbf{0} & \frac{C_1+C_2}{r} & \frac{C_2}{r} + C_1\mu & \frac{C_2}{r} + C_1\mu & \frac{C_2}{r} - C_2\mu & \frac{C_2}{r} - C_2\mu \end{bmatrix}$ with r being the winch radius. The dynamics of the cable-actuated system relating $\hat{\tau}$ to $\dot{\mathrm{P}}_{\mu}$ can be described by

$$\dot{\mathrm{P}}_{\mu} = G(s)\hat{\tau}, \qquad G = \boldsymbol{C}_{sys}\left(s\boldsymbol{I} - \boldsymbol{A}_{sys}\right)^{-1}\boldsymbol{B}_{sys} \tag{6.24}$$

This system is passive if $\int_0^T \dot{\mathrm{P}}_{\mu}\hat{\tau}\,dt \geq 0,\ \forall T \geq 0$. According to the definition of a passive system stated in section 2.3, a passive system is Hurwitz and has a phase response that satisfies $-90^o < \arg g(j\omega) < 90^o,\ \forall\omega$. In a Nyquist diagram, the definition states that $g(j\omega)$ is in the closed half plane $Re(s) \geq 0$ for a passive system [30]. In what follows, the range of μ leading to passivity of the system will be found numerically by evaluating the frequency response of the system of Eq. (6.24). It will be also shown that this range becomes larger as the payload becomes heavier. The cable parameters for this simulation are as follows: the Young's modulus $E = 437\ MPa$, the density $\rho = 2180\ kg/m^3$, the cable diameter $d = 6.16\ mm$ and the starting lengths $L_1 = L_2 = 0.5\ m$. A pretension of $100\ N$ is applied to the cables and the winches moment of inertia and radius are set to $0.001\ kg.m^2$ and $0.05\ m$ respectively.

Given the payload mass to be 1 kg, the Bode diagram of the transfer function relating $\hat{\tau}$ to $\dot{P}_{\mu}$ is shown in Figure 6.4. The system is passive for $0 \leq \mu \leq \mu_{cr}$. It is indicated by the phase response of $g(j\omega)$ being bounded by $\pm 90^{o}$ in Figure 6.4 a) for $\mu_{cr} = 0.39$. The phase response of the system for $\mu = 0.45$ which is over its critical value is also shown in Figure 6.4 b) which is not bounded by $\pm 90^{o}$ indicating that the system is no longer passive.

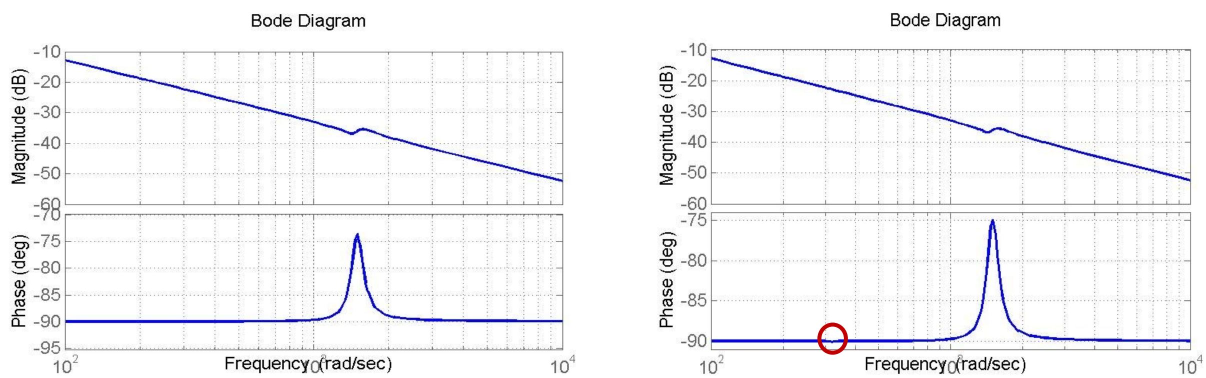

a) $\boldsymbol{\mu_{cr} = 0.39}$ **b)** $\boldsymbol{\mu = 0.45}$

Figure 6.4: Bode diagram: $\boldsymbol{m_{payload}=1\ kg}$

The Nyquist diagram of the cable-actuated system of Eq. (6.24) is shown in Figure 6.5. In Figure 6.5 a), $\mu_{cr} = 0.39$ which is in the range leading to passivity of the system since the Nyquist diagram of $g(j\omega)$ is in the closed half plane $Re(s) \geq 0$. The Nyquist diagram of the system with $\mu = 0.45$ moves to the left half plane that indicates the violation of the passivity property of the system as shown in Figure 6.5 b).

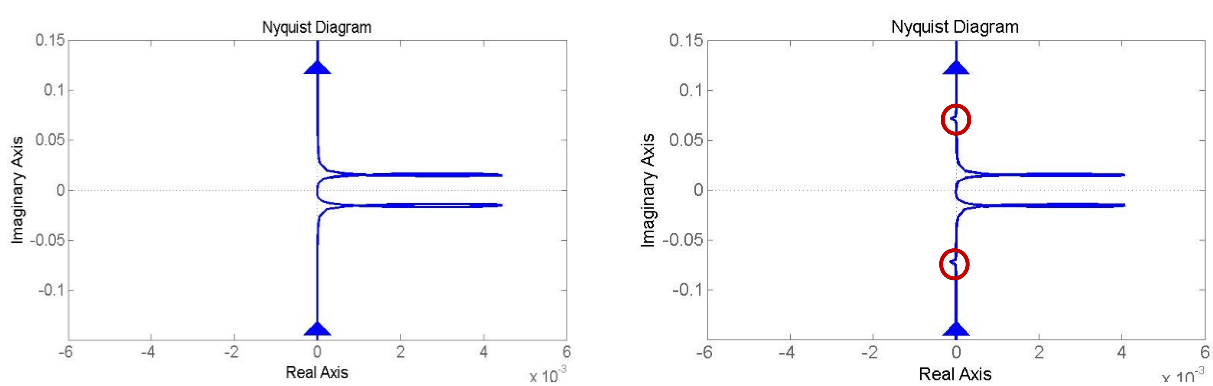

a) $\boldsymbol{\mu_{cr} = 0.39}$ **b)** $\boldsymbol{\mu = 0.45}$

Figure 6.5: Nyquist diagram: $\boldsymbol{m_{payload}=1\ kg}$

In the previous test case, the payload mass of 1 kg was chosen and the range of μ leading to passivity property of the system was found to be $0 \leq \mu \leq 0.39$. In order to show that for a larger payload the passivity property of the system is achieved for a larger range of μ, another test case is considered. In this case, a cable actuated system with the same cable properties and the same winches is modeled where the payload mass is set to $10\ kg$. Figure 6.6 a) shows that shows that by increasing the payload mass to $10\ kg$, the phase response of $g(j\omega)$ is bounded by $\pm 90^o$ up to $\mu_{cr} = 0.45$. Whereas, the phase response falls under -90^o for a larger μ as it is shown in Figure 6.6 b) for $\mu = 0.90$.

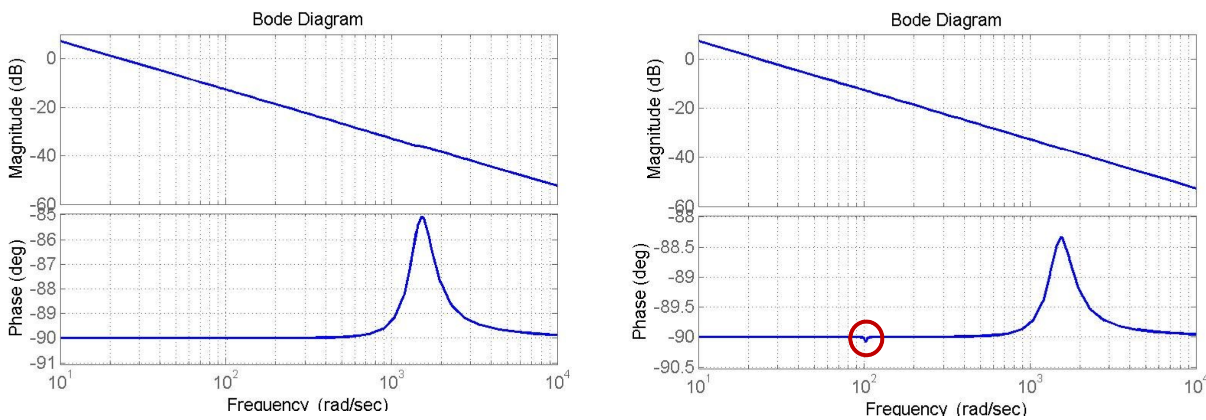

a) $\boldsymbol{\mu_{cr} = 0.45}$ **b)** $\boldsymbol{\mu = 0.90}$

Figure 6.6: Bode diagram: *$m_{payload}$=10 kg*

The Nyquist diagram of the cable-actuated system with a payload mass of $10\ kg$ is shown in Figure 6.7. In Figure 6.7 a) ,the Nyquist diagram is in the closed half plane $Re(s) \geq 0$ for $\mu_{cr} = 0.45$, indicating the passivity property of the system. For $\mu = 0.90$, the Nyquist diagram is no longer in the closed half plane as shown in Figure 6.7 b).

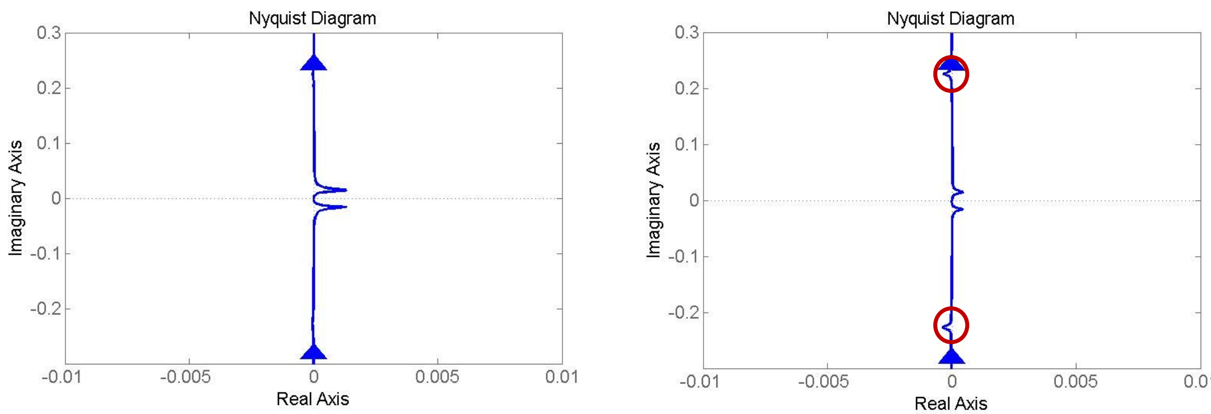

a) $\boldsymbol{\mu_{cr} = 0.45}$ **b)** $\boldsymbol{\mu = 0.90}$

Figure 6.7: Nyquist diagram: ***$m_{payload}$=10 kg***

In conclusion, by increasing the payload mass from $1\ kg$ to $10\ kg$, the range of μ leading to passivity property of the system is increased from $0 \leq \mu \leq 0.39$ to $0 \leq \mu \leq 0.45$.

6.3 Controller design

In the context of control, the objective of this thesis is to design a passivity-based controller that will apply torques through the winches to have the cable-actuated system payload track a prescribed desired trajectory precisely, and at the same time, suppress the cable vibrations. From the Passivity Theorem, it is guaranteed that any controller that is strictly passive with finite gain, such as a simple derivative controller, will stabilize the system. The winch control inputs are adjusted according to the payload tracking error. The desired payload trajectory restricts the payload to move smoothly from its initial position of *0.5 m* to its finial desired position of *0.6 m*. The period of this trajectory is set to *T=0.2 s* and the payload is assumed to be at rest in its initial and final position. This smooth desired trajectory is defined by P_d, $\dot{\mathrm{P}}_d$ and $\ddot{\mathrm{P}}_d$

$$\mathrm{P}_d(t) = 0.5 + 0.05\left(1 - cos\left(\frac{\pi t}{T}\right)\right) \tag{6.25}$$

$$\dot{\mathrm{P}}_d(t) = 0.05\left(\frac{\pi}{T}\right) sin\left(\frac{\pi t}{T}\right) \tag{6.26}$$

$$\ddot{\mathrm{P}}_d(t) = 0.05\left(\frac{\pi}{T}\right)^2 cos\left(\frac{\pi t}{T}\right) \tag{6.27}$$

Given this desired trajectory, it is chosen to design a feedforward control in conjunction with feedback control to get good payload tracking. The objective of feedforward control is to cancel out some parts of the system dynamics while the passivity property is preserved in the error dynamics. Using the generalized coordinates $\begin{bmatrix} \mathrm{P} \\ \boldsymbol{q}_e \end{bmatrix}$, the motion equation of the cable-actuated system of Figure 6.1 is rewritten in order to establish feedforward and feedback elements of the controller.

$$M_{\mathrm{PP}}\ddot{\mathrm{P}} + \mathrm{C_P}\dot{\mathrm{P}} = \hat{\tau} \tag{6.28}$$

$$\widehat{\boldsymbol{M}}_{\mathrm{ee}}\ddot{\mathbf{q}}_{\mathrm{e}} + \mathbf{K}_{\mathrm{ee}}\dot{\mathbf{q}}_{\mathrm{e}} = -[\mathrm{C_1}\mathbf{J}_{1\mathrm{e}} \quad \mathrm{C_2}\mathbf{J}_{2\mathrm{e}}]^{\mathrm{T}}\hat{\tau} \tag{6.29}$$

where,

$$M_{\mathrm{PP}} \triangleq J_{1\theta}^{-T} M_{zz,rr} J_{1\theta}^{-1} \tag{6.30}$$

$$\widehat{\boldsymbol{M}}_{\mathrm{ee}} \triangleq \boldsymbol{M}_{zz,ee} - \boldsymbol{M}_{zz,re}^{T} M_{zz,rr}^{-1} \boldsymbol{M}_{zz,re} \tag{6.31}$$

M_{PP} is equal to the moment of inertia of the winch, I, and $\mathrm{C_P}\dot{\mathrm{P}} = \dot{M}_{\mathrm{PP}}\dot{\mathrm{P}} - \frac{1}{2}\frac{\partial(\dot{\mathrm{P}}^T M_{\mathrm{PP}}\dot{\mathrm{P}})}{\partial \mathrm{P}}$ is zero for the cable-actuated system of Figure 6.1. A similar set of equations for a flexible system with closed-loop is derived by Damaren [38]. Eq. (6.28) is the rigid-body motion equation and Eq. (6.29) is the elastic motion equation.

Given the desired trajectory P_d, the desired form of $\mathrm{P}_\mu$is approximated by P_d and the tracking errors are

$$\tilde{\mathrm{P}} = \mathrm{P} - \mathrm{P}_d \tag{6.32}$$

$$\tilde{\mathrm{P}}_\mu = \mathrm{P}_\mu - \mathrm{P}_{\mu d} \tag{6.33}$$

A filtered error S_μ is introduced as [38]

$$S_\mu = \dot{\tilde{\mathrm{P}}}_\mu + \Lambda \tilde{\mathrm{P}}_\mu \tag{6.34}$$

where, $\Lambda = (\boldsymbol{J}_c \boldsymbol{M}^{-1} \boldsymbol{J}_c^T)^{-1}$ is positive definite. A virtual reference trajectory and its corresponding error are now proposed by

$$\dot{\mathrm{P}}_r = \dot{\mathrm{P}}_\mathrm{d} - \Lambda \tilde{\mathrm{P}}_\mu \tag{6.35}$$

$$\dot{\tilde{\mathrm{P}}}_r = \dot{\mathrm{P}} - \dot{\mathrm{P}}_r = \dot{\tilde{\mathrm{P}}} + \Lambda \tilde{\mathrm{P}}_\mu \tag{6.36}$$

The feedforward element of the controller is defined by

$$M_{\mathrm{PP}} \ddot{\mathrm{P}}_\mathrm{r} = \hat{\tau}_\mathrm{d} \tag{6.37}$$

Damaren [38] proved the passivity of the system from $\hat{\tau} - \hat{\tau}_\mathrm{d}$ to S_μ by considering the function

$$\nu = \frac{1}{2} \dot{\tilde{\mathrm{P}}}_r^T M_{\mathrm{PP}} \, \dot{\tilde{\mathrm{P}}}_\mathrm{r} + \frac{1}{2}(1 - \mu)\left[\dot{\tilde{\mathbf{q}}}_e^T \widehat{\boldsymbol{M}}_{\mathrm{ee}} \dot{\tilde{\mathbf{q}}}_e + \tilde{\boldsymbol{q}}_e^{\boldsymbol{T}} \boldsymbol{K}_{ee} \tilde{\boldsymbol{q}}_e\right] \tag{6.38}$$

where, $\tilde{\boldsymbol{q}}_e = \boldsymbol{q}_e - \boldsymbol{q}_{ed}$. He showed that the derivative of ν gives

$$\dot{\nu} = S_\mu^T (\hat{\tau} - \hat{\tau}_\mathrm{d}) \tag{6.39}$$

Integration of this equation shows the passivity property of the system from $\hat{\tau} - \hat{\tau}_\mathrm{d}$ to S_μ. The procedure of proving the passivity property of the cable actuated system is similar to this. Using the passivity theorem, the stabilization of the passified cable-actuated system is guaranteed with a feedback strictly passive controller. Selecting a simple PD controller as feedback with the gains K_p and K_d, we get

$$\hat{\tau} = \hat{\tau}_{\mathrm{d}} - K_d\left(\dot{\tilde{\mathrm{P}}}_{\mu} + \Lambda\tilde{\mathrm{P}}_{\mu}\right) - K_p\tilde{\mathrm{P}}_{\mu} \quad \textbf{(6.40)}$$

where, $S_{\mu} = \dot{\tilde{\mathrm{P}}}_{\mu} + \Lambda\tilde{\mathrm{P}}_{\mu}$. The final form of the control law follows from Eq. (6.21), Eq. (6.37) and Eq. (6.40)

$$\boldsymbol{\tau} = [C_1 J_{1\theta} \quad C_2 J_{2\theta}]^T \left[M_{\mathrm{PP}}\left(\ddot{\mathrm{P}}_d - \Lambda\dot{\tilde{\mathrm{P}}}_{\mu}\right) - K_d\left(\dot{\tilde{\mathrm{P}}}_{\mu} + \Lambda\tilde{\mathrm{P}}_{\mu}\right) - K_p\tilde{\mathrm{P}}_{\mu}\right] \quad \textbf{(6.41)}$$

which is simple to design and implement.

6.4 Analyzing the controlled response

The control law of Eq. (6.41) is applied to the cable actuated system defined by Eq. (6.22) and Eq. (6.23) and the closed-loop response to a prescribed payload trajectory is discussed here. The closed-loop response of the system is compared applying the passivity-based controller designed in Chapter 5 by introducing an observer with the one designed in this Chapter by introducing μ-tip rate. The cables parameters for this simulation are as follows: the Young's modulus $E = 437\ MPa$, the density $\rho = 2180\ kg/m^3$, the cable diameter $d = 6.16\ mm$ and the starting lengths $L_1 = L_2 = 0.5\ m$. A pretension of $100\ N$ is applied to the cables and the winches moment of inertia and radius are set to $0.001\ kg.m^2$ and $0.05\ m$ respectively. The payload mass is $1\ Kg$ and the payload desired trajectory is defined by Eq. (6.25), Eq. (6.26) and Eq. (6.27). The design parameters are given as $K_P = 2000, K_d = 10, \mu = 0.3$ and $C_1 = C_2 = 0.5$. Figure 6.8 a) shows the position of the payload and the prescribed trajectory using the μ-tip rate technique. Figure 6.8 b) shows the payload position of the same system and the same the prescribed trajectory while using the observer-based technique of Chapter 5. The simulations show reasonably good payload tracking in both case, while the μ-tip rate technique seems to be more effective in vibration suppression.

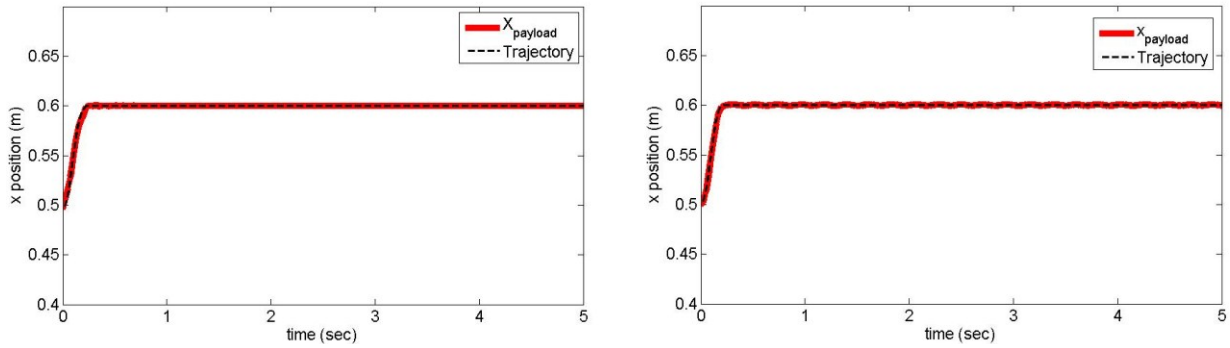

a) μ-tip rate method **b) Observer-based method**

Figure 6.8: Payload tracking and longitudinal oscillation using different passification techniques

Figure 6.9 a) and Figure 6.9 b) compares the μ-tip rate technique and the observer-based technique in terms of tension in the first cable element. It is clear that by using the μ-tip rate technique, the variation of tension in the first cable element damps out more quickly.

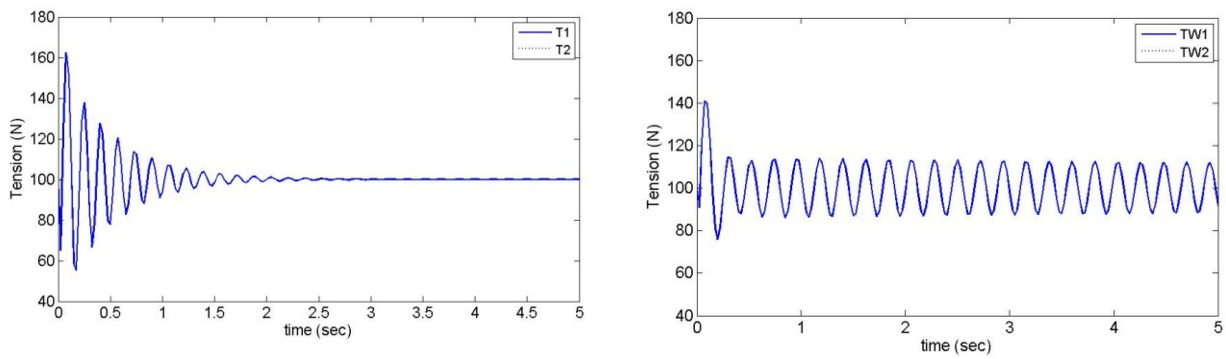

a) μ-tip rate method **b) Observer-based method**

Figure 6.9: Variation of tension in the first cable element using different passification techniques

Therefore, the controller designed based on the μ-tip rate technique is more effective in vibration suppression compared to the controller designed based on the observer-based technique.

Figure 6.10 a) and Figure 6.10 b) compares the μ-tip rate technique and the observer-based technique in terms of control signals. In μ-tip rate technique, the control signals are the input torques applied through the winches. In observer-based technique, the control signals are the changes in the unstretched length of the first elements on each cable. Therefore, these figures are plotted in different units.

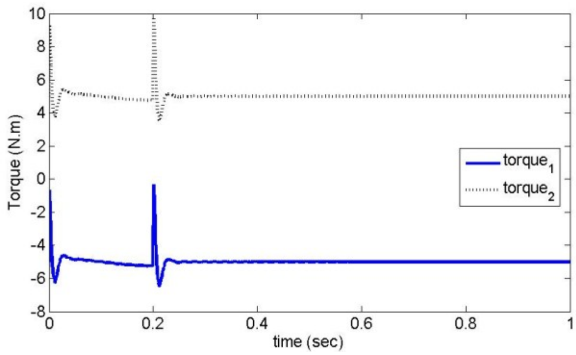

a) μ-tip rate method

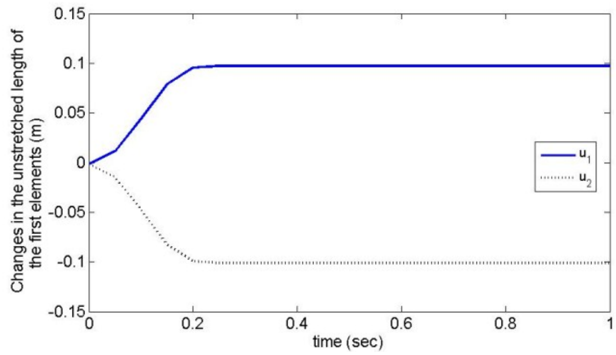

b) Observer-based method

Figure 6.10: Control signals using different passification techniques

7 Conclusion

The focus of this thesis is the dynamics modeling and control of cable-actuated-systems consisting of a payload and several actuated cables. The objective was to design a stabilizing controller that positions the payload precisely, while suppressing the cable vibrations. In this thesis, we modeled the cables using the lumped mass method that properly modeled the longitudinal and transverse dynamics behavior of cables. In the process of designing a controller, PID and LQG control algorithms were first used. Although it was simple to implement the PID controller, its performance was limited as a result of its suboptimal gains. Using the LQG controller increased the performance in payload positioning and vibration suppression, but its implementation procedure was complicated, and there was no guarantee of robustness. The robust nature of the passivity-based control and the fact that it has the potential to lead to a simple controller design motivated us to investigate its application to our systems. Cable-actuated systems are usually non-square with non-collocated actuators and sensors, which limits the use of passivity-based control. In order to overcome these limitations, we first considered a dynamic embedding where an observer state-feedback was used to construct a new output that realizes a passive input-output map. Later, we considered an alternative passification technique, called μ-tip rate. In this technique, an input-output map is considered where the output is a scaled version of the true payload velocity and the input is a combination of the winch torques.

We found the dynamics model of the system by discretizing the cables into a series of lumped masses connected by viscoelastic massless elements. We performed several simulations to determine the precision and the reliability of the dynamics model. Considering two elements on each cable, the first three simulated natural frequencies associated with the transverse vibration of the first cable were within $8\ \%$, $8.3\ \%$ and $7.4\ \%$ of the theoretical ones. The accuracy of the dynamics model was shown to be improved by increasing the number of elements. Using ten elements on each cable, the simulated natural frequencies associated with the transverse vibration of the first cable were within $0.04\ \%$, $4.2\ \%$ and $2.7\ \%$ of the theoretical ones. Ignoring the internal damping of the system, an energy analysis verified the conservation of the mechanical energy of the system in absence of external forces. These results create an adequate level of confidence that the model is capable of predicting realistic behavior of the cable-actuated system.

Designing the PID and LQG controllers, a series of closed-loop simulation were performed by actuating the winches according the payload position error feedback. The control input applied by each winch was approximated by the change in the unstretched length of the first cable element. Comparing the performance of the LQG controller and the PID controller applied to the same example system illustrated that the LQG controller leads to smaller oscillations of the cables and smoother control signal. In addition, the tension oscillations were much smaller when using the LQG controller. The PID controller was able to stabilize the system in $4\ sec$, when the desired trajectory was defined with a step of *0.1 m* in the payload position. The LQG controller has the potential to stabilize the system more quickly. When the desired trajectory was formulated as $0.5 + 0.05\left(1 - cos\left(\frac{\pi t}{0.2}\right)\right)$ which is slower compared to the step input, the LQG controller stabilize the system in $0.2\ sec$, with good tracking performance.

The Passivity Theorem states that the negative feedback interconnection of a passive system and a very strictly passive system is input-output stable. In order to realize a passive input-output map for the cable actuated system, we first considered an observer state-feedback in series with a dynamic embedding. The proposed observer-based passification technique applied to the unstable linearized system does not require the system to have relative degree -1, 0 or $+1$. The original system has non-square transfer function with two inputs and one output. Given the modified LTI system, we verified the positive realness of the system in the frequency domain. The modified design consisting of the linearized system with the observer, state-feedback controller and the dynamic embedding had positive minimum Hermitian part over all frequencies, verifying that it has SPR properties. Later an integral term was added to the control law guaranteeing zero steady-state tracking error. We revised the positive realness condition of the system in order to properly satisfy the requirements of the KYP lemma. The new system consisting of the linearized system with the observer, state-feedback controller, dynamic embedding and integral action was also shown to be SPR with positive minimum Hermitian part over all frequencies. The controller designed based on the observer-based technique stabilized the system in 0.2 sec with good tracking performance.

Although a passive input-output map was found for the cable-actuated system by using the observer-based technique, we found the controller design procedure and thus its implementation to be complicated for a steady-state tracking problem. Therefore, as an alternative, we considered μ-tip rate passification technique which led to a more practical and simpler controller design. After incorporating the dynamics of the winches, we defined a new output, called $\mu - \text{tip}$ rate, as a scaled version of the true payload velocity. We found the range of the design parameter μ leading to passivity of the system numerically from the frequency response of the system. The system passivity property was shown to be dependent on the payload mass, and for heavier payloads the modified system was passive for a larger range of μ. Given the payload mass to be 1 kg, the system was shown to be passive for $0 \leq \mu \leq 0.39$, while for a 10 kg payload mass, this range increased to $0 \leq \mu \leq 0.45$. Both observer-based and μ-tip technique led to design controllers capable of stabilizing the system and bring the payload to its desired position in 0.2 sec, while, the controller designed based on the μ-tip rate technique was more effective in vibration suppression of the cables. The controller designed based on μ-tip rate technique was able to decrease the variations of tension in the cable to 4 % of its final value in 1.4 sec, while it took 50 sec for the controller designed based on the observer-based technique to accomplish the same task. Consequently, compared to the observer-based passification technique, we found the μ-tip rate to be a more effective controller.

Future work

Future work for designing a controller for the cable-actuated system can be broken down into the following steps:

- The μ-tip rate technique was applied to the linearized model of the cable-actuated system where we did not see the transverse vibration of the lumped masses. Effort should be made to apply the μ-tip rate technique to a linearized model that considers cable deformations in both longitudinal and transverse directions. This way, one can study the effect of the designed controller on damping the transverse vibration of the cables.
- The stability of the closed-loop system and the robustness of the controller with respect to parameter uncertainties of the system should be studied first numerically and then analytically.
- In order to damp the cable vibrations, it may be necessary to extend the control procedure to a nonlinear case. A first approach could be to design a gain scheduled SPR controller.
- Efforts should be made to generalize the developed control technique to be applicable to two or three dimensional cable actuated systems.
- The same load sharing parameters that we used in forming the $\mu-\mathrm{tip}$ rate were used for distributing the required torque between the two winches. Alternative methods of load sharing could be investigated, for example optimal distribution of the winch torque, while satisfying the desired net force on the payload.
- Efforts should be made to validate the proposed control algorithm experimentally on a physical testbed.

References

1. Leonard, J.W., *Tension structures: Behavior and analysis*. 1988.
2. *Multi-Thethered Aerostat*. [cited 2013 Febuary 28]; Available from: http://people.mcgill.ca/meyer.nahon/research/.
3. *Modern Elevator*. [cited 2013 Febuary 28]; Available from: http://www.explainthatstuff.com/how-elevators-work.html.
4. *Towed AUV*. [cited 2013 Febuary 2013]; Available from: http://www.mtiltd.com/.
5. Chen, L.Q., *Analysis and control of transverse vibrations of axially moving strings.* Applied Mechanics Reviews, 2005. 58(1-6): p. 91-115.
6. Zhu, W.D. and Y. Chen, *Forced response of translating media with variable length and tension: Application to high-speed elevators.* Proceedings of the Institution of Mechanical Engineers, Part K: Journal of Multi-body Dynamics, 2005. 219(1): p. 35-53.
7. Zhu, W.D. and Y. Chen, *Theoretical and experimental investigation of elevator cable dynamics and control.* Journal of Vibration and Acoustics, Transactions of the ASME, 2006. 128(1): p. 66-78.
8. Grant, D.A., *Beam vibrations with time-dependent boundary conditions.* Journal of Sound and Vibration, 1983. 89(4): p. 519-522.
9. Pota, H.R., et al. *Robust Control of Residual Motion of Cable Transporter Systems*. 2003.
10. Zhang, Y. and S. Agrawal. *Coupled vibrations of a varying length flexible cable transporter system with arbitrary axial velocity*. 2004.
11. Zhang, Y., S.K. Agrawal, and P. Hagedorn, *Longitudinal vibration modeling and control of a flexible transporter system with arbitrarily varying cable lengths.* JVC/Journal of Vibration and Control, 2005. 11(3): p. 431-456.
12. Zhang, Y. and S.K. Agrawal, *Lyapunov controller design for transverse vibration of a cable-linked transporter system.* Multibody System Dynamics, 2006. 15(3): p. 287-304.
13. Otsuki, M., et al., *Nonstationary robust control for vibration of elevator-rope.* Nihon Kikai Gakkai Ronbunshu, C Hen/Transactions of the Japan Society of Mechanical Engineers, Part C, 2005. 71(3): p. 859-866.
14. Otsuki, M., et al., *Application of nonstationary sliding mode control to suppression of transverse vibration of elevator rope using input device with gaps.* JSME International Journal, Series C: Mechanical Systems, Machine Elements and Manufacturing, 2006. 49(2): p. 385-394.
15. Zhu, W.D. and N.A. Zheng. *Exact response of a translating string with arbitrarily varying length under general excitation*. 2008.
16. Howell, C.T., *Investigation of the dynamics of low-tension cables*, 1992, DTIC Document.
17. Triantafyllou, M.S. and C.T. Howell, *Nonlinear impulsive motions of low-tension cables.* Journal of engineering mechanics, 1992. 118(4): p. 807-830.
18. Burgess, J., *Bending stiffness in a simulation of undersea cable deployment.* International Journal of Offshore and Polar Engineering, 1993. 3(3).
19. Buckham, B.J., *Dynamics modelling of low-tension tethers for submerged remotely operated vehicles*, 2004, National Library of Canada = Bibliothèque nationale du Canada: Ottawa.

20. Driscoll, F.R., R.G. Lueck, and M. Nahon, *Development and validation of a lumped-mass dynamics model of a deep-sea ROV system.* Applied Ocean Research, 2000. 22(3): p. 169-182.
21. Lambert, C. and M. Nahon. *An aerostat positioning system with cable control*. 2008.
22. Malahy, R. *A nonlinear finite element method for the analysis of offshore pipelines, risers and cable structures*. in *5. International Offshore Mechanics and Arctic Engineering(OMAE) Symposium*. 1986.
23. Meunier, G., B. Boulet, and M. Nahon, *Control of an overactuated cable-driven parallel mechanism for a radio telescope application.* IEEE Trans Control Syst Technol IEEE Transactions on Control Systems Technology, 2009. 17(5): p. 1043-1054.
24. Gattulli, V., R. Alaggio, and F. Potenza, *Analytical prediction and experimental validation for longitudinal control of cable oscillations.* International Journal of Non-Linear Mechanics, 2008. 43(1): p. 36-52.
25. Zhu, W.D. and J. Ni, *Energetics and Stability of Translating Media with an Arbitrarily Varying Length.* Transaction- American Society of Mechanical Engineers Journal of Vibration and Acoustics, 2000. 122: p. 295-304.
26. Zhu, W.D., J. Ni, and J. Huang, *Active Control of Translating Media With Arbitrarily Varying Length.* Transaction- American Society of Mechanical Engineers Journal of Vibration and Acoustics,2001. 123: p. 347-358.
27. Fujino, Y. and T. Susumpow, *Active control of cables by axial support motion.* Smart Materials and Structures, 1995. 4(1A): p. A41-A51.
28. Susumpow, T. and Y. Fujino, *Active Control of Multimodal Cable Vibrations by Axial Support Motion.* Journal of engineering mechanics /, 1995. 121(9): p. 964.
29. Marquez, H.J., *Nonlinear control systems*. 2003: John Wiley.
30. Brogliato, B., et al., *Dissipative systems analysis and control: theory and applications*. 2007: Springer.
31. Alli, H. and T. Singh, *Passive control of overhead cranes.* Journal of Vibration and Control, 1999. 5(3): p. 443-459.
32. Wang, D. and M. Vidyasagar, *Passive Control of a Stiff Flexible Link Communication.* The International journal of robotics research, 1992. 11(6): p. 572-578.
33. JUANG, J. and M. Phan, *Robust controller designs for second-order dynamic systems- A virtual passive approach.* Journal of guidance, control, and dynamics, 1992. 15(5): p. 1192-1198.
34. Lee, F., H. Flashner, and M. Safonov, *Positivity embedding for noncolocated and nonsquare flexible systems.* Applied mathematics and computation, 1995. 70(2): p. 233-246.
35. Collado, J., R. Lozano, and R. Johansson, *Using an observer to transform linear systems into strictly positive real systems.* Automatic Control, IEEE Transactions on, 2007. 52(6): p. 1082-1088.
36. Damaren, C.J., *Passivity analysis for flexible multilink space manipulators.* Journal of Guidance Control Dynamics, 1995. 18: p. 272-279.
37. Damaren, C.J., *Modal properties and control system design for two-link flexible manipulators.* The International Journal of Robotics Research, 1998. 17(6): p. 667-678.
38. Damaren, C.J., *On the dynamics and control of flexible multibody systems with closed loops.* The International Journal of Robotics Research, 2000. 19(3): p. 238-253.

39. Damaren, C.J., *An adaptive controller for two cooperating flexible manipulators.* Journal of Robotic Systems, 2003. 20(1): p. 15-21.
40. Christoforou, E.G. and C.J. Damaren. *Application of passivity-based techniques to the control of structurally flexible gantry robots*. in *Robotics and Automation (ICRA), 2011 IEEE International Conference on*. 2011. IEEE.
41. Boulet, P.B., *Notes for a course on Linear Systems*, 2010: McGill University.
42. Schaft, A.J.v.d., *L2-gain and passivity techniques in nonlinear control*. 1996, London; New York: Springer.
43. Forbes, J.R., *Extensions of Input-Output Stability Theory and the Control of Aerospace Systems*, 2011, University of Toronto.
44. Skogestad, S. and I. Postlethwaite, *Multivariable feedback control: analysis and design*. Vol. 2. 2007: Wiley.
45. Desoer, C.A. and M. Vidyasagar, *Feedback systems: input-output properties*. Vol. 55. 2009: Society for Industrial Mathematics.
46. Harder, D.W. *Positive-definite matrices*. 17 March 2013]; Available from: https://ece.uwaterloo.ca/dwharder/NumericalAnalysis/04LinearAlgebra/posdef/.
47. *Schur complement*. 28 Febuary 2013 14 March 2013]; Available from: http://en.wikipedia.org/wiki/Schur_complement.
48. Buckham, B., et al., *Dynamics and control of towed underwater vehicle system, part II: Model validation and turn maneuver optimization.* Ocean Engineering, 2003. 30(4): p. 471-485.
49. Irvine, H.M., *Cable structures*. 1981.
50. Meirovitch, L., *Fundamentals of vibrations*. 2001, Boston: McGraw-Hill.
51. Masciola, M.D. *Dynamic analysis of a coupled and an uncoupled tension leg platform*. 2011; Available from: http://digitool.Library.McGill.CA/R/?func=dbin-jump-full&object_id=104726.
52. Gawronski, W., *Advanced structural dynamics and active control of structures*. 2004: Springer.
53. Meirovitch, L. and R. Parker, *Fundamentals of vibrations.* Applied Mechanics Reviews, 2001. 54: p. 100.